Institut für Wasserbau · Universität Stuttgart

Mitteilungen

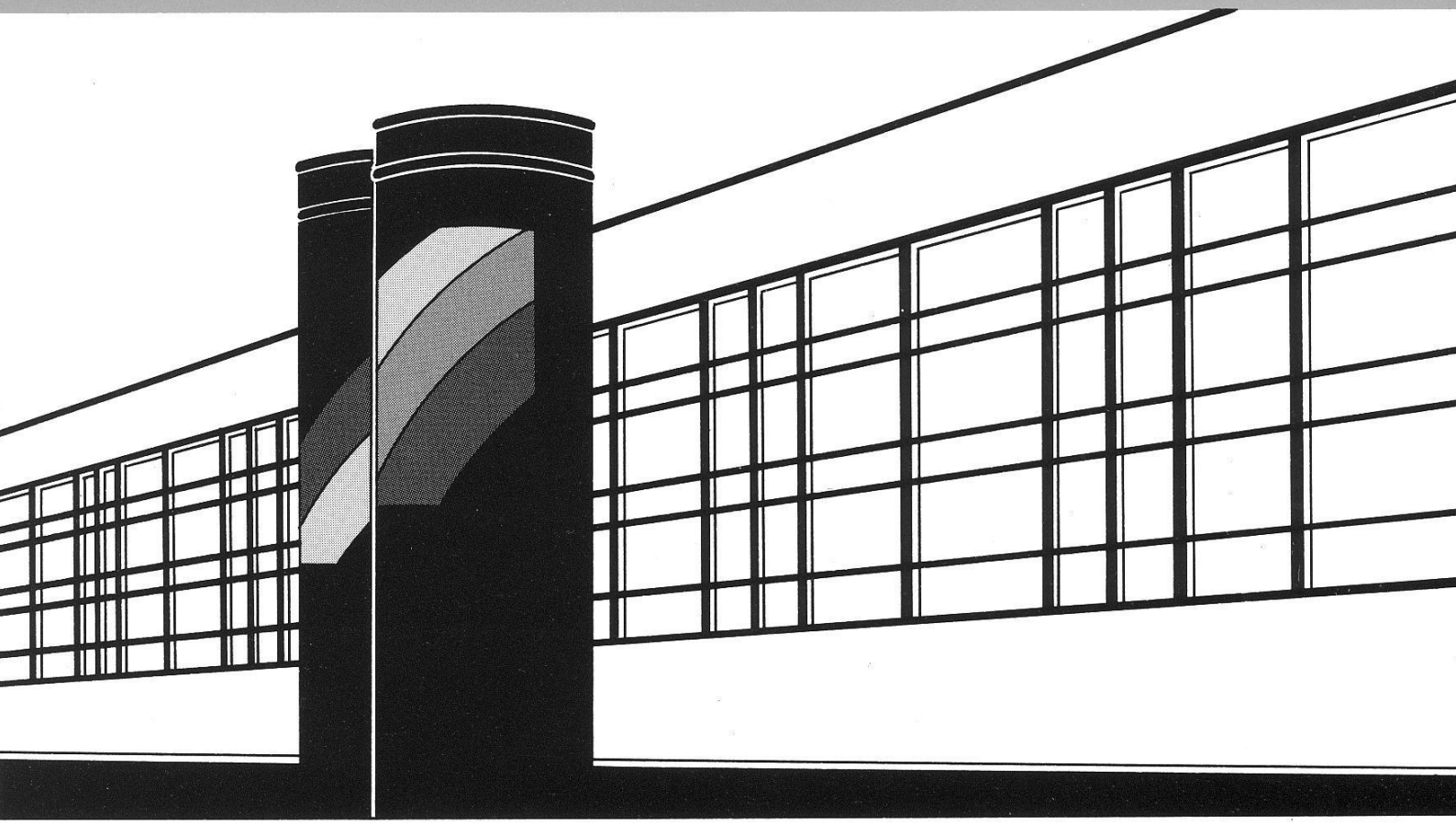

Heft 183 Anozie Ebigbo

Modelling of biofilm growth and its influence on CO_2 and water (two-phase) flow in porous media

Modelling of biofilm growth and its influence on CO_2 and water (two-phase) flow in porous media

Von der Fakultät Bau- und Umweltingenieurwissenschaften der Universität Stuttgart zur Erlangung der Würde eines Doktor-Ingenieurs (Dr.-Ing.) genehmigte Abhandlung

Vorgelegt von

Anozie Ebigbo

aus Enugu / Nigeria

Hauptberichter:	Prof. Dr.-Ing. Rainer Helmig
Mitberichter:	Prof. Alfred B. Cunningham, Ph.D.
	Prof. Dr. phil. Karsten Pruess
Tag der mündlichen Prüfung:	25. Mai 2009

Institut für Wasserbau der Universität Stuttgart

2009

Heft 183

Modelling of biofilm growth and its influence on CO_2 and water (two-phase) flow in porous media

von
Dr.-Ing.
Anozie Ebigbo

Eigenverlag des Instituts für Wasserbau der Universität Stuttgart

D93 Modelling of biofilm growth and its influence on CO_2 and water (two-phase) flow in porous media

Titelaufnahme der Deutschen Bibliothek

Ebigbo, Anozie:
Modelling of biofilm growth and its influence on CO_2 and water (two-phase) flow in porous media / von Anozie Ebigbo. Institut für Wasserbau, Universität Stuttgart. - Stuttgart: Inst. für Wasserbau, 2009

(Mitteilungen / Institut für Wasserbau, Universität Stuttgart: H. 183)
Zugl.: Stuttgart, Univ., Diss., 2009
ISBN **978-3-933761-87-3**
NE: Institut für Wasserbau <Stuttgart>: Mitteilungen

Herausgegeben 2009 vom Eigenverlag des Instituts für Wasserbau
Druck: Document Center S. Kästl, Ostfildern

Acknowledgement

This work was carried out within the framework of the International Research Training Group NUPUS (http://www.nupus.uni-stuttgart.de) funded by the German Research Foundation DFG (GRK 1398) and the Netherlands Organisation for Scientific Research NWO (DN 81-754). I also acknowledge support by the US Department of Energy Zero Emissions Research and Technology (ZERT) programme (DOE Award No. DE-FC26-04NT42262) and from the US Department of Energy EPSCoR programme under grant number DE-FG02-08ER46527.

I would like to express my gratitude to all those who helped make this work possible. In particular, thank you to my supervisor, Rainer Helmig, for believing in me, creating the appropriate environment for research in our department, and for his fairness, motivation, and constant support.

I would also like to thank Al Cunningham for his supervision and numerous discussions on this work. I had the pleasure on two occasions of visiting Al and the very friendly Center for Biofilm Engineering in beautiful Montana.

Special thanks to Holger Class for his support, supervision, guidance, and for always making sure I am on the right track.

I deeply appreciate the work of the organisers and speakers of the doctoral programmes "Non-linearities and Upscaling in Porous Media, NUPUS" and "Environment and Water, ENWAT." These two programmes certainly helped me and many others by providing a perfect framework for the training of graduate students.

Thank you to Karsten Pruess for taking part in the examination as a member of the examination committee.

I would also like to thank Helge Dahle and Jan Nordbotten for inviting me to and hosting me at the Department of Applied Mathematics, University of Bergen for three months.

Thank you to Hans Bruining for the four weeks I spent in the Geo-Engineering Section, TU Delft and for co-supervising my work within the NUPUS framework.

Within my time at the IWS, I was fortunate enough to work with a number of friendly and helpful colleagues including Andreas Bielinski, Andreas Kopp, Ulrich Ölmann, Prudence Lawday, Melanie Darcis, Hartmut Kuhnke, Steffen Ochs, Jennifer Niessner, Maria Costa, Insa Neuweiler, Anongnart Assteerawatt, Sabine Manthey, Alexandros Papafotiou, Yufei Cao, Birgitte Eikemo, Anna Kuhlmann, David Werner, Markus Wolff, Jochen Fritz, Bernd Flemisch, Sandra Freiboth, Klaus Mosthaf, Michelle Hartnick, Karin Erbertseder, Rainer Enzenhöfer, Maren Paul, Onur Doğan, Andreas Lauser, Miloš Vasin, Veronica Heiss, Alexandru Tatomir, Lena Walter, Li Yang, Thomas Breiting, and Hussam Sheta.

Naturally, I owe a lot to my family – Mama, Papa, Esther, Alanna, and Njiko. There's just no place like home.

Finally, I would like to thank Meike for being there for me every single day.

In loving memory of Josef Raab

Contents

List of Figures

List of Tables

Notation

The following table shows the significant symbols used in this work. Local notations are explained in the text.

Symbol	Definition	Dimension
Greek Letters:		
Ω	control volume	[m^3]
Γ	control volume boundary	[m^2]
ε	biofilm porosity	[-]
ϕ	porosity	[-]
ϕ_0	porosity of porous medium unaffected by biofilm	[-]
ϕ_κ	porosity of Continuum κ	[-]
$\phi_{p,c}, \phi'_{p,c}$	parameters for the calculation of K_p and K_f	
λ	pore-size distribution index	[-]
μ_α	dynamic fluid viscosity of phase α	[kg/(m s)]
μ_κ	growth rate of biomass in Continuum κ	[1/s]
ϱ_α	fluid density of phase α	[kg/m^3]
ϱ_b	biofilm density	[kg/m^3]
σ	interfacial tension	[N/m^2]
θ	contact angle	[$^\circ$]
Latin Letters:		
C_w^b	concentration of biomass in water	[kg/m^3]
C_w^s	concentration of substrate/solute in water	[kg/m^3]
D	diffusion/dispersion coefficient	[m^2/s]
F	continuum accounting for fluid flow in biofilm	
P	continuum accounting for fluid flow in porous matrix	
$\mathbf{K}$	tensor of intrinsic permeability	[m^2]
K	isotropic intrinsic permeability	[m^2]
K_0	permeability of biofilm-free porous medium	[m^2]
$K_{\min}$	permeability of biofilm-filled porous medium	[m^2]
K_s	Monod half-saturation coefficient	[kg/m^3]

M	specific surface	[m^2/m^3]
N	ansatz function	
R	mass ratio of electron acceptor per substrate consumed	[-]
S_α	saturation of phase α	[-]
$S_{\alpha r}$	residual saturation of phase α	[-]
S_e	effective saturation	[-]
T	temperature	[° C]
V_0	pore volume of porous medium unaffected by biofilm	[m^3]
V_B	bulk volume	[m^3]
V_b	biofilm volume including biofilm pores	[m^3]
V_f	volume of pores within biofilm	[m^3]
V_p	pore volume of porous medium excluding biofilm pores	[m^3]
W	weighting function	
Y	yield coefficient	[-]
a	exchange paramter	[s/m^2]
b	biomass decay rate	[1/s]
b_0	endogenous biomass decay rate	[1/s]
b_c	biomass decay rate due to lysis	[1/s]
c_c	paramter for the calculation of b_c	
$c_{a,1}, c_{a,2}$	paramters for the calculation of k_a	
$c_{d,1}, c_{d,2}, \tilde{c}_{d,2}$	paramters for the calculation of k_d	
d_r	characteristic pore diameter	[m]
e	exchange term	[$kg/(m^3 s)$]
$\mathbf{g}$	vector of gravitational acceleration $(0, 0, -\mathrm{g})^T$	[m/s^2]
g	(scalar) gravitational acceleration	[m/s^2]
k_μ	maximum substrate utilisation rate	[1/s]
k_a	attachment function	[1/s]
k_d	detachment function	[1/s]
k_d^τ	detachment due to shear	[1/s]
k_d^μ	detachment due to biological factors	[1/s]
$k_{r\alpha}$	relative permeability of phase α	[-]
$\mathbf{n}$	unit normal vector	[-]
n_c	paramter for the calculation of b_c	
n_k	parameters for the calculation of K_p	
p_α	pressure of phase α	[N/m^2]
p_d	entry pressure	[N/m^2]
p_c	capillary pressure	[N/m^2]
q	soure/sink	[$kg/(m^3 s)$]
r_g	biomass growth	[$kg/(m^3 s)$]
r_b	biomass decay	[$kg/(m^3 s)$]
r_a	biomass attachment rate	[$kg/(m^3 s)$]
r_d	biomass detachment rate	[$kg/(m^3 s)$]

$\mathbf{v}$	Darcy flux/velocity	[m/s]

Subscripts:

α	phase, either w or n
n	non-wetting phase
w	wetting phase
κ	continuum, either p or f
p	Continuum P
f	Continuum F

Superscripts:

b	biomass
s	substrate/solute

Abstract

Bacterial biofilms are groups of microbial cells attached to surfaces and to each other. Cells in a biofilm are protected from adverse external conditions. In natural environments, this attached mode of growth is more successful than the suspended mode (Costerton *et al.*, 1978), and a major portion of microbial activity takes place at surfaces (van Loosdrecht *et al.*, 1990; Bouwer *et al.*, 2000). In porous media, biofilms are used as bioreactors (e.g, in wastewater treatment) and as biobarriers (e.g., in enhanced oil recovery). They are also used in the containment and degradation of contaminants in groundwater aquifers. It has been proposed that biofilms be used as biobarriers for the mitigation of carbon dioxide (CO_2) leakage from a geological storage reservoir (Mitchell *et al.*, 2009).

The concentration of greenhouse gases – particularly carbon dioxide (CO_2) – in the atmosphere has been on the rise in the past decades. One of the methods which have been proposed to help reduce anthropogenic CO_2 emissions is the capture of CO_2 from large, stationary point sources and storage in deep geological formations. The caprock is an impermeable geological layer which prevents the leakage of stored CO_2, and its integrity is of utmost importance for storage security. As mentioned above, biofilms could be used as biobarriers which help prevent the leakage of CO_2 through the caprock in injection well vicinity. Due to the high pressure build-up during injection, the caprock in the vicinity of the well is particularly at risk of fracturing. The biofilm could also protect well cement from corrosion by CO_2-rich brine.

The goal of this work is to develop and test a numerical model which is capable of simulating the development of a biofilm in a CO_2 storage reservoir. This involves the description of the growth of the biofilm, flow and transport in the geological formation, and the interaction between the biofilm and the flow processes. Important processes which are accounted for in the model include the effect of biofilm growth on the permeability of the formation, the hazardous effect of supercritical CO_2 on suspended and attached bacteria, attachment and detachment of biomass, and two-phase fluid flow processes. The partial differential equations which describe the system are discretised in space with a vertex-centered finite volume method, and an implicit Euler scheme is used for time discretisation. The model is tested by comparing simulation results to experimental data.

In a test case simulation, the model predicts the extent of biomass accumulation near an injection well and its effect on the permeability of the formation. The simulations show that the biobarrier is only effective for a limited amount of time. Regular injection of nutrients would be necessary to sustain the biofilm. In future work, the model could be extended to account for the active precipitation of minerals by the biofilm which would lead to a more enduring barrier. The model also needs to be extended to account for more than one

growth-limiting factor. This would allow for the simulation of injection strategies which aim at growing a biofilm at some distance from the injection well.

Zusammenfassung

Die vorliegende Arbeit behandelt im Wesentlichen die Entwicklung eines numerischen Modells, um die Anreicherung von mikrobieller Biomasse im Untergrund simulieren zu können. Das entwickelte Modell soll in der Lage sein, das Abdichten der beschädigten geologischen Deckschicht einer unterirdischen Kohlendioxid-Lagerstätte mit Hilfe von Biofilmen zu simulieren. Dafür müssen einerseits Strömungsprozesse und andererseits auch die mikrobielle Aktivität sowie die Interaktion dieser Vorgänge in porösen Medien richtig beschrieben werden. Die Anreicherung von Bakterien in einem porösen Medium beeinflusst die hydraulischen Eigenschaften des Mediums und als Folge davon auch die darin stattfindende Strömung. Im Gegenzug bestimmt die Strömung den Transport der mikrobiellen Nährstoffe und damit auch die Verteilung mikrobieller Wachstumsraten. Dementsprechend ist die richtige Beschreibung der Wechselwirkung zwischen Strömung und mikrobiellen Prozessen eine wesentliche Herausforderung in der Modellbildung.

Mikrobielle Biomasse im Untergrund

Mikroben (z. B. Bakterien) können als in einer Flüssigkeit schwebende Zellen vorkommen, d. h. planktonisch. Allerdings sind die meisten Zellen im Untergrund sessil, d. h. fest an einer Oberfläche sitzend. Diese Form ist die für das Wachstum bevorzugte und auch erfolgreichere. Eine Gruppe festsitzender Zellen, die von extrazellulären Polymeren biologischen Ursprungs (EPS) zusammengehalten werden, wird als Biofilm bezeichnet. Ein Biofilm entsteht an einer Oberfläche wie in den folgenden Schritten schematisiert:

- Gelöste organische Moleküle haften an einer festen Oberfläche und bilden einen Konditionierungsfilm.
- Freischwebende Zellen, die an diese vorkonditionierte Oberfläche gelangen, können an der Oberfläche adsorbieren.
- Adsorbierte Zellen produzieren EPS und festigen so ihre Bindung zu der Oberfläche und zueinander.
- In einer nährstoffreichen Umgebung vermehren sich diese festsitzende Zellen und ein Biofilm ensteht.
- Biofilmzellen können abgelöst, mit der Strömung transportiert und stromabwärts wieder an der Oberfläche angeheftet werden.

Biofilme weisen sehr heterogene Strukturen auf. Zellen innerhalb eines Biofilms neigen dazu, sich an bestimmten Stellen zu konzentrieren, während andere Bereiche des Biofilms frei bleiben. Daher werden Biofilme in gewisser Weise auch selbst als poröse Medien betrachtet, die durch Eigenschaften wie Porositäten und Dichten charakterisierbar sind.

Biofilme, die in einem porösen Medium wachsen, blockieren Poren und verändern dabei die Eigenschaften des porösen Mediums. Diese veränderten Eigenschaften werden bei der biologischen Filtration (z. B. bei der Abwasserbehandlung), bei der biologischen Altlastensanierung (z. B. für die Erstellung hydraulischer Barrieren) und bei anderen Fragestellungen auf diesem Gebiet genutzt. Eine hydraulische Barriere biologischen Ursprungs könnte z. B. auch in einer geologischen CO_2-Lagerstätte eingesetzt werden, um das Entweichen von CO_2 zu verhindern.

CO_2-Speicherung in geologischen Formationen

CO_2 ist das derzeit für am Wichtigsten erachtete anthropogene Treibhausgas. Die globale Erderwärmung wird demnach sehr stark durch die in den letzten Jahrzehnten stattfindende Anreicherung von anthropogenen Treibhausgasen in der Atmosphäre mitverursacht. Die Freisetzung von CO_2 kann mit Hilfe effizienterer Technologien und alternativer Energiequellen reduziert werden. CO_2-Emissionen können aber auch reduziert werden, indem man CO_2 aus Kraftwerksabgasen abscheidet und in tiefen geologischen Formationen speichert. Bei den physikalischen Bedingungen, die in diesen unterirdischen Lagerstätten herrschen, liegt CO_2 im überkritischen Zustand vor, gekennzeichnet durch eine hohe Dichte und geringe Viskosität. Diese Lagerstätten enthalten oft salzhaltiges Wasser, das dichter ist als CO_2. Eine möglichst undurchlässige geologische Deckschicht verhindert das Aufsteigen des leichteren CO_2 an die Erdoberfläche. Jedoch müssen, z. B. im Rahmen von Risikostudien, mögliche Störungen oder Risse in dieser Deckschicht betrachtet werden, die zu einem Entweichen des CO_2 führen könnten. Die Deckschicht in der Nähe eines CO_2-Injektionsbrunnens ist besonders gefährdet. Der hohe Druckanstieg während der ersten Injektionsphase, Zementkorrosion am Brunnen aufgrund des CO_2-reichen Formationswassers und eventuelle Beschädigungen der Deckschicht während der Erstellung des Bohrlochs sind als mögliche Ursachen für gestörte Deckschichten zu nennen. Biobarrieren könnten verwendet werden, um solche Risiken zu minimieren, z. B. indem sie Risse in der Deckschicht abdichten oder den Bohrlochzement vor Korrosion schützen. Eine Biobarriere kann aus einem Biofilm selbst bestehen, aber auch aus vom Biofilm begüngstigten mineralischen Ablagerungen.

Modellkonzept

Bei der Modellierung von Strömungs- und Transportvorgängen in porösen Medien unterscheidet man mindestens zwei charakteristische Skalen. Auf der Mikroskala werden die Geometrie des porösen Mediums und die Strömung der einzelnen Fluide beschrieben. Zur Makroskala gelangt man durch eine Mittelung der Mikroskala. Mikroskalische Information, wie die Geometrie des porösen Mediums, wird auf der Makroskala mit effektiven Pa-

rametern, z. B. Porosität und Permeabilität, abgebildet. Das Modell, das in dieser Arbeit beschrieben wird, ist auf der Makroskala definiert.

Das Formationswasser und das injizierte CO_2 bilden separate Phasen. Die Strömung dieser beiden Phasen im porösen Medium wird mit der erweiterten Darcy-Gleichung beschrieben. Die Wechselwirkungen zwischen den Fluiden werden durch konstitutive Beziehungen berücksichtigt.

Wie bereits erwähnt, haben auch Biofilme selbst oft eine poröse Struktur. Beide Fluide, Wasser und CO_2, könnten innerhalb der Biofilmporen vorliegen. Allerdings fließen die Fluide innerhalb eines Biofilms offensichtlich deutlich langsamer als außerhalb. Im Modell werden deshalb zwei Kontinua definiert, um diese Prozesse unterschiedlicher Geschwindigkeit zu beschreiben. Ein Kontinuum beschreibt die Strömungsprozesse in den Poren des Biofilms, während das zweite Kontinuum die Strömungsprozesse in den Poren des porösen Mediums beschreibt. Es müssen auch Austauschterme definiert werden, die die Wechselwirkung der beiden Kontinua beschreiben. Dementsprechend werden Bilanzgleichungen für jedes Kontinuum aufgestellt und mit den Austauschtermen gekoppelt. Mit Vereinfachungen kann man die Komplexität des Systems reduzieren. Manche dieser Vereinfachungen sind allerdings einschränkend und müssen in weiteren Arbeiten näher untersucht werden. Die wichtigsten Annahmen, die im Modell gemacht werden, sind nachfolgend aufgelistet.

- Der Austausch gelöster Stoffe zwischen den beiden Kontinua ist diffusiv, d. h. aufgrund von Konzentrationsgradienten zwischen den beiden Kontinua.
- Die Verteilung der beiden Fluide innerhalb der Kontinua wird ausschließlich von Kapillarkräften bestimmt.
- Empirische Funktionen beschreiben den Austausch von Biomasse zwischen den Kontinua, d. h. das Anhaften freischwebender und das Ablösen festsitzender Biomasse.
- Das Modell berücksichtigt nur einen Nährstoff, dessen Verfügbarkeit das Biomassenwachstum bestimmt. Dies setzt voraus, dass alle anderen Voraussetzungen für Wachstum gegeben sind.

Das Verstopfen des Porenraums durch den Biofilm ist offensichtlich ein wichtiger Teil eines jeden Modells, das sich mit Biobarrieren im Untergrund befasst. In dem hier beschriebenen Modell wird jedem der oben beschriebenen Kontinua eine Permeabilität zugewiesen. Biofilmwachstum verursacht Änderungen in der Permeabilität jedes Kontinuums. Diese Änderungen werden mit konstitutiven Beziehungen berücksichtigt. Die totale Permeabilität des mit Biofilmen gefüllten porösen Mediums ist die Summe der Permeabilitäten der Kontinua. Typische Permeabilitäts-Porositäts-Beziehungen aus Experimenten (z. B. Cunningham *et al.*, 1991) können so beschrieben werden.

Fluideigenschaften sind essentiell bei der Beschreibung von Strömungprozessen. Das Wasser in tiefen geologischen Formationen ist meistens sehr salzhaltig, was bei der Berechnung der Dichte und der Viskosität des Wassers berücksichtigt werden muss. Die Eigenschaften des CO_2 können stark mit Druck und Temperatur variieren – der kritische Punkt

von CO_2 liegt bei 73,8 bar und $31\,^{\circ}\mathrm{C}$. Für die Berechnung der CO_2-Dichte werden die Zustandsgleichungen von Span and Wagner (1996) verwendet. Überkritisches CO_2 ist ein sehr gutes Lösungsmittel und verursacht daher bei Bakterien ein Austreten des intrazellulären Materials. Dementsprechend ist überkritisches CO_2 ein effizientes Biozid. Diese Tatsache wird im Modell berücksichtigt, indem der Verfall des Biofilms von den Fluidsättigungen im Biofilm abhängt.

Die partiellen Differentialgleichungen, die aus den Massenbilanzgleichungen enstehen, werden mit einer knotenzentrierten Finite-Volumen-Methode – der sogenannten Box-Methode – räumlich diskretisiert. Jedem Knoten wird ein Kontrollvolumen (eine Box) zugewiesen. Ansatzfunktionen erster Ordnung werden für die Approximation der Unbekannten und der Geometrie verwendet. Die Wichtungsfunktion eines jeden Knotens wird innerhalb des Kontrollvolumens, das dem Knoten zugeordnet ist, gleich eins gesetzt und außerhalb gleich null. Für die zeitliche Diskretisierung wird das implizite Euler-Verfahren verwendet. Das numerische Modell ist im Rahmen des Mehrphasenströmungssimulators MUFTE-UG implementiert. Einen Überblick über die Anwendungsgebiete des Programms MUFTE-UG findet man in Assteerawatt *et al.* (2005).

Modellverifizierung

Jedes numerische Modell, das zur Voraussage verwendet werden soll, sollte verifiziert werden, z. B. durch einen Vergleich von Modellergebnissen mit experimentellen Daten. Zwei Experimente aus der Literatur wurden ausgesucht, um das Modell zu testen. Jedes Experiment besteht aus zwei Durchläufen.

In den Experimenten von Taylor and Jaffé (1990a) wird vornehmlich die Wechselwirkung zwischen Biofilmwachstum und Strömungsprozessen untersucht. Der Austausch von Biomasse zwischen den Kontinua steht im Vordergrund. Biofilme wurden in Sandsäulen erzeugt, dabei wurden die Fließgeschwindigkeiten des Wassers in den Säulen konstant gehalten. Drei Modellparameter wurden an die Daten aus einem der zwei Durchläufe des Experiments angepasst. Die gleichen Parameter wurden dann für die Simulation des anderen Durchlaufs verwendet. Die Ergebnisse der numerischen Simulationen sind zufriedenstellend.

Mitchell *et al.* (2009) führten Experimente durch, bei denen überkritisches CO_2 in Sandstein-Bohrkerne injiziert wurde. Dabei wurde der Druck und die Temperatur so reguliert, dass das CO_2 immer im überkritischen Zustand war. Zwei Bohrkerne wurden mit biofilmbildenden Bakterien geimpft. Die Permeabilitäten der Bohrkerne wurden regelmäßig gemessen. Das Biofilmwachstum führte in beiden Fällen zu einer Permeabilitätsabnahme von ungefähr 95 %. Anschließend wurde überkritisches CO_2 in die Bohrkerne injiziert. Dabei erhöhten sich die Permeabilitäten wieder etwas. Für die Simulation dieser Experimente müssen aufgrund fehlender Information zu dem genauen Ablauf der Experimente einige Annahmen getroffen werden. Dadurch wurde eine erheblich vereinfachte Version des Modells für die Simulation verwendet. Ein strenger quantitativer Vergleich der Simulationen mit den Experimenten ist daher leider nicht möglich. Trotzdem kann das Modell die beobachteten

Permeabilitätsveränderungen in einem der beiden Durchläufe gut nachbilden. Hierzu wurden drei Simulationsparameter an die experimentellen Daten angepasst. Eine Simulation des zweiten Durchlaufs mit den gleichen Simulationsparametern liefert eine gute Übereinstimmung mit den experimentellen Ergebnissen.

Diese Vergleiche können dazu beitragen, ein besseres Verständnis der wichtigen Prozesse und Parameter bei den gegeben Bedingungen zu erreichen. Sie sind natürlich auch eine hervorragende Methode, um Fehler und falsche Annahmen im Modell zu finden.

Modellapplikation

Wie bereits erwähnt, ist die Simulation von Biofilmen in unterirdischen CO_2-Lagerstätten das Ziel der Modellentwicklung. Das beschriebene Modell berücksichtigt unter anderem folgende Prozesse:

- Biomassewachstum,
- Biomasseverfall,
- Anhaftung planktonischer Zellen an die Oberfläche des Formationsgesteins,
- Ablösung sessiler Zellen,
- Biomassetransport im Formationswasser,
- die Auswirkung der Biofilmbildung auf die hydraulischen Eigenschaften der Formation
- und die Auswirkung des überkritischen CO_2 auf die mikrobiellen Zellen.

Dieses Modell wird für einen hypothetischen Testfall angewendet, bei dem die Deckschicht in der Nähe eines Bohrlochs einer CO_2-Lagerstätte beschädigt ist. Das injizierte CO_2 würde in einem solchen Fall durch das beschädigte Gestein entweichen. Bakterielle Zellen und Nährstoffe werden unterhalb der Deckschicht injiziert bis sich ein Biofilm im beschädigten Bereich gebildet hat. Anschließend wird CO_2 in die Formation injiziert. Die Simulationen zeigen, dass die Biobarriere das Entweichen des injizierten CO_2 verhindert – allerdings nur für eine gewisse Zeit. In einer weiteren Simulation wurde ein System untersucht, bei dem die Nährstoffe in gewissen zeitlichen Abständen injiziert werden, um die Biobarriere aufrecht zu erhalten. Cunningham *et al.* (2009) beschreibt eine Methode, bei der bestimmte Biofilme benutzt werden, die als Katalysatoren für die Ausfällung von Mineralien dienen können. Die so gebildete Biobarriere wäre beständiger. Allerdings kann das Modell in seinem jetzigen Zustand solche Prozesse nicht abbilden. In einer letzten Simulation konnte gezeigt werden, dass die Biobarriere auch in einer Formation gebildet werden kann, in der CO_2 bereits vorhanden ist. In allen drei Simulationen hemmte das überkritische CO_2 die Entwicklung des Biofilms. Obwohl bakterielle Zellen innerhalb eines Biofilms vor den schädlichen Effekten des CO_2 geschützt werden, kann sich ein Biofilm nur ausbreiten, indem sich Zellen davon lösen, in den freischwebenden Zustand übergehen, mit dem Strom transportiert werden und stromabwärts wieder an einer Oberfläche haften. Dieser Kreislauf wird von dem Biozid unterbrochen und macht ein Ausbreiten des Biofilms sehr schwierig.

Weitere Modellapplikationen

Das Modell kann – mit einigen Erweiterungen – auch für andere Applikationen, bei denen mikrobielle Aktivität und Zweiphasenströmung in porösen Medien miteinander interagieren, angewendet werden. Zwei Beispiele solcher Applikationen sind die biologische Altlastensanierung und die mikrobiell verbesserte Ölgewinnung.

- In der biologischen Altlastensanierung werden toxische Substanzen von Mikroorganismen abgebaut. Diese Mikroorganismen könnten natürlich in einem Grundwasserleiter vorkommen oder hinzugefügt worden sein. Biobarrieren werden in der biologischen Altlastensanierung auch für die Eindämmung von Schadstoffwolken verwendet. Am Beispiel einer Simulation konnte in-situ biologischer Schadstoffabbau im Untergrund gezeigt werden
- Die Produktion von Erdöl kann mit Hilfe mikrobieller Aktivität verbessert werden. Bakterien, die an der Grenzfläche zwischen Öl und Wasser haften, können Tenside produzieren, die die Oberflächenspannung zwischen den Fluiden herabsetzen, und damit die Mobilität des Öls erhöhen. Außerdem können Biofilme genutzt werden, um die Permeabilitätsverteilung einer Ölformation zu homogenisieren. Damit soll erreicht werden, dass beim Fluten einer solchen Formation mit Wasser die Verdrängung des Erdöls gleichmäßig verläuft.

Die wichtigsten Modellerweiterungen, die nötig wären, um die oben genannten Prozesse angemessen zu beschreiben, sind eine Berücksichtigung mikrobieller Aktivität an der Grenzfläche zwischen den Fluiden und das Lösen der Fluide ineinander.

Ausblick

Diese Arbeit beschreibt die Bildung und Verifizierung eines numerischen Modells und dessen Anwendung in einem Testfall. Das Modell ist in der Lage, Biofilmentwicklung im Untergrund zu beschreiben. Allerdings ist es noch verbesserungsfähig. Weitere Arbeiten zu diesem Thema sollten folgende Punkte beinhalten:

- Manche Vereinfachungen, die während der Entwicklung des Modells gemacht wurden, sind einschränkend und sollten näher untersucht werden. Ein gutes Beispiel hierfür ist die Annahme, dass der gleiche Druck in beiden Kontinua herrscht. Somit kann der advektiver Austausch gelöster Stoffe zwischen den Kontinua nicht berücksichtigt werden. Stattdessen könnte nach beiden Drücken unabhängig voneinander gelöst werden und nur mit Austauschtermen verlinkt werden. Der Austausch gelöster Stoffe wäre dann getrieben von einer Überlagerung von Druck- und Konzentrationsgradienten.
- Das Modell nimmt an, dass das Wachstum der Bakterien ausschließlich von der Verfügbarkeit eines Nährstoffs abhängt, d. h. alle anderen Bedingungen für Wachstum sind gegeben. Dies schränkt das Modell stark ein. Um einen Biofilm in einer

gewissen Entfernung vom Injektionsbrunnen zu erzeugen, könnte man den Elektronendonator und den Elektronenakzeptor zeitlich versetzt injizieren. Solche Szenarien können bislang nicht vom Modell beschrieben werden. Daher sollten der Transport und die Verfügbarkeit eines Elektronakzeptors vom Modell berücksichtigt werden.

- Es werden viele empirische Parameter für die Simulationen benötigt. Sensitivitätsstudien könnten darüber Aufschluss geben, auf welche Parameter das System am empfindlichsten reagiert. Diese Parameter müssten dann durch Experimente genauer bestimmt werden. Experimente sind allgemein für das bessere Verständis der relevanten Mechanismen erforderlich.

- Alle Gleichungen, Korrelationen und Parameter, die vom Modell verwendet werden, sind auf der Makroskala definiert. Es ist jedoch meistens einfacher, die Prozesse auf der Mikroskala zu verstehen und zu beschreiben. Dementsprechend sollten Prozesse, die auf der Mikroskala gut zu beschreiben sind, auf der Makroskala angemessen dargestellt werden, was oft nicht einfach ist. Daher ist die Entwicklung von Skalierungsmethoden auf diesem Gebiet (z. B. Golfier *et al.*, 2009) absolut erforderlich.

- Die Erhaltungsgleichungen der verschiedenen Komponenten (Wasser, CO_2, Biomasse und Substrat) werden gekoppelt gelöst. Weiterführende Arbeiten könnten sich mit der möglichen Entkopplung der Prozesse, die auf unterschiedlichen Zeitskalen ablaufen, beschäftigen. Dies mit der Absicht, ein effizienteres numerisches Modell zu erhalten. Die Strömung der Fluide könnte beispielsweise zumindest zum Teil von den biologischen Prozessen entkoppelt betrachtet werden.

- Eine Biobarriere aus Biofilmen verliert in Abwesenheit ausreichender Nahrung an Effizienz. Eine dauerhaftere Lösung könnte eine Biobarriere darstellen, die aus Biofilmen besteht, die aktiv Mineralien ausfällen und so für eine nachhaltige Barrierewirkung sorgen. Um solche Prozesse zu beschreiben, ist eine Erweiterung des Modells dahingehend nötig, dass der Transport der chemischen Spezies, die für solche Ausfällungen nötig sind, beschrieben wird.

1 Introduction

The effects of global warming on the environment – including sea level rise, extreme weather conditions, etc. – are diverse and often beyond human control. Anthropogenic emissions of greenhouse gases, particularly carbon dioxide (CO_2), are primarily responsible for the temperature increase. The use of more efficient technology and regenerative energy sources are ways of reducing emissions. Additionally, CO_2 could be captured from flue gases of power plants and stored in geological formations. Suitable storage formations should have the capacity to accommodate large amounts of CO_2 and guarantee a high storage security. Substantial leakage of CO_2 from a reservoir would render any storage operation useless and could even compromise groundwater resources and human life. Hence, the proper assessment of the risk of CO_2 leakage from a potential storage reservoir is a key issue that needs to be addressed (see Oldenburg, 2008; Kopp *et al.*, 2009). Minimising the risk of leakage could include sealing potential leakage pathways. Cunningham *et al.* (2009) propose the use of microbial biofilms to plug such pathways. Experiments show that biofilms can significantly increase the resistance of a porous medium (e.g., sand, rock) to flow (Taylor and Jaffé, 1990a; Vandevivere and Baveye, 1992; Mitchell *et al.*, 2009). Setting up such a hydraulic barrier in the subsurface requires proper judgment of relevant flow, transport, and microbial processes. Numerical models are indispensable for the study of these processes and their interactions with each other. This work deals with the development and application of a numerical model capable of describing the above-mentioned processes. In the following, introductions to the topics of microbial biofilms and CO_2 storage in geological formations are given.

1.1 Microbial Biofilms in Porous Media

1.1.1 Bacteria and Biofilms

Bacteria are single-celled microorganisms and belong to the group of living organisms called prokaryotes. In contrast to the eukaryotes, which include fungi, algae, and plant and animal cells, they have a very simple cell structure and lack a nucleus. Bacterial cell diameters are typically between 0.2 μm and 3.0 μm (Tchobanoglous *et al.*, 2003) with exceptions. There is a great diversity in bacterial cell shape – spherical, rod-shaped, spiral, oval, etc.

Bacteria and other microorganisms can exist as suspended or floating cells in a bulk fluid, in which case, they are referred to as planktonic. However, in natural environments, microbial cells tend to be sessile, i.e., attached to a solid surface. The surfaces onto which these cells are attached may be immobile or may be suspended in a fluid. Cullimore (2000) refers to cells

attached to immobile surfaces as *sessile attached* and those attached to suspended surfaces as *sessile suspended*. Sessile suspended microbes form flocs called river/marine snow in surface water (De Beer and Stoodley, 2006) or well snow in borehole water columns (Cullimore, 2000).

Attached cells are often embedded in a matrix of extrapolymeric substances (EPS) which protects the bacterial cells from environmentally harsh conditions. This assembly of EPS and microbial cells attached to a solid surface (substratum) is referred to as a biofilm. Bryers (2000) defines a biofilm as

a surface accumulation, which is not necessarily uniform in time or space, that comprises cells immobilised at a substratum and frequently embedded in an organic polymer matrix of microbial origin.

1.1.2 Porous Media

The term *porous medium* (see Corey, 1994) as used in this text refers to a material consisting of a solid (matrix) and interconnected non-solid space (pores). Corey (1994) gives important restrictions to this definition including that the pores must be large enough to contain fluids and fluid flow, but small enough to ensure that the orientation of the interfaces between two fluids in the pores is controlled by interfacial forces. Typical examples of porous media include soils, groundwater aquifers, petroleum reservoirs, living tissue, textiles, wood, etc.

Properties with which porous media are often characterised include porosity, pore size distribution, specific surface area, etc. Porous media have a very high specific surface area which is the ratio of interfacial area (between the solid matrix and the pore space) to volume. This property of porous media indicates that, in such systems, most microbial processes occur on the solid surfaces. Biofilms in porous media play a significant role in bioremediation of groundwater aquifers, leaching of metals from ores, enhanced oil recovery, and biological wastewater treatment (Bouwer *et al.*, 2000; Rittmann, 1993; De Beer and Stoodley, 2006).

1.1.3 Biofilm Formation

The growth of a biofilm on a solid surface is preceded by the adsorption of dissolved organic molecules to the surface. These molecules form a film on the surface, called conditioning film, which affects the colonisation of the surface by microorganisms by changing the physicochemical properties of the surface and serving as a concentrated nutrient source for microbes (Lewandowski and Cunningham, 1998). Microbial cells floating in a fluid may be transported to a conditioned surface by diffusive forces, convective forces, and/or active movement. Some of the cells in contact with the substratum adsorb to it. The adsorption can be reversible or irreversible. Adsorbed cells produce EPS, "slimy adhesive substances" (Lewandowski and Cunningham, 1998), which ensure the attachment of the cells to the substratum and to one another. In porous media, microbial cells also get attached if pore openings are not large enough to allow the passage of the cells (straining). Provided the conditions are conducive, the bacterial cells reproduce and form colonies. A conducive environment is one with the appropriate pH, temperature, salinity, as well as the energy and

carbon sources, and the electron acceptor needed by the bacteria for metabolism. Detachment of microbes from the biofilm can occur due to erosion and sloughing. Erosion occurs due to shear stress exerted by the bulk fluid on the biofilm-fluid interface and is a process in which single cells are continuously detached from the biofilm. Sloughing, however, is an irregular process in which large pieces are removed from the biofilm. De Beer and Stoodley (2006) summarise biofilm formation in three main processes:

the attachment of cells to a surface (colonisation), growth of the attached cells into a mature biofilm, and the detachment of single cells (erosion) or large pieces (sloughing).

1.1.4 Structure of Biofilms

Biofilms are characteristically very heterogeneous. The concentration of solutes, the distribution of cells, cell clusters, and EPS within the biofilm can vary strongly. Hence, the structure of a biofilm is also thought to be highly heterogeneous. De Beer and Stoodley (2006) describe biofilms as complex porous structures with cell clusters and open spaces which can act as channels for convective fluid flow as shown in Figure 1.

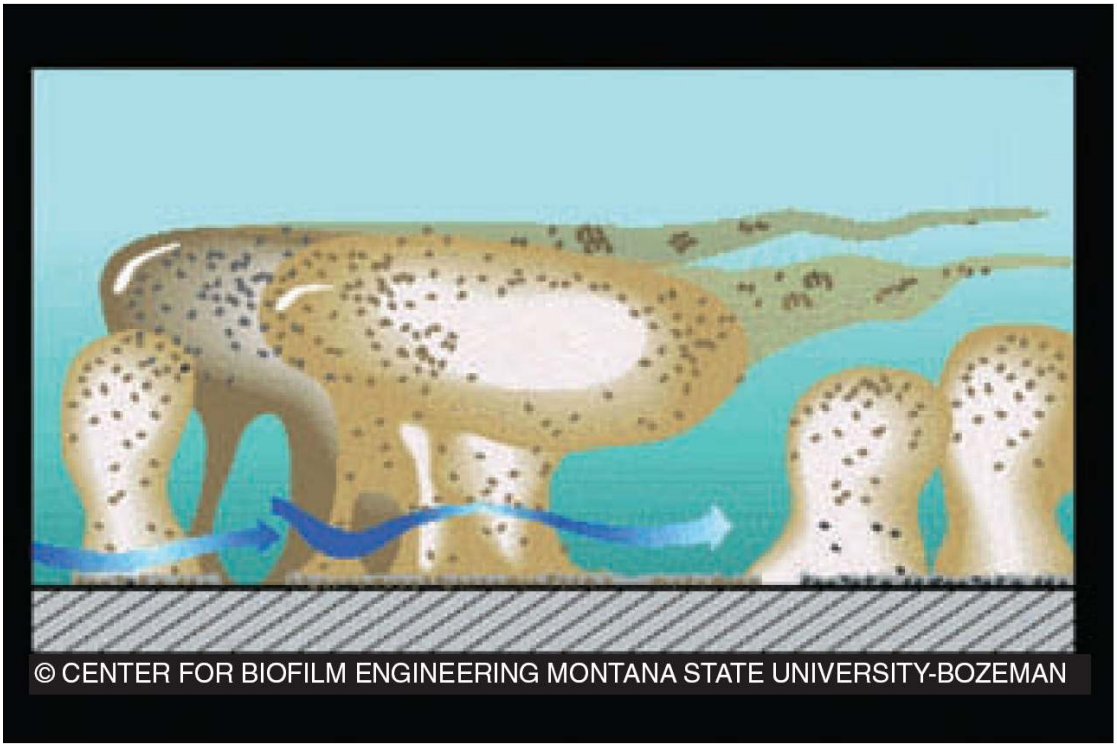

Figure 1: Biofilm structure as depicted by De Beer and Stoodley (2006). Reprinted with permission from the Center for Biofilm Engineering, Montana State University.

van Loosdrecht *et al.* (1995) state that the structure of a biofilm is strongly dependent on such factors as shear stress and the substrate mass transfer rate between the bulk fluid and

the biofilm (see Figure 2). Wimpenny and Colasanti (1997) describe different concepts of biofilm structure including that of dense biofilms with no pores or channels, citing dental plaque as an example. In general, the structure of a biofilm can vary a lot depending on

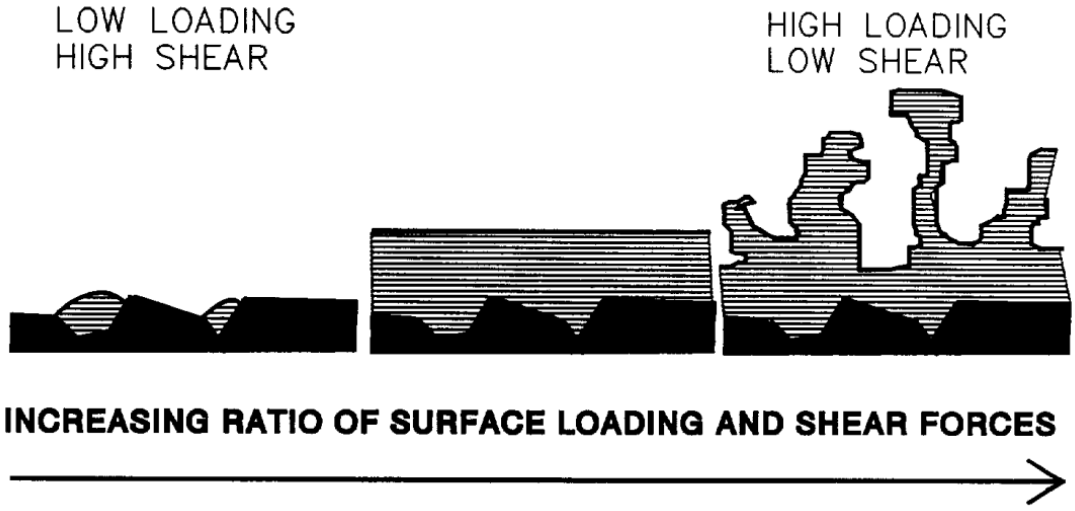

Figure 2: Variations in biofilm structure as a result of changing flow conditions and substrate mass transfer rate. Figure from van Loosdrecht *et al.* (1995) (reprinted with permission from the copyright holders, IWA).

a number of factors including hydrodynamic conditions, nutrient availability, growth rate, species, quorum sensing (cell-to-cell communication), etc. The influence of some of these factors are discussed in van Loosdrecht *et al.* (2002). A slow mass transfer of substrate into the biofilm leads to a porous biofilm structure while a slow substrate utilisation rate by the bacterial cells in the biofilm leads to a compact biofilm structure (van Loosdrecht *et al.*, 2002). Obviously, shear stress also has a strong influence on biofilm structure. Strong shear forces result in high detachment rates which tend to reduce the level of heterogeneity of the biofilm.

Biofilm Porosity

A parameter often used to characterise biofilm structure and heterogeneity is biofilm porosity which is the volume ratio of the pore space within a biofilm to its total volume. It can be determined by evaluating microscope images of biofilms or by determining the areal porosities of biofilm slices (Lewandowski, 2000; Zhang and Bishop, 1994). Porosity can vary significantly with distance from the substratum. Zhang and Bishop (1994) and Lewandowski (2000) observed lower porosities at the substratum than at the surface of the biofilm.

Biofilm Density

This is a measure of the amount of biomass within a biofilm. Different ways of defining biofilm density are given in Zhang and Bishop (1994). They describe the terms *dry density* and *wet density* of biofilms. van Loosdrecht *et al.* (2002) define biofilm density "as the amount of biomass per volume of biofilm excluding the pore volume." In this work, biofilm density is defined as the amount of biomass per volume of biofilm *including* the pore volume.

1.1.5 Effect of Biofilm Accumulation on Properties of Porous Media

Biofilms in porous media grow on the surface of the solid matrix, occupying pore space and obstructing fluid flow through pore throats (see Figure 3). Hence, the accumulation

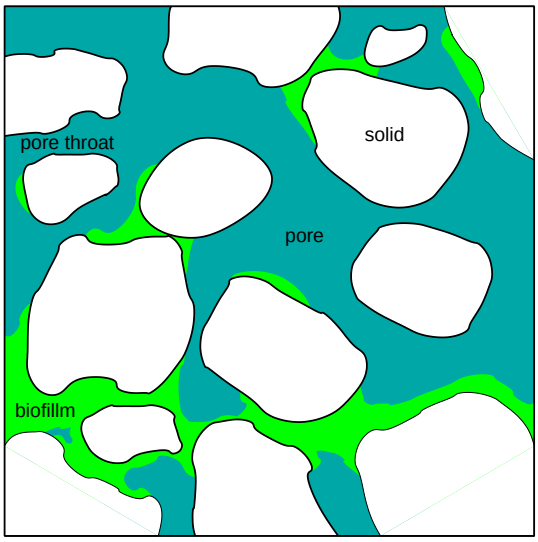

Figure 3: Biofilm growing in a porous medium.

of biomass in a porous medium can lead to changes in the hydraulic properties (porosity, permeability) of the medium. This and the ability of attached bacteria to degrade certain compounds give rise to a range of applications in which biofilm-affected porous media are used as biofilters and biobarriers. Biofilters are used in the treatment of drinking water and wastewater (Rittmann, 1993). In enhanced oil recovery, biobarriers are used to selectively plug high-permeability zones improving the overall recovery of oil (Zekri, 2001). Biofilms in aquifers are used for the treatment of contaminated groundwater (Cunningham *et al.*, 1991). As discussed in Section 1.3 and in Mitchell *et al.* (2009), biofilms could be used to help prevent leakage of carbon dioxide (CO_2) from a geological storage reservoir. An introduction to the topic of CO_2 storage in geological formations is given in Section 1.2.

1.2 CO_2 Storage in Geological Formations

The capture and storage of CO_2 from large stationary sources, such as power plants and industrial facilities, could be a substantial contribution to the goal of reducing anthropogenic greenhouse gas emissions. A very good overview of the technology including capture, transport, geological storage, ocean storage, risk analysis, and economic implications is given in a report by the Intergovernmental Panel on Climate Change, IPCC (2005). Geological storage sites include deep saline aquifers, depleted oil and gas reservoirs, and coal seams. The CO_2 is injected into geological formations at great depths (>800 m). Due to the

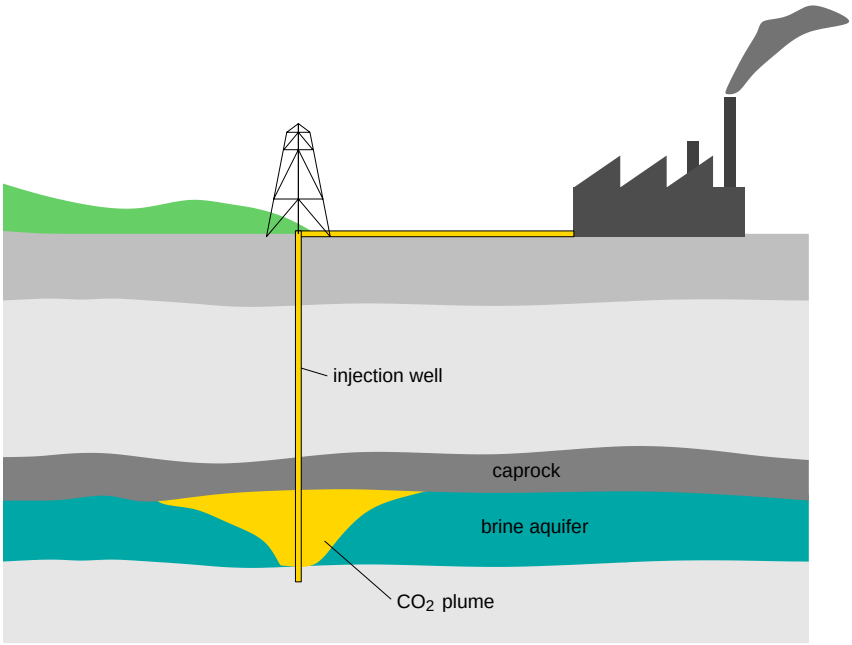

Figure 4: Concept of CO_2 storage in a brine aquifer.

high pressures and temperatures at such depths, the injected CO_2 would be either a liquid or a supercritical fluid. The injected CO_2, which is lighter and less viscous than the formation water (brine), would form a separate phase. The resulting CO_2 plume would, driven by the injection pressure, move radially into the formation. Due to buoyancy, it would also be driven upwards. An impermeable geological layer (caprock) is necessary to prevent the buoyant CO_2 plume from rising to the surface (see Figure 4). Fractures in the caprock or leaky wells can act as leakage pathways for the injected CO_2 (Pruess, 2005; Nordbotten *et al.*, 2005; Ebigbo *et al.*, 2007). Leakage of CO_2 from a storage site could cause pollution of shallow aquifers and the atmosphere, and would undermine the main aim of the sequestration project.

1.2.1 Trapping Mechanisms

Injected CO_2 is expected to remain stored in the geological formation for centuries. Different physical and chemical processes are involved in immobilising or trapping the CO_2 in the formation. The concept of *stratigraphic trapping* has been mentioned in Section 1.2. A caprock prevents mobile CO_2 from escaping from the storage formation. Some of the injected CO_2 is immobilised by capillary forces (*residual trapping*). CO_2 also dissolves in brine (*solubility trapping*). This increases the density of the brine causing it to sink to deeper layers. *Mineral trapping* occurs with the precipitation of CO_2-trapping minerals. As can be seen in Figure 5, the trapping mechanisms which guarantee a higher storage security gain significance with time.

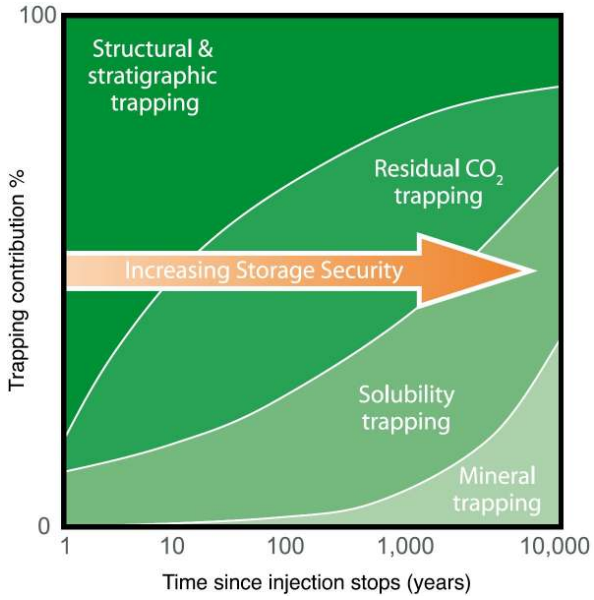

Figure 5: CO_2 trapping mechanisms and time scales. This is Figure 5.9 of the *Special Report on Carbon Capture and Storage* by the Intergovernmental Panel on Climate Change (IPCC, 2005).

1.2.2 Injection Well and Caprock Integrity

Wells used for the injection of CO_2 into geological formations need to be able to withstand the high pressure build-up during injection and corrosion by CO_2-rich brine. The pressure increase due to injection is highest in the vicinity of the injection well. Its magnitude is dependent on the viscosities of CO_2 and brine and on relative permeability effects. Due to low CO_2 saturations during the initial injection phase, the pressure build-up can be quite significant. This can cause fractures in the caprock. If the gas pressure exceeds the capillary entry pressure of the caprock, the CO_2 can penetrate the caprock. The injection rate can be regulated to prevent pressures that exceed some preestimated critical pressure. Injection

well integrity can be undermined by corrosive CO_2-water mixtures causing degradation of well cement.

1.3 Motivation and Goals

In Section 1.2, the topic of carbon capture and storage (CCS) was introduced. The risk of CO_2 leakage through fractures in the caprock, especially in the vicinity of the injection well, and the danger of well cement corrosion were discussed. The effect of biofilm accumulation on porous media properties (especially permeability) was introduced in Section 1.1.5. Mitchell *et al.* (2009) and Cunningham *et al.* (2009) have suggested the use of engineered biofilms and biomineralisation deposits to plug CO_2 leakage pathways. Figure 6 illustrates this concept. This would entail injecting microbial cells and nutrients at the caprock-aquifer interface before the injection of CO_2 into the formation with the intention of growing a biofilm which would plug potential leakage pathways. Cunningham *et al.* (2009) also propose the use of biofilms which are capable of actively precipitating calcium carbonate ($CaCO_3$) minerals, in which case, a medium containing calcium would be injected after the biofilm has developed. There are a number of open questions which arise.

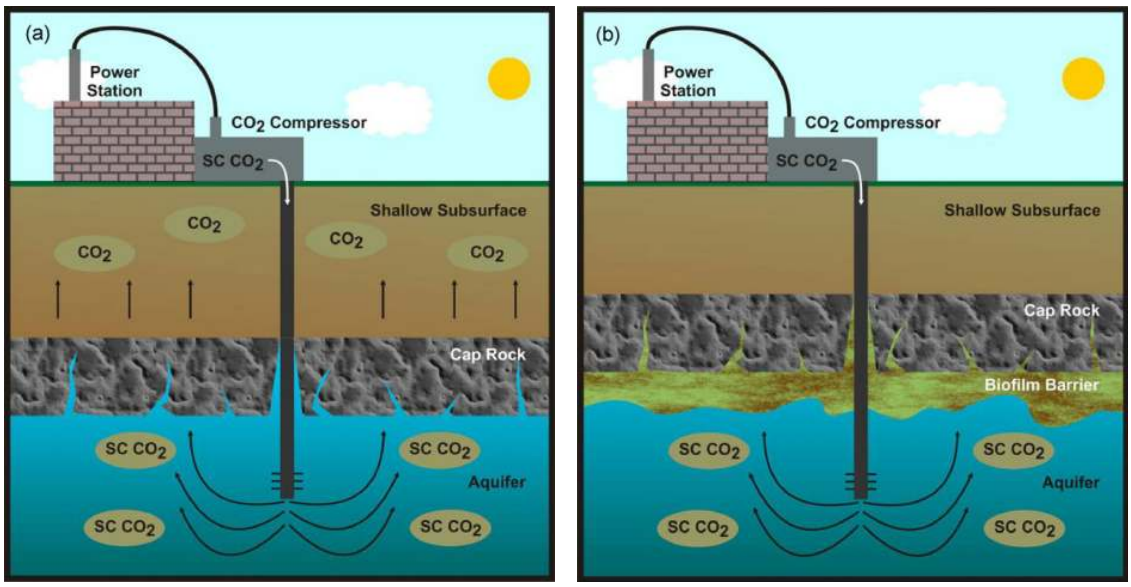

(a) Potential leakage pathways of CO_2 through caprock.

(b) Engineered biofilm and biomineral barrier plugging leakage pathways.

Figure 6: Concept of leakage mitigation in injection well vicinity. Figures from Mitchell *et al.* (2009) (reprinted with permission from the copyright holders, Elsevier).

- Can the microbial cells and nutrients be transported to and biofilm growth be stimulated in the right places?
- Can the biomineral deposits be formed in the right places?

- How long would it take to form a biofilm or biobarrier?
- What is the extent of the barrier?
- Which factors have the strongest influence on the questions mentioned above?
- What is the most efficient injection strategy?

The aim of this work is to develop a numerical model which could aid in assessing the feasibility of the use of biobarriers to increase CO_2 storage security. Numerical simulations should also make it easier to answer the questions posed above. However, due to the significance of biofilms in porous media, the model could also have a number of other applications such as in bioremediation, microbially enhanced oil recovery, or transport in natural soils.

1.3.1 Structure

A short overview of the structure of this thesis is given below.

- Chapter 2 deals with the development of a conceptual model and the implementation in a numerical context. Basic terms needed for the description of such a model concept are explained. A set of equations is derived using the mass conservation principle. Constitutive relations are determined with which the effects of the biofilm on the properties of the porous medium can be accounted for. And finally, the implementation in a numerical model is described.
- In Chapter 3, the model is tested by comparing simulation results to those of two experiments chosen from literature. The two experiments differ in that each one focuses on a different set of processes. The definition of initial and boundary conditions which properly describe the conditions in the experiments is a serious challenge.
- The experiments modelled in Chapter 3 are bench-scale problems. In Chapter 4, a fictitious field-scale test case is simulated with the aim of exploring the feasibility of the biobarrier technology described above.
- Finally, other fields in which the model could be applied are discussed in Chapter 5. Possible extensions of the model to properly describe these applications are stated.

2 Physical and Mathematical Model

This chapter focuses on the description of a conceptual model capable of representing the relevant processes involved in a system which consists of a natural porous medium, two fluid phases (water and CO_2), and a biofilm (see Figure 7). The grains of the porous medium,

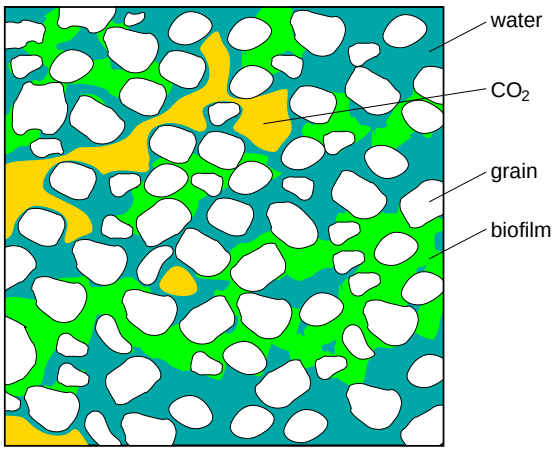

Figure 7: Two-phase fluid system with biofilm and solid phase.

which make up the solid phase, are impermeable. The biofilm is attached to the solid phase and occupies part of the porous medium's void space. The rest of this space is occupied by the fluids. Both fluids can also be present within the pores of the biofilm as is shown in Figure 8. This is in accordance with the discussion in Section 1.1.4 on the porous structure of biofilms.

2.1 Scale

Physical processes and properties are typically defined on different spatial scales, i.e., on different levels of resolution. On the *molecular scale*, for example, one would describe the properties and motion of individual molecules and their interaction with other molecules. One could also describe the behaviour of a group of molecules. If the amount of molecules in this group is sufficiently large, then specific properties which do not exist on the molecular scale such as density and viscosity can be assigned to such a group. This averaging of the properties of individual molecules and molecular interactions gives rise to the continuum concept which assumes that matter is continuous and neglects molecular-scale heterogeneities.

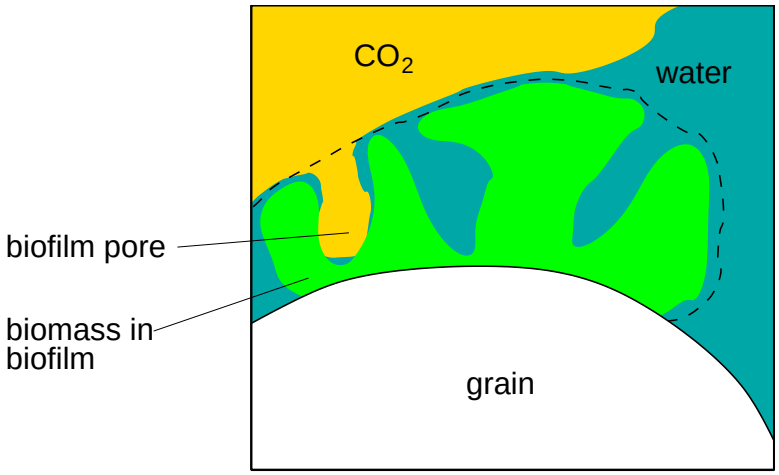

Figure 8: Conceptual model of microscale fluid distribution within the void spaces of the porous medium and the biofilm. Both fluids (water and CO_2) can be present within and outside the biofilm.

Biofilm as a Continuum The concept of a continuum as described above can also be applied to a biofilm. This gives rise to the biofilm continuum in which there is no differentiation between the individual microbial cells, the pores within the biofilm, and the extracellular material. With this, the properties discussed in Section 1.1.4, i.e., density and porosity can be assigned to the biofilm.

In this text, two distinct scales will be considered as is done in Helmig (1997).

- The *microscale* is the scale one derives from the consideration of a continuum and averaging over the molecular scale. At this scale, there is a clear description of the fluids, solids, and their interfaces.
- The *macroscale* represents an averaging of microscale properties. The volume over which this averaging is done (*representative elementary volume*, REV) needs to be large enough to ensure that the average properties are independent of the size of the REV (see Figure 9). It should also be much smaller than the size of the entire domain (Bear, 1988). This gives rise to a macroscopic continuum with effective properties and also to new basic equations like the Darcy equation. Note that the model developed and used in this work is defined on the macroscale.

As can be seen in Figure 10, the interfaces and discontinuities which exist between the fluid, the biofilm, and the solid on the microscale are averaged out on the macroscale. This loss of microscale information is often compensated by introducing constitutive relationships. As shown in Figure 8, both fluids can be present in the pores of the biofilm. Flow processes within and outside the biofilm may differ significantly. Neither the presence of fluids nor

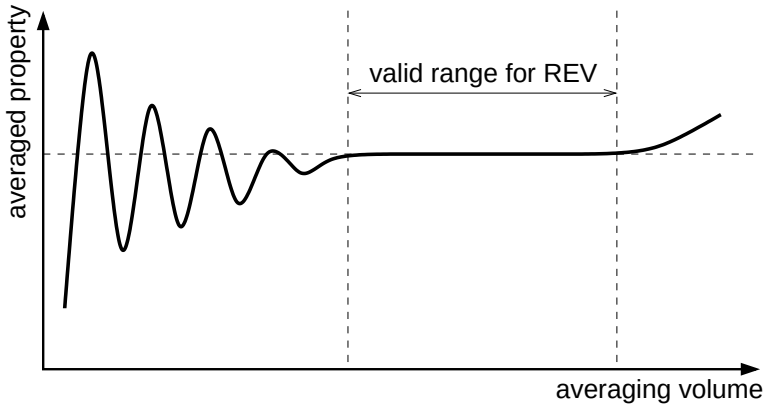

Figure 9: Definition of a representative elementary volume (REV) (adapted from Bear, 1988). The concept of an REV is only valid if the value of the average property does not depend on the size of the REV. As shown above, the averaging volume has to be large enough to ensure this. At some point, however, the value of the averaged quantity changes with REV size due to large-scale heterogeneities such as lenses.

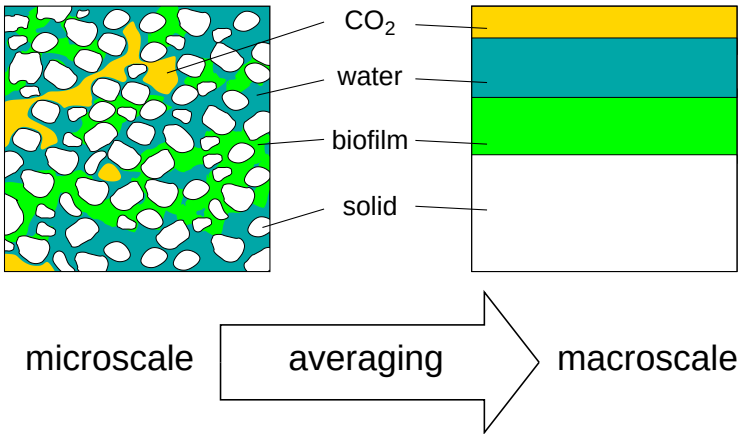

Figure 10: Micro- and macroscale view of a porous medium occupied by a biofilm and two fluids. Microscale information such as the geometry of the solid matrix, the distribution of the biofilm, and the fluids within the pore space is all but lost on the macroscale.

their flow within the biofilm phase is accounted for in the macroscale consideration in Figure 10. One solution to this problem is the introduction of a second REV or continuum which accounts for the flow of the fluids through the biofilm. This is discussed in Section 2.2.

2.2 Dual-Continuum Concept

The concept of modelling separate but coupled components of a porous medium has been applied numerous times in the modelling of fluid flow in fractured porous media (see Dietrich *et al.*, 2005; Wu *et al.*, 2004; Pruess *et al.*, 1999; Barenblatt and Zheltov, 1960). One assumes that each component is distributed continuously within an REV. Typically, a network of fractures is defined as one continuum and the porous matrix as another. Effective parameters are assigned to each continuum, and flow processes are described in each continuum by a set of conservation equations. These are coupled by mass exchange terms. These concepts are called *dual-* or *multi-continuum* concepts.

Flow through a porous medium containing a biofilm can be divided into two components – fast flow through the open pores of the porous medium and slow flow through the biofilm. This can be seen in analogy to the dual-continuum concepts of fractured porous media. Two continua can be defined as shown in Figure 11. Continuum P accounts for flow through the open pores and Continuum F for flow through the biofilm. Mass balance equations can be set up for each continuum and the variables of both continua linked by mass transfer terms.

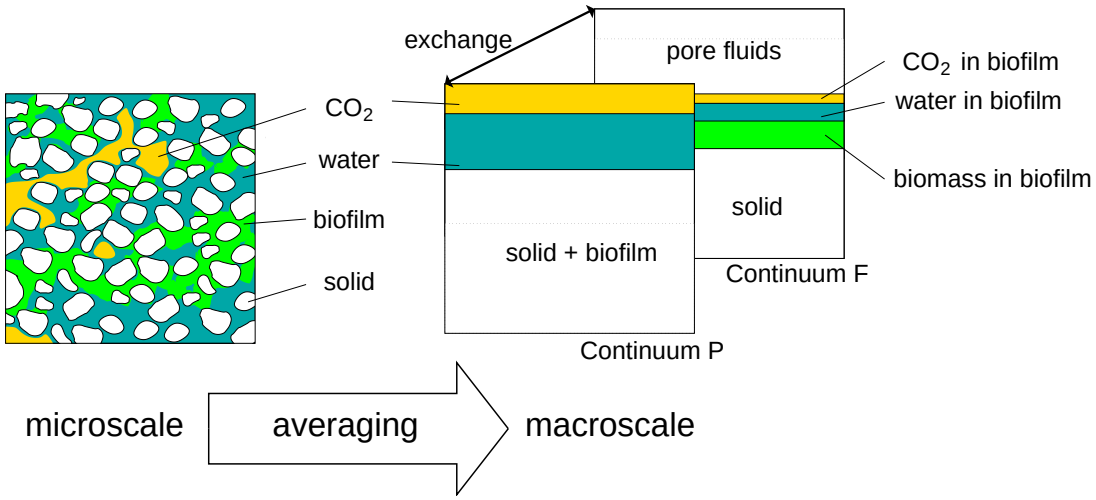

Figure 11: Schematic diagram of dual-continuum concept applied to biofilm-affected porous media. Continuum P accounts for flow through the pores of the porous medium and Continuum F for flow through the biofilm.

In each continuum, different volume fractions are important. Clear definitions of these volume fractions are given in the following.

- ϕ_0 is the original porosity of the porous medium.

$$\phi_0 = \frac{\text{pore volume of unaffected porous medium within REV } V_0}{\text{bulk volume of REV } V_B} \tag{1}$$

- ϕ_p is the porosity of Continuum P.

$$\phi_p = \frac{\text{pore volume of porous medium excluding biofilm pores } V_p}{\text{bulk volume of REV } V_B} \tag{2}$$

- ϕ_f is the porosity of Continuum F.

$$\phi_f = \frac{\text{volume of pores within biofilm } V_f}{\text{bulk volume of REV } V_B} \tag{3}$$

- ε is the biofilm porosity.

$$\varepsilon = \frac{\text{volume of pores within biofilm } V_f}{\text{biofilm volume including biofilm pores } V_b} = \frac{\phi_f}{\phi_0 - \phi_p} \tag{4}$$

The volumes used above V_0, V_B, V_p, V_f, and V_b are shown in Figure 12.

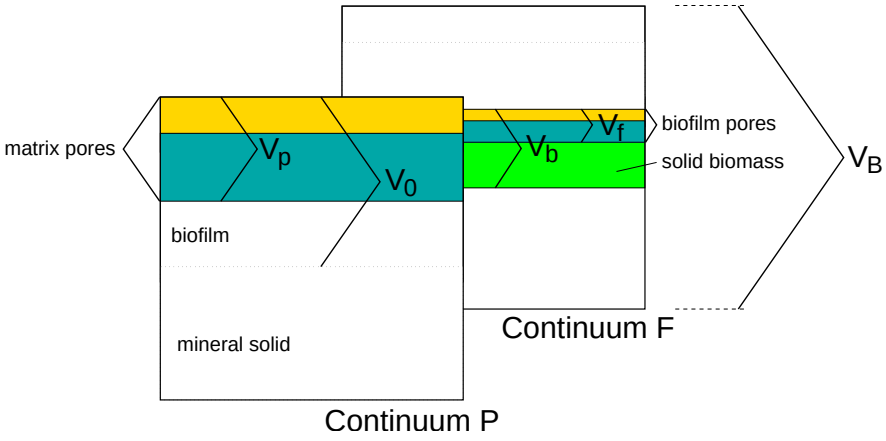

Figure 12: Volumes needed for the definition of different volume fractions.

2.3 Definitions of Basic Terms and Properties

The terms needed for the mathematical description of the flow of multiple fluids through porous media including the properties of the fluids and of the porous structure are defined in this section.

Phase

The term *phase* refers to a continuum with distinct properties. In a geological CO_2 storage reservoir with biofilm accumulation, there is a solid phase (porous material), two immiscible fluid phases (water/brine and CO_2), and a biofilm phase. However, in this thesis, only the fluids will be referred to as phases. The fluid with greater affinity to the solid matrix is the *wetting* phase, and the other is the *non-wetting* phase.

2.3.1 Properties of Porous Matrix

Some properties of porous materials have already been introduced in Section 1.1.2, the most obvious of them being *porosity* ϕ. It is the ratio of the interconnected pore volume to the total volume of the porous medium. *Specific surface* M was defined in Section 1.1.2. Other important properties of porous media are given below.

- *Pore-size distribution* can be characterised by an index λ (Brooks and Corey, 1964). In theory, λ can be any positive number. A completely uniform pore-size distribution would have a λ-value approaching infinity, whereas media with small values of λ have a wide range of pore sizes (Corey, 1994).
- *Intrinsic permeability* is the property of a porous medium that describes the ease with which a fluid can flow through it. It is a proportionality factor in the Darcy equation (see Equation 14). Generally, intrinsic permeability is a tensorial quantity $\mathbf{K}$. For a homogeneous medium, however, intrinsic permeability is a scalar value K.

2.3.2 Fluid Properties

Fluid properties of interest for the description of fluid flow and transport include *density* and *viscosity*.

- The density ϱ of a fluid is defined as its mass per unit volume.
- Viscosity is a measure of a fluid's reluctance to flow (White, 2003). Dynamic viscosity μ, for Newtonian fluids, is a proportionality factor between shear stress and shear strain rate.

Both density and viscosity of a given phase vary with pressure p and temperature T. The composition of a given phase also alters its properties. Note that in this work, temperature and phase composition are assumed to be constant.

Physical Properties of CO_2 and Water

The properties of fluids necessary for the description of flow and transport include density and viscosity. Definitions of these two properties have been given above. Depending on temperature and pressure, these properties may vary considerably. In this section, the densities and viscosities of CO_2 and water and their variation within the temperature and pressure range of interest will be discussed.

Properties of CO_2

The properties of any fluid depend strongly on the fluid's state of aggregation. At atmospheric conditions, CO_2 is a gas with a density of about $1.9\,\mathrm{kg/m^3}$. Figure 13 shows the saturation vapour curve of CO_2 for a given pressure and temperature range. The regions within which CO_2 is gaseous, liquid, or supercritical are also shown. The critical conditions for CO_2 are $p = 73.8\,\mathrm{bar}$ and $T = 31\,^\circ\mathrm{C}$. As discussed in Bielinski (2006), supercritical CO_2 has a liquid-like (high) density and gas-like (low) viscosity. For the storage of CO_2 in geo-

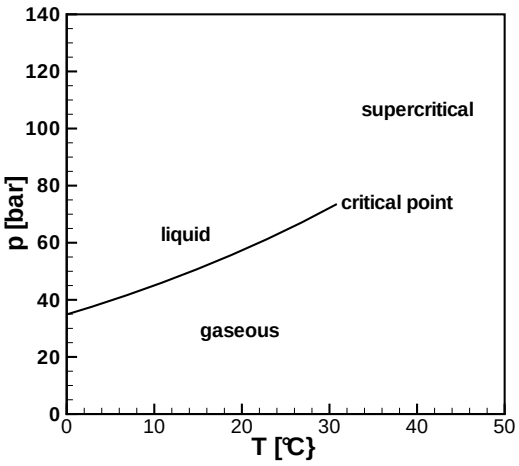

Figure 13: CO_2 saturation vapour pressure curve and the different states of aggregation.

logical formations, a high CO_2 density is necessary since dense CO_2 requires less space and is less buoyant. This implies high storage effectivity and safety. Thus, the conditions within the storage reservoir should be such that the stored CO_2 is either liquid or supercritical. In other words, the reservoir should have the right depth since both pressure and temperature vary with depth. Pressure increases hydrostatically with depth. Temperature also increases with depth at a rate that is called the *geothermal gradient*. 0.03–0.04 °C/m are typical values for geothermal gradients. Suitable storage reservoir depths could range between 700 and 3000 m – deep enough to ensure that the CO_2 is not gaseous, but shallow enough to guarantee economic feasibility.

In Figure 14, the density of CO_2 at 40 °C as a function of pressure is shown. Within the pressure range of 60–140 bar, CO_2 density ranges between about 150 and $760\,\mathrm{kg/m^3}$. Also

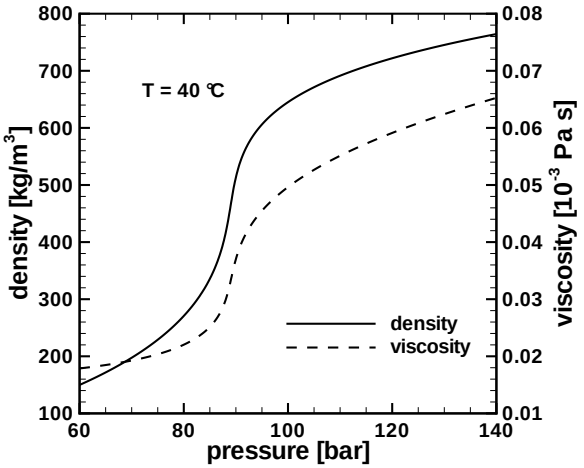

Figure 14: Density and viscosity of CO_2 at 40 °C. Both properties of CO_2 vary considerably. The strongest variations occur near the critical point which marks the end of the saturation vapour pressure curve (see Figure 13).

shown in the figure is the dynamic viscosity of CO_2. The properties of CO_2 needed for the balance equations are determined as is done in the work by Bielinski (2006). Density is calculated using the equation of state of Span and Wagner (1996), and viscosity is calculated as given by Fenghour *et al.* (1998).

Supercritical CO_2: As shown in Figure 13, when pressure and temperature exceed critical values, CO_2 is supercritical. Supercritical CO_2 is a particularly good solvent and is used industrially in extraction processes (see Mukhopadhyay, 2009). Its high solvency also makes it an efficient biocide (see Section 2.6.2).

Properties of Water

At the conditions which prevail in potential CO_2 reservoirs, the density and viscosity of water vary only slightly. For this reason, the properties of water are assumed to be constant in this work. The salinity of water or brine in geological formations can vary significantly. An overview of the salinities of brines in different formations is given in Batzle and Wang (1992) with values ranging from 0 to 0.3 $kg_{salt}/kg_{solution}$. Formation brines are solutions of different salts. Sodium chloride (NaCl) is usually the most abundant. When determining physical properties of brine, it is often assumed that the solution only contains NaCl. To compensate for this, an *equivalent NaCl content* is sometimes used in which the effects of the other salts are accounted for (see Michaelides, 1981). The density and viscosity of saline water vary with its salinity. Figure 15 shows these two properties of brine as functions of salinity as given by Batzle and Wang (1992) (see also Bielinski, 2006).

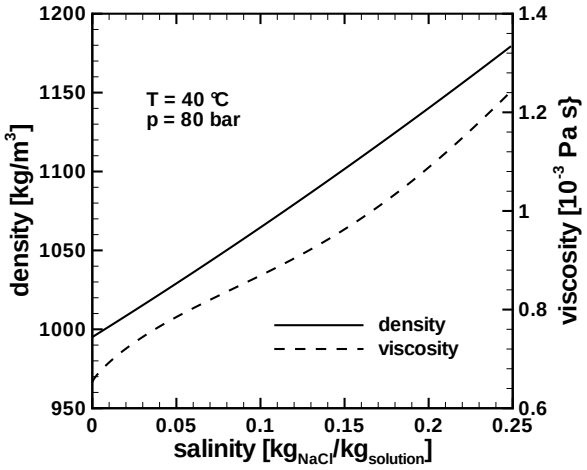

Figure 15: Density and viscosity of brine at 40 °C and 80 bar.

2.3.3 Interaction between Fluid Phases and Porous Matrix

Section 2.3.2 deals with fluid properties relevant for the description of flow and transport, and Section 2.3.1 introduced parameters which characterise a porous medium. Fluids flowing through the pores of a porous matrix interact with the matrix and with each other. These interactions also need to be described with parameters and properties of the system. These are introduced in this section.

Saturation

The ratio of the volume occupied by a phase α to the total pore volume within an REV is called the *saturation* S_α of that phase. It follows that the sum of saturations must be equal to one.

$$S_w + S_n = 1 \tag{5}$$

Capillarity

Interfacial tension exists at the boundary between immiscible fluids as a results of the differences in intermolecular forces between the molecules at the interface. It acts to reduce the interfacial area between the fluids. The angle which forms between the surface of a solid and the boundary of two immiscible fluids in contact with the solid is called *contact angle* θ (see Figure 16). The fluid with the acute contact angle is the wetting fluid. Such a fluid adheres preferentially to the solid surface. The non-wetting fluid has an obtuse contact angle.

Consider an interface between two fluids of different densities as shown in Figure 17. Fluid 2 is the wetting fluid and is denser than Fluid 1. A capillary tube with radius r connects the

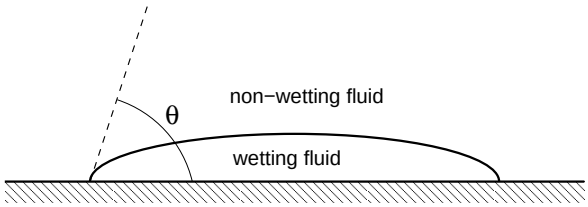

Figure 16: Contact angle θ between two fluids in contact with a solid surface.

two fluids. Due to interfacial tension, Fluid 2 has risen up the capillary tube to Point B. The pressure at Point A of both fluids are equal.

$$p_1^A = p_2^A = p^A \tag{6}$$

However, at the interface within the capillary tube (Point B), there is a difference between the pressures of the two fluids.

$$\begin{array}{rcl} p_1^B & = & p^A - \varrho_1 g h \\ p_2^B & = & p^A - \varrho_2 g h \end{array} \tag{7}$$

h is the height Fluid 2 has risen in the capillary tube, and g is acceleration due to gravity. This

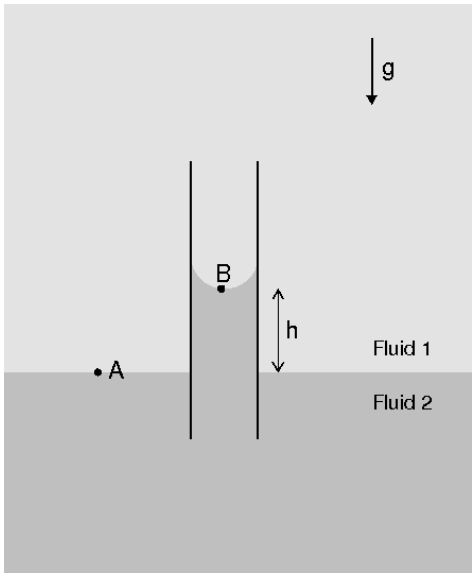

Figure 17: Capillary tube connecting two immiscible fluids.

implies that the difference between the two pressures, called *capillary pressure* p_c, is exactly

$$p_1^B - p_2^B = (\varrho_2 - \varrho_1) g h = p_c^B. \tag{8}$$

p_c^B is often approximated as follows

$$p_c^B = \frac{2\sigma}{r} \cos\theta, \tag{9}$$

which shows its dependence on interfacial tension σ, contact angle θ, and on the radius r of the capillary tube.

In much the same way as in the capillary tube, there is a discontinuity in pressure across the interface of two immiscible fluids in a porous medium which is the capillary pressure. It is defined as

$$p_c = p_n - p_w. \tag{10}$$

p_w and p_n are the pressures of the wetting and non-wetting fluids, respectively. Equation 9 can be transferred to capillary pressure in porous media by using an idealised model in which the porous medium consists of a bundle of capillary tubes. Each tube represents interconnected pores with a given radius. Even though this model oversimplifies the geometry of the porous medium, it is very useful in explaining microscale concepts.

On the macroscale, capillary pressure can be related to the saturation of the wetting phase. Low wetting-phase saturations mean that the wetting phase is primarily located in pores with small radii which in turn means that the capillary pressure must be high. If the wetting-phase saturation increases, the interfaces between the two fluids shift to larger pores, and hence, the capillary pressure reduces.

$$p_c = p_c(S_w) \tag{11}$$

There are several empirical expressions which link p_c and S_w. Brooks and Corey (1964) propose the relationship

$$S_e = \frac{S_w - S_{wr}}{1 - S_{wr}} = \left(\frac{p_d}{p_c}\right)^{\lambda} \quad \text{for } p_c \geq p_d. \tag{12}$$

S_e is called *effective* saturation, S_{wr} is the *residual* wetting-phase saturation, and p_d is the entry pressure of the porous medium. See Figure 18 for a plot of the relationship.

Relative Permeability

Intrinsic permeability was introduced in Section 2.3.1 as a property of the porous matrix. *Relative permeability* $k_{r\alpha}$ scales the intrinsic permeability, and therefore, is a value between zero and one. It accounts for the increased resistance to flow for a given phase due to the presence of the other phase. Like capillary pressure, relative permeabilities are strongly dependent on phase saturations. In this work, the following expressions are used to describe the relationship between the relative permeability of each phase and effective saturation (see Figure 18).

$$\begin{aligned} k_{rw} &= S_e^{\frac{2+3\lambda}{\lambda}} \\ k_{rn} &= (1 - S_e)^2 \left(1 - S_e^{\frac{2+\lambda}{\lambda}}\right) \end{aligned} \tag{13}$$

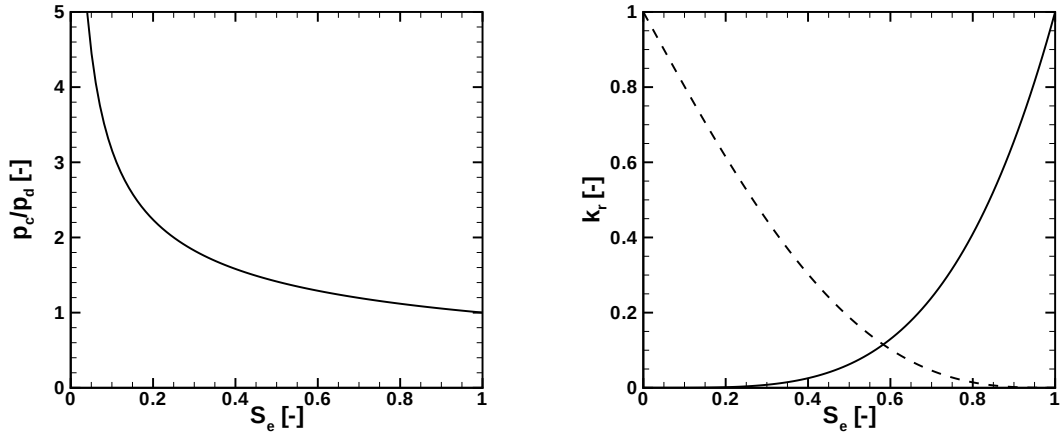

(a) Capillary pressure–saturation relationship. In theory, p_c increases infinitely as S_e decreases, but for practical reasons, it can be assumed that $p_c \leq p_{c,max}$.

(b) Relative permeability–saturation relationships. The continuous line shows wetting-phase relative permeability and the dashed line non-wetting-phase relative permeability.

Figure 18: Capillary pressure and relative permeabilities as functions of effective saturation using Equations 12 and 13, and $\lambda = 2$.

2.3.4 Fluid Flow in Biofilm

In Section 1.1.4, the concept of a porous biofilm structure with pores and channels was discussed. In experiments, Stoodley *et al.* (1994) and De Beer *et al.* (1994) could show the advective flow of water through the voids of a biofilm. In a natural porous medium, fluid flow through a biofilm is mostly much slower than through the pores of the porous medium. This leads to the assumption often made when modelling fluid flow through biomass-affected porous media, which is that the biofilm is impermeable to advective flow. However, depending on the amount of biomass in the system and on the processes that are of interest, advective flow through the biofilm can have an important and non-negligible effect on the system (see Thullner and Baveye, 2008). In two-phase fluid systems, the presence of a porous biofilm has an effect on the distribution of the fluids, and hence, on capillary pressure and relative permeabilities. It may also be important for the growth dynamics of the biofilm to know which fluids occupy the voids in the biofilm. For these reasons, the permeability and porosity of the biofilm are not neglected in this work.

2.4 General Equations of Two-Phase Fluid Flow in Porous Media

In this section, the equations generally used to describe two-phase fluid flow in a porous medium without biomass will be discussed briefly. These include equations for velocities and mass conservation equations. In Section 2.5, these conservation equations will be extended within the framework of a dual-continuum concept to account for biomass accumulation.

2.4.1 The Darcy Equation

Two-phase fluid fluxes through porous media can be approximated with the extended Darcy equation as given below.

$$\mathbf{v}_\alpha = -\frac{k_{r\alpha}}{\mu_\alpha} K(\nabla p_\alpha - \varrho_\alpha \mathbf{g}) \tag{14}$$

The flux $\mathbf{v}_\alpha$ of a given phase, also called Darcy velocity, is proportional to the "driving forces" which include pressure gradient and gravity with $\frac{k_{r\alpha}}{\mu_\alpha} K$ as the proportionality factor.

2.4.2 Mass Conservation Equations

Consider a fluid α flowing through a fixed control volume Ω as shown in Figure 19. The

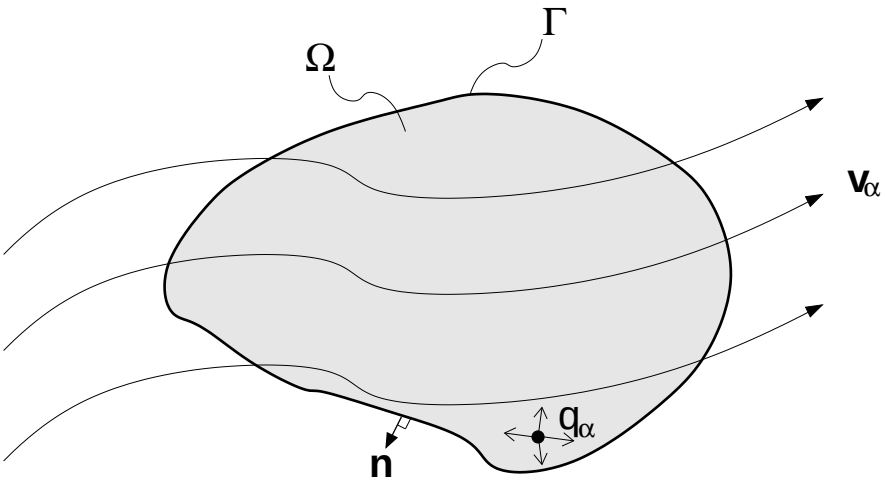

Figure 19: Stationary control volume Ω for balance equation. $\mathbf{v}_\alpha$ is the Darcy velocity with which the fluid α flows through the control volume and over its boundary Γ. q_α is a source or sink.

mass of the fluid α can only change if there is a difference between the inflow and outflow of the fluid or due to sources or sinks.

$$\text{Rate of change of mass} = \text{inflow} - \text{outflow} + \text{sources/sinks} \tag{15}$$

This leads to the following equation.

$$\int_\Omega \frac{\partial(\phi S_\alpha \varrho_\alpha)}{\partial t} d\Omega + \int_\Gamma (\varrho_\alpha \mathbf{v}_\alpha \cdot \mathbf{n}) d\Gamma = \int_\Omega q_\alpha d\Omega, \tag{16}$$

where q_α is a source or sink, and $\mathbf{n}$ is the unit vector normal to the surface Γ. The advective term can be reformulated using the Gauss theorem.

$$\int_\Omega \left\{ \frac{\partial(\phi S_\alpha \varrho_\alpha)}{\partial t} + \nabla \cdot (\varrho_\alpha \mathbf{v}_\alpha) - q_\alpha \right\} d\Omega = 0 \tag{17}$$

Equation 17 is valid if the integrand vanishes.

$$\frac{\partial(\phi S_\alpha \varrho_\alpha)}{\partial t} + \nabla \cdot (\varrho_\alpha \mathbf{v}_\alpha) = q_\alpha \tag{18}$$

Equation 18 is the continuity equation for the fluid α. Note that the mutual dissolution of the fluids has been neglected.

Similarly, the continuity equation for a solute s flowing with the fluid α through the control volume can be derived.

$$\frac{\partial(\phi S_\alpha C_\alpha^s)}{\partial t} + \nabla \cdot \{(C_\alpha^s \mathbf{v}_\alpha) - D^s \nabla C_\alpha^s\} = q_s, \tag{19}$$

where C_α^s in kg/m^3 is the concentration of the solute s within the fluid phase α. Equation 19 contains a term which accounts for the diffusive flux of the solute.

2.5 Mass Conservation Equations

Two continua were defined in Section 2.2. For each continuum κ, a set of continuity equations similar to those given in Section 2.4.2 can be derived. In the following, this will be done for the fluid phases, biomass, and a substrate.

2.5.1 Conservation of Mass of Water and CO_2

$$\frac{\partial(\phi_\kappa S_{\alpha,\kappa} \varrho_{\alpha,\kappa})}{\partial t} + \nabla \cdot (\varrho_{\alpha,\kappa} \mathbf{v}_{\alpha,\kappa}) = q_{\alpha,\kappa} + e_{\alpha,\kappa}; \quad \alpha \in \{w, n\}, \quad \kappa \in \{p, f\}. \tag{20}$$

The Darcy velocity $\mathbf{v}_{\alpha,\kappa}$ is calculated as given in Equation 14. $q_{\alpha,\kappa}$ is a source/sink term; $e_{\alpha,\kappa}$ accounts for the exchange of mass between two continua. The dissolution of CO_2 in water and water in CO_2 is neglected. Note that Equation 20 is supplemented by Equations 5 and 10, and by the constitutive relationships given in Equations 12 and 13. These are summarised below.

$$\begin{aligned} 1 &= S_{w,\kappa} + S_{n,\kappa} \\ p_{c,\kappa} &= p_{n,\kappa} - p_{w,\kappa} \\ p_{c,\kappa} &= p_{c,\kappa}(S_{w,\kappa}) \\ k_{r\alpha,\kappa} &= k_{r\alpha,\kappa}(S_{w,\kappa}) \end{aligned} \tag{21}$$

The above equations assume that each continuum can be characterised with a set of parameters such as porosity ϕ_κ, entry pressure $p_{d,\kappa}$, and pore-size distribution index λ_κ.

2.5.2 Conservation of Biomass

Conservation equations for the biomass in the system also need to be formulated. Again, this is done for each continuum. At this point, the following assumptions are made.

- In Continuum P, biomass exists only as suspended cells within the water phase and can be accounted for with a concentration C_w^b[kg/m^3]. Biomass in the CO_2 phase is neglected since supercritical CO_2 is a biocide (Mitchell *et al.*, 2008).
- In Continuum F, biomass exists only in the biofilm, i.e., attached. The properties of the biofilm, namely, biofilm density ϱ_b and biofilm porosity ε are taken to be constant. See Section 1.1.4 and Equation 4 for definitions of ϱ_b and ε.

Thus, the conservation equation for biomass in Continuum P (suspended) reads

$$\frac{\partial(\phi_p C_w^b S_{w,p})}{\partial t} + \nabla \cdot (C_w^b \mathbf{v}_{w,p}) - \nabla \cdot (D_p^b \nabla C_w^b) = q_p^b + e_p^b. \tag{22}$$

C_w^b is the concentration of biomass in the water phase, q_p^b is a source/sink term with which biomass growth and decay can be accounted for, and e_p^b is an exchange term. The coefficient of dispersion of suspended biomass in the water phase D_p^b varies with porosity and saturation; $D_p^b = \hat{D}_p^b \phi_p S_{w,p}$. $\hat{D}_p^b$ is a constant diffusion coefficient.

In Continuum F, biomass is immobile, therefore, the mass balance equation consists of only storage and source/sink terms.

$$\frac{\partial([\phi_0 - \phi_p]\varrho_b)}{\partial t} = q_f^b + e_f^b \tag{23}$$

Inserting Equation 4, yields

$$\left(\frac{\varrho_b}{\varepsilon}\right) \frac{\partial \phi_f}{\partial t} = q_f^b + e_f^b, \tag{24}$$

ε and ϱ_b have been pulled out of the differential because they are taken to be constant. Note that

$$e_f^b = -e_p^b. \tag{25}$$

2.5.3 Conservation of Mass of Growth-Limiting Substrate

As stated in Section 1.1.3, bacterial cells, both attached and floating, need the appropriate pH, temperature, salinity, etc. to survive. They also need energy, carbon, and an electron acceptor source for metabolism and reproduction. So many different factors affect the growth of biomass. However, it is assumed here that the availability of one substrate limits bacterial growth. Therefore, the growth of biomass is essentially a function of the concentration of this substrate in water. A mass balance of the growth-limiting substrate gives

$$\frac{\partial(\phi_\kappa S_{w,\kappa} C_{w,\kappa}^s)}{\partial t} + \nabla \cdot (C_{w,\kappa}^s \mathbf{v}_{w,\kappa}) - \nabla \cdot (D_\kappa^s \nabla C_{w,\kappa}^s) = q_{w,\kappa}^s + e_{w,\kappa}^s, \quad \kappa \in \{p, f\}. \tag{26}$$

D_κ^s is a porosity-dependent dispersion coefficient. $D_\kappa^s = \hat{D}_\kappa^s \phi_\kappa S_{w,\kappa}$, where $\hat{D}_\kappa^s$ is a constant diffusion coefficient.

In Equation 26, the dissolution of substrate in CO_2 has been neglected. Depending on the substrate, its solubility in supercritical CO_2 may not be negligible. In that case, a balance equation which accounts for the transfer of substrate between the phases would be necessary.

2.6 Simplifying Assumptions and Exchange Terms

A total of eight conservation equations, four in each continuum, were set up in Section 2.5. Some of the equations can be linked by exchange terms which describe the flow of mass from one continuum to the other as a function of a difference in potential. On the other hand, assumptions can be made which significantly reduce the complexity of the system without compromising its validity.

2.6.1 Fluid Exchange

Mass exchange of water and CO_2 between the continua can be achieved with an exchange term e_α[kg/(m^{3}s)] which is a function of the pressure difference between the two continua.

$$\begin{aligned} &e_\alpha = a_\alpha(p_{\alpha,p} - p_{\alpha,f}), \\ &\text{with } e_\alpha = -e_{\alpha,p} = e_{\alpha,f}. \end{aligned} \tag{27}$$

a_α is a parameter which describes the rate at which the exchange takes place. It could depend on the intrinsic and relative permeabilities of the continua, on the characteristic length separating components of the two continua, etc. (e.g., Gerke and van Genuchten, 1993). If a_α is zero, the exchange processes are infinitely slow compared to the characteristic fluxes of the system. If a_α is infinity, the pressure difference is equilibrated instantaneously.

For simplicity and as a first step in the development of this model, the pressures in the two continua are assumed to be equal. The consequence of this simplification is that fluid exchange takes place instantaneously, and it is not possible to quantify the exchange rate which may be important for the determination of solute exchange. In this work, solute exchange is assumed to be driven primarily by concentration gradients (see Section 2.6.5). The topic of further work has to be the investigation of the importance of solute exchange due to advection and the implementation into the model.

As stated above, it is assumed that for each local REV

$$p_{\alpha,p} = p_{\alpha,f} = p_\alpha. \tag{28}$$

Since fluid properties depend on pressure, the following expressions are direct consequences of Equation 28.

$$\begin{aligned} \varrho_{\alpha,p} &= \varrho_{\alpha,f} = \varrho_\alpha \\ \mu_{\alpha,p} &= \mu_{\alpha,f} = \mu_\alpha \end{aligned} \tag{29}$$

The capillary pressures at the interface between the two continua have to be the same.

$$p_{c,p} = p_{c,f} = p_c \tag{30}$$

Note that no wettability changes will be accounted for in this work, i.e., both the porous medium and the biofilm are taken to be hydrophilic media. Since p_c can be expressed as a function of $S_{e,p}$ or $S_{e,f}$, $S_{e,p}$ and $S_{e,f}$ are not independent. If one of the two is known

(e.g., $S_{e,p}$), the other can be calculated as a function of p_c in the following manner (see also Figure 20).

$$\begin{aligned} p_c &= p_{d,p} S_{e,p}^{-\frac{1}{\lambda_p}}, \\ S_{e,f} &= \left(\frac{p_{d,f}}{p_c}\right)^{\lambda_f} \quad \text{if } p_c > p_{d,f}, \\ S_{e,f} &= 1 \qquad\qquad\quad \text{otherwise.} \end{aligned} \tag{31}$$

This means that the distribution of the two fluids within the two continua is determined by capillary forces. It is assumed that $p_{d,f} > p_{d,p}$, so that the non-wetting phase invades Con-

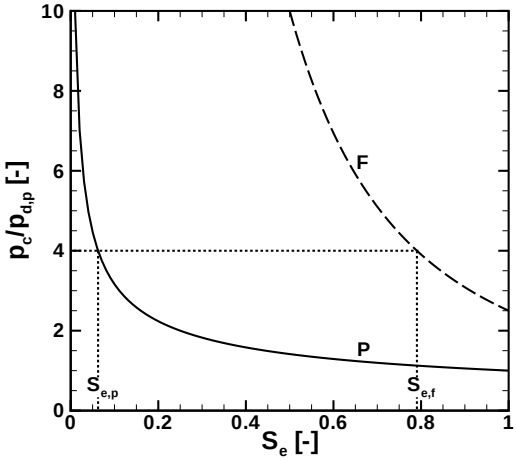

Figure 20: $S_{e,p}$ and $S_{e,f}$ resulting from one p_c-value. $\lambda_p = 2$, $\lambda_f = \frac{1}{2}$, $p_{d,f} = 2.5 \cdot p_{d,p}$.

tinuum P first before Continuum F. This results from the assumption that the largest pores of the porous medium are larger than those of the biofilm. Figure 21 shows the microscale view of a biofilm in a pore and depicts the assumptions discussed above.

Equation 20 for the water phase becomes

$$\frac{\partial(\phi_p S_{w,p} \varrho_w)}{\partial t} + \nabla \cdot (\varrho_w \mathbf{v}_{w,p}) = q_{w,p} - e_\alpha \tag{32}$$

and

$$\frac{\partial(\phi_f S_{w,f} \varrho_w)}{\partial t} + \nabla \cdot (\varrho_w \mathbf{v}_{w,f}) = q_{w,f} + e_\alpha. \tag{33}$$

Adding Equations 32 and 33, gives

$$\frac{\partial([\phi_p S_{w,p} + \phi_f S_{w,f}] \varrho_w)}{\partial t} + \nabla \cdot (\varrho_w [\mathbf{v}_{w,p} + \mathbf{v}_{w,f}]) = q_w, \tag{34}$$

where $q_w = q_{w,p} + q_{w,f}$. Similar reformulations can be done for the CO_2 phase.

$$\frac{\partial([\phi_p S_{n,p} + \phi_f S_{n,f}] \varrho_n)}{\partial t} + \nabla \cdot (\varrho_n [\mathbf{v}_{n,p} + \mathbf{v}_{n,f}]) = q_n \tag{35}$$

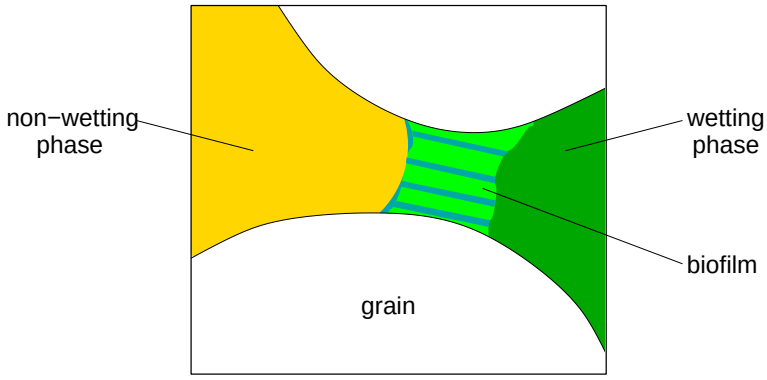

Figure 21: Microscale idealisation of a biofilm growing in a pore at the interface between two fluids. The biofilm b is idealised as a bundle of capillary tubes. The non-wetting phase n would have to overcome the biofilm entry pressure in order to displace the wetting phase w.

2.6.2 Biomass Growth and Decay

The terms q_f^b and q_p^b, from Equations 22 and 24, are sources or sinks. They comprise biomass growth $r_{g,\kappa}$, biomass decay $r_{b,\kappa}$, and external sources or sinks $\hat{q}_\kappa^b$.

$$q_\kappa^b = r_{g,\kappa} - r_{b,\kappa} + \hat{q}_\kappa^b \tag{36}$$

The growth of biomass $r_{g,\kappa}$ is a function of the biomass concentration or density and a growth rate μ_κ.

$$\begin{aligned} r_{g,p} &= \mu_p \phi_p S_{w,p} C_w^b \\ r_{g,f} &= \mu_f (\phi_f / \varepsilon) \varrho_b \end{aligned} \tag{37}$$

The growth rate μ_κ depends on the concentration of the growth-limiting substrate and is traditionally modelled with Monod kinetics.

$$\mu_\kappa = k_\mu Y \frac{C_{w,\kappa}^s}{K_s + C_{w,\kappa}^s} \tag{38}$$

k_μ is the maximum substrate utilisation rate, and $Y[\mathrm{kg}_{\mathrm{biomass}}/\mathrm{kg}_{\mathrm{substrate}}]$ is the yield coefficient which accounts for the fraction of substrate actually used for growth. A great deal of the utilised substrate goes into *cell maintenance*. Notice that both k_μ and Y have been assumed to be the same for both continua, i.e., for both planktonic and sessile cells. K_s is the Monod half-saturation coefficient. It is the value of $C_{w,\kappa}^s$ at which $\mu_\kappa = k_\mu Y/2$. These three parameters are species-specific.

Biomass decay refers to processes which reduce the amount of active biomass present in a sample. It can be caused by *endogenous decay*, *grazing*, and *lysis*. Endogenous decay is caused by respiration of an electron acceptor using internal components of the cell. Cell lysis refers to the death of microbial cells due to harsh external conditions such as exposure to biocides. van Loosdrecht and Henze (1999) make it clear that endogenous respiration does not

significantly reduce the number of microbial cells, even though it reduces the amount and activity of biomass. Lysis and grazing, however, reduce the number, amount, and activity of biomass. In this work, the endogenous decay rate is assumed to be constant, whereas lysis is assumed to be dependent on CO_2 saturation.

$$\begin{aligned} r_{b,p} &= b_p \phi_p S_{w,p} C_w^b \\ r_{b,f} &= b_f (\phi_f / \varepsilon) \varrho_b \end{aligned} \tag{39}$$

The decay rate b_κ comprises a constant endogenous decay rate b_0 as mentioned above and a death rate $b_{c,\kappa}$ caused by the cells' exposure to toxic supercritical CO_2.

$$b_\kappa = b_0 + b_{c,\kappa} \tag{40}$$

The above equation suggests that both endogenous decay and cell inactivation by a biocide are linear functions of cell concentration. For endogenous decay, this is a widely used concept. However, it may not be appropriate for the latter. An overview of functions used to model decay due to CO_2 exposure, including linear and non-linear models, is given in Zhang *et al.* (2006). For simplicity, it is assumed that a linear model is sufficient.

Zhang *et al.* (2006) and Mitchell *et al.* (2008) suggest likely mechanisms involved in cell inactivation by CO_2. On the one hand, low intracellular pH caused by CO_2 dissolution within a cell may disrupt processes essential for cell activity or cause enzyme denaturation. On the other hand, supercritical CO_2, which is a good solvent, can cause the extraction of intracellular material. In experiments conducted by Mitchell *et al.* (2009) to investigate the effect of supercritical CO_2 on bacterial cells, biofilm cells proved to be more resilient than planktonic cells. This was attributed to the interaction of CO_2 molecules with the EPS matrix leading to an immobilisation of the molecules.

$b_{c,\kappa}$ is a lumped parameter accounting for the different mechanisms responsible for the increased biomass decay due to exposure to CO_2. The most obvious macroscale parameter with which this exposure may be quantified is saturation. Hence, $b_{c,\kappa}$ is assumed to be a function of $S_{n,\kappa}$.

$$b_{c,\kappa} = c_c S_{n,\kappa}^{n_c}, \tag{41}$$

where c_c and n_c are empirical values which may depend on the bacterial species and on the properties of the natural porous medium and biofilm. Once biomass decays, it is no longer accounted for in the model. In effect, therefore, decayed biomass simply disappears causing slight changes in pressure. It is assumed here that the process of growth and decay of biofilm occurs much slower than the flow processes which would equilibrate any such changes in pressure.

Under harsh environmental conditions, some bacterial cells are capable of forming *spores* – a highly resistant phenotypic state (Chambless *et al.*, 2006). Spores often survive the harsh conditions and are reactivated when the conditions become conducive. Zhang *et al.* (2006) report that spores are resistant to high-pressure CO_2 treatment. Spore formation is very important in *sterilisation*. However, since spores are dormant and make up only about 1 % of the initial population (Chambless *et al.*, 2006), the effect they may have on the mechanisms important for the formation and persistence of the biobarrier is assumed to be negligible and not included in the formulation of the model.

2.6.3 Biomass Exchange

The exchange terms e_p^b and e_f^b from Equations 22 and 24, describe the mass transfer between suspended biomass in Continuum P and attached biomass in Continuum F.

$$e^b = e_f^b = -e_p^b = \underbrace{k_a \phi_p S_{w,p} C_w^b}_{r_a} - \underbrace{k_d (\phi_f/\varepsilon) \varrho_b}_{r_d} \tag{42}$$

r_a is the rate of attachment of suspended biomass to the solid or biofilm, and r_d is the rate at which biomass detaches from the biofilm. k_a and k_d are attachment and detachment functions, respectively. They are an attempt to account for microscale processes leading to either attachment or detachment on the macroscale.

Attachment Function

There are a number of different processes, occurring simultaneously, responsible for the attachment of microbial cells in a porous medium. These could include straining, adsorption, sedimentation, and interception. Straining occurs when a floating cell or cluster of cells is larger than the pore opening through which its medium is flowing. Cells may also be adsorbed at an interface as a result of intermolecular forces. Sedimentation only occurs if the microbial cell density differs from that of the fluid. And interception results from collisions of floating cells with the grains. See Corapcioglu and Haridas (1984) for a more detailed explanation of these processes.

Different expressions have been proposed to determine the attachment coefficient or function. The so-called *colloid filtration theory* (e.g., Tufenkji and Elimelech, 2004), which describes the physicochemical interaction between the *biocolloids* and the porous medium, is often used. Bradford *et al.* (2003) include a depth-dependent straining term in their model. Taylor and Jaffé (1990b) assume k_a to be a linear function of the volume fraction of attached material. However, most research has concentrated on attachment to "clean" porous media. Clement *et al.* (1999) stress the lack of research work which focuses on the quantification of an attachment function in a porous medium with an actively growing biofilm. Obviously, as the volume fraction occupied by a biofilm in a porous medium increases, so also does the importance of the biofilm itself in the attachment processes. The biofilm would change the adsorption rate of cells and increase the possibility of straining by reducing pore diameters.

In light of the factors mentioned above, a simple method to quantify the attachment function seems appropriate. It should also account for variations in attachment with changes in the volume fraction of pore space occupied by attached biomass. Thus, the relationship given by Taylor and Jaffé (1990b) is used in this work.

$$k_a = c_{a,1} + c_{a,2} \phi_f / \varepsilon \tag{43}$$

$c_{a,1}$ and $c_{a,2}$ are empirical parameters.

In two-phase fluid flow, microorganisms also attach to the interface between the two fluids. This is often incorporated in models with an additional attachment term (Rockhold *et al.*,

2004; Schaefer *et al.*, 1998; Gargiulo *et al.*, 2007). The attachment rate at the fluids' interface is then a function of the interfacial area between the two fluids. This interfacial area can be estimated from the pore-size distribution of the porous medium and is a non-linear function of the wetting-phase saturation (Niemet *et al.*, 2002; Cary, 1994). However, in this work, one of the fluid phases is a biocide which means that cells attached to the fluids' interface are exposed to the toxic fluid. These are then accounted for by decay term $b_{c,p}$ (see Equation 41).

Detachment Function

Detachment is defined here as any process that causes the transfer of biomass from the biofilm to the aqueous fluid phase. Detachment processes, relevant to this work, include erosion and sloughing. Erosion is the continuous release of small particles (cells and small cell clusters) from the biofilm mostly due to shear stress, while sloughing is the random release of large pieces of biofilm (Bryers, 2000).

Many expressions to determine detachment rate exist. Good overviews of the different expressions are given by Stewart (1993) and by Lewandowski and Cunningham (1998). The expressions usually correlate the attachment rate with biofilm thickness L_f, amount of biomass, shear stress τ, and even biofilm growth rate μ_f. Peyton and Characklis (1993) and Tijhuis *et al.* (1995) tested the performance of some of these expressions with different experimental data. Many of the expressions were not transferable from one set of experimental data to another.

Particles are removed from the biofilm if the force exerted on the biofilm by the fluid exceeds the strength of the biofilm. Rittmann (1982) relates detachment to shear stress. In this case, changes in the force exerted on the biofilm (shear stress) are accounted for as well as the reduction in the strength of the biofilm with increasing thickness. Speitel and DiGiano (1987) suggest that an additional detachment term be added to that of Rittmann (1982). This is motivated by experimental data suggesting that fast-growing biofilms detach more readily than slow-growing biofilms. This could be as a result of differences in the production rate of EPS compared to cell reproduction. It could also result from an increasingly uneven growth as growth rate increases. Picioreanu *et al.* (2001) could show, using numerical simulations, that differences in shape and structure between fast and slow-growing biofilms is one reason for the differences in susceptibility to shear.

In light of the factors mentioned above, a detachment function needs to account for the force exerted on the biofilm by the fluid and changes in strength of biofilm. It should also be as simple as possible and should incorporate only readily available information. In the model presented here, for example, information on biofilm thickness is not readily available, hence, a detachment function dependent on biofilm thickness seems inappropriate here. Available macroscale information include Darcy velocity, pressure gradient, biomass growth rate, and saturations. The detachment function given in Equation 44 is a function of the magnitude of the water-phase pressure gradient $|\nabla p_w|$. It is assumed that the pressure gradient accounts for the shear forces exerted on the biofilm by the water phase. It is also assumed, as discussed above, that a higher growth rate increases biofilm susceptibility to shear. This is

accounted for, as suggested by Speitel and DiGiano (1987), by the term k_d^μ.

$$k_d = \underbrace{c_{d,1}(\phi_p S_{w,p}|\nabla p_w|)^{n_d}}_{k_d^\tau} + \underbrace{c_{d,2}\mu_f(\phi_f/\varepsilon)\varrho_b}_{k_d^\mu} \tag{44}$$

$c_{d,1}$, $c_{d,2}$, and n_d are empirical parameters. Assuming the dependence of k_d^τ on the pressure gradient behaves in the same way as its dependence on shear stress, the exponent n_d can be taken from Rittmann (1982) to be $n_d = 0.58$. The detachment term k_d^μ is proportional to the rate of biofilm growth. Speitel and DiGiano (1987) give values for the proportionality factor $c_{d,2}$ ranging from 0.319 to 0.665 depending, for example, on the substrate. In this work, it is assumed that the proportionality between k_d^μ and growth rate varies with the amount of biofilm in place ϕ_f/ε.

$$c_{d,2} = \tilde{c}_{d,2}\phi_f/\varepsilon \tag{45}$$

The dependence of $c_{d,2}$ on ϕ_f/ε accounts for the increase in variation of the substrate distribution within the biofilm with increase in biofilm thickness resulting in uneven biofilm growth, and hence in greater detachment.

2.6.4 Substrate Consumption

Substrate is utilised by biomass in both continua. Therefore, $q_{w,\kappa}^s$ in Equation 26 is a sink and a function of the bacterial substrate utilisation rates.

$$q_{w,\kappa}^s = -r_{g,\kappa}/Y \tag{46}$$

$r_{g,\kappa}$ can be calculated as given in Equation 37. The substrate consumption rate is obviously higher than the sum of the two growth rates because some of the utilised substrate is not used for growth. This is accounted for with the division by the yield coefficient Y.

2.6.5 Substrate Exchange

The transfer of substrate between the two continua is accounted for by the term $e_{w,\kappa}^s$ in Equation 26. It is a function of the difference in substrate concentration in the two continua.

$$e_w^s = -e_{w,p}^s = e_{w,f}^s = a_w^s(C_{w,p}^s - C_{w,f}^s) \tag{47}$$

The parameter a_w^s describes the rate at which the exchange takes place. This process is often assumed to be mainly diffusive. An effective diffusion coefficient D_{eff}^s can be defined which accounts for both diffusive and advective fluxes of dissolved substrate across the interface.

$$e_w^s = D_{eff}^s \frac{A_{pf}}{L}(C_{w,p}^s - C_{w,f}^s) \tag{48}$$

L is a characteristic length over which the concentration difference exists, and A_{pf} is the specific interfacial area between the two continua. These two parameters are difficult to determine and have to be estimated. One way to estimate A_{pf}/L could be by assuming that the surface area available for mass transfer is equal to the specific surface M of the

porous medium, and the characteristic length over which the substrate fluxes occur is the characteristic pore radius $d_r/2$. This gives

$$e_w^s = D_{eff}^s \frac{M}{d_r/2}(C_{w,p}^s - C_{w,f}^s). \tag{49}$$

D_{eff}^s can be interpreted as the effective diffusivity of the solute in the biofilm. The measurement of effective diffusion coefficients in biofilms has been the subject of many studies, a review of which is given in Stewart (1998). Wood *et al.* (2002) provide a numerical scheme for calculating diffusivities in biofilms.

2.7 Clogging

Biofilms growing in a porous medium occupy pore space and obviously change the properties of the porous medium. The changes in porosity caused by the biofilm can be determined from the mass balance equations. Other properties such as permeability or pore-size distribution are a lot more difficult to describe. Many studies have focused on deriving a mathematical expression linking the intrinsic permeability of a porous medium to its porosity, e.g., Taylor *et al.* (1990), Vandevivere (1995), Clement *et al.* (1996), Seki and Miyazaki (2001),Thullner *et al.* (2002). There are also some studies on the effect of bacterial accumulation on changes in permeability or pore-size distribution in an unsaturated porous medium, e.g., Rockhold *et al.* (2002), Maggi and Porporato (2007), Mostafa and Van Geel (2007). In experiments, the effect of biofilm growth on permeability has been shown (Cunningham *et al.*, 1991; Vandevivere and Baveye, 1992). They generally show a strong initial decrease in intrinsic permeability with decrease in porosity followed by a region in which only minor changes in permeability are observed (see Figure 22). The shape of the permeability–porosity curve is dependent on both the properties of the porous medium and of the biofilm.

In the model developed in this work, two permeabilities exist. Each continuum is assigned a permeability. The relationship between the intrinsic permeabilities K_p and K_f, and the total intrinsic permeability K can be obtained from the summation of the individual fluxes within a control volume.

$$\mathbf{J} \cdot \mathbf{A} = \mathbf{J}_p \cdot \mathbf{A}_p + \mathbf{J}_f \cdot \mathbf{A}_f, \tag{50}$$

where $\mathbf{J}$ is the total mass flux of a fluid through a control volume with the permeability K, $\mathbf{J}_\kappa$ stands for the mass flux contribution of the continuum κ, $\mathbf{A}$ is the total cross-sectional area through which the flux takes place, and $\mathbf{A}_\kappa$ is the area through which the flux $\mathbf{J}_\kappa$ takes place. Using the Darcy equation and assuming only one fluid (e.g., water) is present yields

$$-K\frac{\varrho_w}{\mu_w}(\nabla p_w - \varrho_w \mathbf{g}) \cdot \mathbf{A} = -(K_p + K_f)\left(\frac{\varrho_w}{\mu_w}(\nabla p_w - \varrho_w \mathbf{g}) \cdot \mathbf{A}\right). \tag{51}$$

Due to the assumptions made in Section 2.6.1, the pressure gradients and the fluid properties are the same for both continua, and due to the concept of Darcy velocities, the same goes for the cross-sectional areas.

$$K = K_p + K_f \tag{52}$$

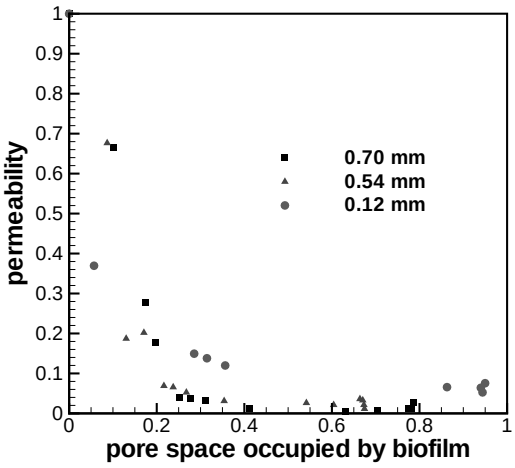

Figure 22: Decrease in permeability with increase in biomass in sands with different median particle sizes (0.12 mm, 0.54 mm, and 0.70 mm). This is experimental data taken from Cunningham *et al.* (1991). The values are normalised with the initial values.

This means that one can determine the individual permeability–porosity relationships for each continuum and sum them up for comparison with experimental values. Obviously, the permeability of a porous medium with small amounts of biofilm is mainly dependent on K_p, while that of a biofilm-filled porous medium is mainly dependent on K_f. Thus, the following expressions have to be fulfilled.

$$\begin{array}{lll} \text{If } \phi_p = \phi_0 \text{ and } K = K_0 & \Longrightarrow & K_p = K_0 \text{ and } K_f = 0, \\ \text{if } \phi_p = 0 \text{ and } K = K_{\min} & \Longrightarrow & K_p = 0 \text{ and } K_f = K_{\min}. \end{array} \tag{53}$$

K_0 is the permeability of the biofilm-free porous medium, while $K_{\min}$ is the permeability of the biofilm-filled porous medium.

The permeability of Continuum P can be described using the expression given by Xu *et al.* (2004).

$$\begin{array}{ll} K_p/K_0 = \left(\frac{\phi_p - \phi_{p,c}}{\phi_0 - \phi_{p,c}}\right)^{n_k} & \text{if } \phi_p > \phi_{p,c}, \\ K_p = 0 & \text{otherwise.} \end{array} \tag{54}$$

$\phi_{p,c}$ is the porosity at which $K_p = 0$, and n_k is an empirical parameter which is strongly dependent on the geometry of the porous medium. From Figure 22, one can determine values of $K_{\min}$ for the different sands, and since these values are relatively constant, it seems appropriate to assign K_f the constant value $K_{\min}$. However, at $\phi_p = \phi_0$, K_f has to be zero. Thus, one could think of some $\phi_p = \phi'_{p,c}$ for which the following holds.

$$\begin{array}{ll} K_f = K_{\min} & \text{if } \phi_p \leq \phi'_{p,c}, \\ K_f < K_{\min} & \text{otherwise.} \end{array} \tag{55}$$

For the region in which $K_f < K_{\min}$, there could be a number of different concepts to describe the behaviour of K_f. For example, one could imagine that there is no advective flow

through Continuum F when ϕ_p is greater than $\phi'_{p,c}$, i.e., $K_f = 0$. If ϕ_p starts to decrease due to biofilm growth, at some point, Continuum F suddenly becomes connected, and fluids can flow advectively through it. On the other hand, one could think of a continuously increasing K_f from zero to K_{min} as ϕ_p decreases from ϕ_0 to $\phi'_{p,c}$. In any case, the concept used is not very important because its contribution to the overall flow process is very small. The permeability–porosity relationship resulting from this concept is show in Figure 23.

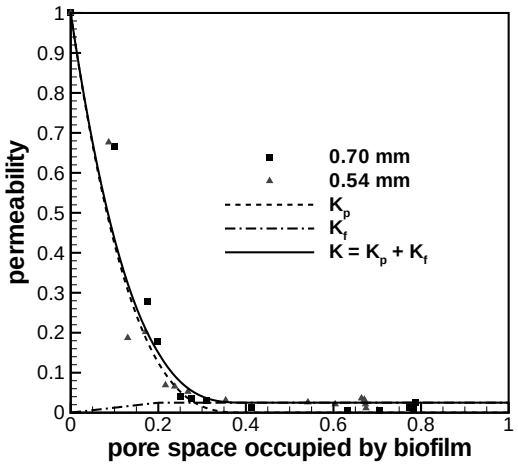

Figure 23: Mathematical description of permeability decrease with increase in biomass fitted to data from Cunningham *et al.* (1991) with two sands of different median particle sizes (0.54 mm and 0.70 mm). The x-axis corresponds to $1 - \phi_p/\phi_0$, and the y-axis corresponds to K/K_0. K is the sum of K_p and K_f. The values of the parameters used are $\phi_{p,c}/\phi_0 = 0.6$, $\phi'_{p,c}/\phi_0 = 0.8$, $K_{\text{min}} = 0.025 \cdot K_0$ and $n_k = 3$. K_f is assumed to increase linearly from zero with decreasing ϕ_p until $\phi'_{p,c}$ at which point $K_f = K_{\text{min}}$.

Vandevivere (1995) described a similar expression for the permeability–porosity relationship. He identified two clogging mechanisms, and their weighted contributions were summed to get the permeability of the porous medium.

2.7.1 Neglected Effects of Biofilm Growth on Porous Medium

Biofilm growth in a porous medium would probably also change the pore-size distribution represented in this work by the pore-size distribution index λ. Maggi and Porporato (2007) introduced concepts with which one could account for these changes. Such changes in pore-size distribution are not included in the presented model. Also neglected are potential changes in entry pressure due to biofilm growth.

2.8 System of Equations

In an attempt to summarise the previous sections, the equations which describe the model concept including mass balance equations, sources/sinks, exchange terms, and constitutive relationships are given in Table 1. The primary variables of the system of equations are wetting phase saturation in Continuum P, non-wetting phase pressure, biomass concentration in water in Continuum P, porosity of Continuum F, and substrate concentrations in water in Continuum P and Continuum F, i.e., $S_{w,p}$, p_n, C_w^b, ϕ_f, $C_{w,p}^s$, $C_{w,f}^s$, respectively.

2.9 Numerical Model

The balance equations in Table 1 form a system of strongly coupled, non-linear partial differential equations. The complexity of the system of equations calls for a numerical solution. The numerical model used in this work is implemented within the framework of the multiphase flow simulator MUFTE-UG (Multiphase Flow, Transport, and Energy model on Unstructured Grids). MUFTE-UG has previously been used in the simulation of the infiltration of non-aqueous phase liquids in saturated and unsaturated soils, CO_2 geosequestration, salt water intrusion, flow in the cathode of fuel cells, and leakage of contaminant gas from atomic waste containers in deep rock repositories (see Assteerawatt *et al.*, 2005).

2.9.1 Spatial and Temporal Discretisation

In this work, the discretisation of the conservation equations in space is done using a vertex-centred finite volume method called the Box method (see Helmig, 1997). In the following, the Box method will be explained using the mass balance equation for water.

$$\frac{\partial([\phi_p S_{w,p} + \phi_f S_{w,f}]\varrho_w)}{\partial t} - \nabla \cdot (\varrho_w[\lambda_{w,p}K_p + \lambda_{w,f}K_f][\nabla p_w - \rho_w \mathbf{g}]) - q_w = 0, \tag{56}$$

where $\lambda_{w,\kappa}$ is the mobility of water in Continuum κ, $\lambda_{w,\kappa} = k_{rw,\kappa}/\mu_w$. Integration over the volume of a given domain Ω gives the weak form of the equation.

$$\begin{aligned} \int_\Omega \tfrac{\partial([\phi_p S_{w,p}+\phi_f S_{w,f}]\varrho_w)}{\partial t} d\Omega \quad - \int_\Omega \nabla \cdot (\varrho_w[\lambda_{w,p}K_p + \lambda_{w,f}K_f][\nabla p_w - \rho_w \mathbf{g}]) d\Omega \\ - \int_\Omega q_w d\Omega = 0 \end{aligned} \tag{57}$$

The following terms are defined for simplicity,

$$\begin{aligned} \Phi_S &:= \phi_p S_{w,p} + \phi_f S_{w,f}, \\ \psi &:= p_w - \rho_w g z, \end{aligned} \tag{58}$$

where z is vertical distance from a reference height. This gives a simplified form of the equation.

$$\int_\Omega \frac{\partial(\varrho_w \Phi_S)}{\partial t} d\Omega - \int_\Omega \nabla \cdot (\sum_\kappa \varrho_w \lambda_{w,\kappa} K_\kappa \nabla \psi) d\Omega - \int_\Omega q_w d\Omega = 0 \tag{59}$$

Table 1: System of equations ($\kappa \in \{p, f\}$, $\alpha \in \{w, n\}$)

	Continuum P	Continuum F
Mass balance equations		
Water	$\frac{\partial([\phi_p S_{w,p}+\phi_f S_{w,f}]\varrho_w)}{\partial t} + \nabla \cdot (\varrho_w[\mathbf{v}_{w,p} + \mathbf{v}_{w,f}]) = q_w$	
CO_2	$\frac{\partial([\phi_p S_{n,p}+\phi_f S_{n,f}]\varrho_n)}{\partial t} + \nabla \cdot (\varrho_n[\mathbf{v}_{n,p} + \mathbf{v}_{n,f}]) = q_n$	
Biomass	$\frac{\partial(\phi_p C^b_w S_{w,p})}{\partial t} + \nabla \cdot (C^b_w \mathbf{v}_{w,p})$ $-\nabla \cdot (D^b_p \nabla C^b_w) = q^b_p - e^b$	$\left(\frac{\varrho_b}{\varepsilon}\right) \frac{\partial \phi_f}{\partial t} = q^b_f + e^b$
Substrate	$\frac{\partial(\phi_p S_{w,p} C^s_{w,p})}{\partial t} + \nabla \cdot (C^s_{w,p} \mathbf{v}_{w,p})$ $-\nabla \cdot (D^s_p \nabla C^s_{w,p}) = q^s_{w,p} - e^s_w$	$\frac{\partial(\phi_f S_{w,f} C^s_{w,f})}{\partial t} + \nabla \cdot (C^s_{w,f} \mathbf{v}_{w,f})$ $-\nabla \cdot (D^s_f \nabla C^s_{w,f}) = q^s_{w,f} + e^s_w$
Sources and sinks		
Biomass	$q^b_\kappa = r_{g,\kappa} - r_{b,\kappa} + \hat{q}^b_\kappa$ $r_{g,p} = \mu_p \phi_p S_{w,p} C^b_w$ $\mu_\kappa = k_\mu Y \frac{C^s_{w,\kappa}}{K_s + C^s_{w,\kappa}}$ $r_{b,p} = b_p \phi_p S_{w,p} C^b_w$ $b_\kappa = b_0 + c_c S^{n_c}_{n,\kappa}$	$r_{g,f} = \mu_f (\phi_f/\varepsilon)\varrho_b$ $r_{b,f} = b_f (\phi_f/\varepsilon)\varrho_b$
Substrate	$q^s_{w,\kappa} = -r_{g,\kappa}/Y$	
Exchange terms		
Biomass	$e^b = r_a - r_d$ $r_a = k_a \phi_p S_{w,p} C^b_w$ $k_a = c_{a,1} + c_{a,2}\phi_f/\varepsilon$	$r_d = k_d (\phi_f/\varepsilon)\varrho_b$ $k_d = c_{d,1}(\phi_p S_{w,p} \lvert\nabla p_w\rvert)^{0.58}$ $+\tilde{c}_{d,2}\mu_f (\phi_f/\varepsilon)^2 \varrho_b$
Substrate	$e^s_w = D^s_{eff} \frac{M}{d_r/2}(C^s_{w,p} - C^s_{w,f})$	
Supplementary equations and constitutive relationships		
Volume fractions	$\phi_p + \phi_f/\varepsilon = \phi_0$	
Saturations	$\sum_\alpha S_{\alpha,\kappa} = 1$	
Capillary pressure	$p_c = p_n - p_w$ $p_{c,p} = p_{d,p} S^{-1/\lambda_p}_{e,p}$ $p_{c,p} = p_{c,f}$	$p_{c,f} = p_{d,f} S^{-1/\lambda_f}_{e,f}$
Intrinsic permeability	$\frac{K_p}{K_0} = \left(\frac{\phi_p - \phi_{p,c}}{\phi_0 - \phi_{p,c}}\right)^{n_k}$ for $\phi_p > \phi_{p,c}$	$K_f = K_{\min}$ for $\phi_p \leq \phi'_{p,c}$
Relative permeabilities	$k_{rw,\kappa} = S^{\frac{2+3\lambda_\kappa}{\lambda_\kappa}}_{e,\kappa}$ $k_{rn,\kappa} = (1 - S_{e,\kappa})^2 \left(1 - S^{\frac{2+\lambda_\kappa}{\lambda_\kappa}}_{e,\kappa}\right)$	
Velocities	$\mathbf{v}_{\alpha,\kappa} = -\frac{k_{r\alpha,\kappa}}{\mu_\alpha} K_\kappa (\nabla p_\alpha - \varrho_\alpha \mathbf{g})$	

The domain Ω can be discretised into elements of finite size. In the Box method, the finite volume mesh is then constructed by connecting the element barycentres with the barycentres of the element faces to obtain a dual mesh of control volumes. Each element is subdivided into n subcontrol volumes, where n is the number of vertices or nodes of the element. This is shown for two-dimensional elements in Figure 24. The spatial discretisation of the

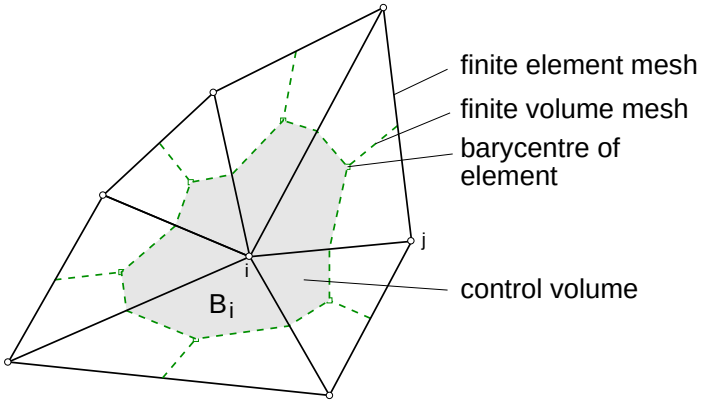

Figure 24: Construction of a control volume with the Box scheme. Each node i is assigned a control volume B_i.

equations involves describing the unknowns u exactly only at the nodes. Within each element, u is approximated using first-order ansatz functions. A given ansatz function N_j is equal to unity at the node j and zero at all other nodes. Thus, the approximated function $\tilde{u}$ is given by

$$\tilde{u} = \sum_{j=1}^{n} u_j N_j. \tag{60}$$

u_j is the exact value of u at the node j. Gradients are described in the same manner.

$$\nabla \tilde{u} = \sum_{j \in \eta_i} N_j (u_j - u_i) \tag{61}$$

η_i is the set of neighbouring nodes of the node i in a given element. Note that the geometry of the domain is approximated with the same ansatz functions as the unknowns. Insertion of the approximated values $\tilde{u}$ into Equation 59 produces an error or residual ϵ. If weighted appropriately, the error term (or weighted residual) becomes zero on the average.

$$\int_{\Omega} W_i \epsilon d\Omega \stackrel{!}{=} 0 \tag{62}$$

In the Box method, the weighting functions W_i are defined as

$$W_i = \begin{cases} 1 & \text{within the control volume } B_i \text{ of the node } i, \\ 0 & \text{otherwise.} \end{cases} \tag{63}$$

The insertion of $\tilde{u}$ into Equation 59, the application of the weighting functions W_i, and the

assumption that the time derivative can be pulled out of the volume integral yields

$$\underbrace{\sum_j \frac{\partial(\varrho_w \Phi_S)_j}{\partial t} \int_\Omega W_i N_j d\Omega}_{\text{I}} \underbrace{- \sum_{j\in\eta_i} (\psi_j - \psi_i) \int_\Omega W_i \nabla \cdot \left(\sum_\kappa \varrho_w \lambda_{w,\kappa} K_\kappa \nabla N_j \right) d\Omega}_{\text{II}} \underbrace{- \sum_j q_{wj} \int_\Omega W_i N_j d\Omega}_{\text{III}} = 0. \tag{64}$$

Term II (flux term) can be reformulated in the following way,

$$\begin{aligned} &\textstyle\sum_{j\in\eta_i} (\psi_j - \psi_i) \int_\Omega W_i \nabla \cdot \left(\sum_\kappa \varrho_w \lambda_{w,\kappa} K_\kappa \nabla N_j \right) d\Omega \\ &\quad = \textstyle\sum_{j\in\eta_i} (\psi_j - \psi_i) \int_\Omega \nabla \cdot \left(W_i \sum_\kappa \varrho_w \lambda_{w,\kappa} K_\kappa \nabla N_j \right) d\Omega \\ &\quad - \textstyle\sum_{j\in\eta_i} (\psi_j - \psi_i) \int_\Omega \nabla W_i \left(\sum_\kappa \varrho_w \lambda_{w,\kappa} K_\kappa \nabla N_j \right) d\Omega. \end{aligned} \tag{65}$$

Using the divergence theorem and the fact that $\nabla W_i = 0$, one is left with

$$\begin{aligned} &\textstyle\sum_{j\in\eta_i} (\psi_j - \psi_i) \int_\Omega W_i \nabla \cdot \left(\sum_\kappa \varrho_w \lambda_{w,\kappa} K_\kappa \nabla N_j \right) d\Omega \\ &\quad = \textstyle\sum_{j\in\eta_i} (\psi_j - \psi_i) \sum_\kappa (\varrho_w \lambda_{w,\kappa})_{ij} \oint_{\partial\Omega} W_i K_\kappa \nabla N_j \cdot \mathbf{n} d\Gamma, \end{aligned} \tag{66}$$

where $\partial\Omega$ is the surface of the domain Ω, and $\mathbf{n}$ is the unit vector normal to the surface $\partial\Omega$. The term $(\varrho_w \lambda_{w,\kappa})_{ij}$ which contains density and mobility has to be averaged between the nodes i and j. This will be discussed later. Using the definition of W_i, Term II then becomes

$$\text{Term II} = \sum_{j\in\eta_i} (\psi_j - \psi_i) \sum_\kappa (\varrho_w \lambda_{w,\kappa})_{ij} \oint_{\partial B_i} K_\kappa \nabla N_j \cdot \mathbf{n}_{\partial B_i} d\Gamma_{B_i}, \tag{67}$$

where ∂B_i is the surface of the control volume B_i associated with node i, and $\mathbf{n}_{\partial \mathbf{B_i}}$ is the unit vector normal to the surface ∂B_i. The permeability K_κ is determined as the *harmonic mean* of the permeabilities at the nodes $K_{\kappa,i}$ and $K_{\kappa,j}$.

$(\varrho_w \lambda_{w,\kappa})_{ij}$ is determined using the *fully upwind* method (see Helmig, 1997), in which case, $(\varrho_w \lambda_{w,\kappa})_{ij}$ is assigned the value of the upstream node. In this way, the direction of advective transport is taken into account in the discretisation resulting in a more stable solution.

$$(\varrho_w \lambda_{w,\kappa})_{ij} = \begin{cases} (\varrho_w \lambda_{w,\kappa})_i & \text{if} \quad (\psi_j - \psi_i) \leq 0, \\ (\varrho_w \lambda_{w,\kappa})_j & \text{if} \quad (\psi_j - \psi_i) > 0. \end{cases} \tag{68}$$

At this point, the so-called *mass matrix* M_{ij} is defined as

$$M_{ij} := \int_\Omega W_i N_j d\Omega. \tag{69}$$

The transformation of the above formulations from a finite element to a finite volume form is achieved by the use of the *mass lumping technique* (see Huber, 1999; Helmig, 1997) which involves summing the coefficients of each row of M_{ij} onto the diagonals. That is,

$$M_{ij}^{\text{lump}} = \delta_{ij} \sum_k M_{ik}. \tag{70}$$

This implies that Term I (storage term) in Equation 64 becomes

$$\text{Term I} = \sum_j \frac{\partial(\varrho_w \Phi_S)_j}{\partial t} \delta_{ij} \sum_k \int_\Omega W_i N_k d\Omega. \tag{71}$$

Since $\sum_k N_k = 1$,

$$\text{Term I} = \sum_j \frac{\partial(\varrho_w \Phi_S)_j}{\partial t} \delta_{ij} \int_\Omega W_i d\Omega. \tag{72}$$

Due to the definition of W_i,

$$\int_\Omega W_i d\Omega = \int_{B_i} dB_i = |B_i|, \tag{73}$$

where $|B_i|$ is the magnitude of the control volume B_i. Thus,

$$\begin{aligned} \text{Term I} &= \textstyle\sum_j \frac{\partial(\varrho_w \Phi_S)_j}{\partial t} \delta_{ij} |B_i|, \\ &= \frac{\partial(\varrho_w \Phi_S)_i}{\partial t} |B_i|. \end{aligned} \tag{74}$$

In the same vein, Term III (source term) of Equation 64 becomes

$$\text{Term III} = q_{wi} |B_i|. \tag{75}$$

Terms I, II, and III can be inserted into Equation 64 to give

$$\frac{(\varrho_w \Phi_S)_i}{\partial t} |B_i| - \sum_{j \in \eta_i} (\psi_j - \psi_i) \sum_\kappa (\varrho_w \lambda_{w,\kappa})_{ij} \int_{\partial B_i} K_\kappa \nabla N_j \cdot \mathbf{n}_{\partial B_i} d\Gamma - q_{wi} |B_i| = 0. \tag{76}$$

The spatial discretisation of the balance equations has been shown in this section using the balance equation of water as an example. This can be done accordingly for the other balance equations.

A *fully implicit Euler scheme*, i.e., a backward finite difference method is used for the discretisation in time. Therefore, for a given equation of the form

$$\frac{\partial u}{\partial t} = f(u), \tag{77}$$

the finite difference scheme gives

$$\frac{u^{t+\Delta t} - u^t}{\Delta t} = f(u^{t+\Delta t}), \tag{78}$$

where Δt is the time-step size. The function f is evaluated at the new time-step $t + \Delta t$.

Applying this to Equation 76 yields

$$\begin{aligned} &\left\{ (\varrho_w \Phi_S)_i^{t+\Delta t} - (\varrho_w \Phi_S)_i^t \right\} \tfrac{|B_i|}{\Delta t} \\ &- \textstyle\sum_{j \in \eta_i} (\psi_j - \psi_i)^{t+\Delta t} \sum_\kappa (\varrho_w \lambda_{w,\kappa})_{ij}^{t+\Delta t} \bar{K}_\kappa^{t+\Delta t} \int_{\partial B_i} \nabla N_j \cdot \mathbf{n}_{\partial B_i} d\Gamma - q_{wi}^{t+\Delta t} |B_i| = 0. \end{aligned} \tag{79}$$

$\bar{K}_\kappa$ is the harmonic mean of $K_{\kappa,i}$ and $K_{\kappa,j}$.

2.9.2 Solution of Non-Linear Problem

An assembly of the discretised balance equations for all control volumes gives a system of equations of the form

$$\mathbf{f}(\mathbf{u}) = \mathbf{0}. \tag{80}$$

$\mathbf{u}$ is the set of unknowns, and $\mathbf{f}$ is a non-linear function of $\mathbf{u}$. Non-linearities in the system arise from the constitutive relationships, e.g., relative permeability varies non-linearly with saturation, absolute permeability is a non-linear function of porosity in Continuum P. Using the *Newton-Raphson* method (see Helmig, 1997), the function is linearised in the following manner.

$$\mathbf{u}_{r+1} = \mathbf{u}_r - \left(\frac{\partial \mathbf{f}}{\partial \mathbf{u}}\right)_r^{-1} \cdot \mathbf{f}(\mathbf{u}_r), \tag{81}$$

where the index r stands for the iteration step. The *Jacobian* matrix $\dfrac{\partial \mathbf{f}}{\partial \mathbf{u}}$ is evaluated numerically. The UG software package provides a number of linear solvers for the solution of the linearised problem. See Bastian *et al.* (1997) and Bastian and Helmig (1999) for details.

3 Attempts at Model Verification

An important issue in numerical modelling is *verification*. Since a model is always a simplification of a physical problem, it is necessary to assess the ability of the model to answer the questions posed by the problem. The model presented in this work is based on a number of assumptions and simplifications. It also requires a good deal of empirical parameters, some describing flow in a porous medium, others quantifying biological processes, and again others describing the interaction between flow in the porous medium and biological processes. In order to gain some confidence in the results of a numerical simulation, the model needs to be tested by comparison with experimental results, analytical solutions, or other numerical models. Currently, no analytical solutions exist for the type of models considered in this work. Two experiments have been chosen from literature which deal with problems relevant to this work and with which the model presented in the previous chapter will be tested. They include an experiment with water-saturated flow through a biofilm-affected porous medium by Taylor and Jaffé (1990a) and one by Mitchell *et al.* (2009) which deals with the effect of CO_2 on a biofilm grown in a porous medium. The first experiment focuses particularly on the interaction between fluid flow and biofilm growth, while the second experiment focuses on the effect of supercritical CO_2 on the development of a biofilm.

3.1 One-Phase Flow Experiments by Taylor and Jaffé (1990a)

3.1.1 General Description

In an experimental study, Taylor and Jaffé (1990a) quantified the reduction in permeability of samples of porous media due to biomass accumulation. Two columns were packed with sand, and biofilms were grown in these columns over several months under constant flow conditions. The columns were inoculated with methanol-utilising bacteria for a few hours after which a constant methanol concentration was maintained in the influent. Pressure was measured at regular intervals along the column, and thus the permeability changes could be quantified. These experiments have been simulated with the model described in Chapter 2. In the experiments, there were "*problems with the deionised water source and the subsequent reductions in head at that time indicated that the column may have been dosed with chlorine from the public water supply*" (Taylor and Jaffé, 1990b). This makes the quantitative comparison between simulated and observed results difficult. Still, a qualitative comparison can aid in understanding the important processes and parameters.

3.1.2 Simulation Parameters

In Table 2, a list of parameters as used in the experiments by Taylor and Jaffé (1990a) is given. These include column dimensions, sand properties, temperature, flow rate, and the substrate concentration of the influent medium. In Column 1, the flow rate and the influent substrate concentration were reduced after 149 days, whereas only the influent substrate concentration was reduced in Column 2.

Table 2: Parameters for experiments by Taylor and Jaffé (1990a).

Parameter	Column 1	Column 2
Column length	0.52 m	
Column diameter	0.0508 m	
Sand porosity ϕ_0	0.347	
Sand permeability K_0	$2.93 \times 10^{-10}\,\mathrm{m}^2$	
Mean grain diameter of sand	0.7 mm	
Specific surface of sand M	$4.85 \times 10^{3}\,\mathrm{m}^{-1}$	
Temperature	15 °C	
Total operation time	284 days	356 days
For t $\leq$ 149 days		
Influent substrate concentration	$7.20 \times 10^{-3}\,\mathrm{kg/m^3}$	$5.59 \times 10^{-3}\,\mathrm{kg/m^3}$
Flow rate	$2.22 \times 10^{-5}\,\mathrm{m^3/s}$	$7.38 \times 10^{-6}\,\mathrm{m^3/s}$
For t $>$ 149 days		
Influent substrate concentration	$5.20 \times 10^{-3}\,\mathrm{kg/m^3}$	$4.70 \times 10^{-3}\,\mathrm{kg/m^3}$
Flow rate	$1.37 \times 10^{-5}\,\mathrm{m^3/s}$	$7.38 \times 10^{-6}\,\mathrm{m^3/s}$

Taylor and Jaffé (1990b) developed a numerical model with which they simulated part of the experiment described above. The parameters used in those simulations are listed in Table 3.

Table 3: Parameters used for simulation in Taylor and Jaffé (1990b).

Parameter	Value	
	Column 1	Column 2
Water viscosity μ_w	$1.139 \times 10^{-3}\,\mathrm{Pa \cdot s}$	
Maximum substrate utilisation rate k_μ	$8.91 \times 10^{-5}\,\mathrm{s^{-1}}$	
Monod half-saturation coefficient K_s	$7.99 \times 10^{-4}\,\mathrm{kg/m^3}$	
Yield coefficient Y	0.0975 kg/kg	
Endogenous decay rate b_0	$3.18 \times 10^{-7}\,\mathrm{s^{-1}}$	
Biofilm density ϱ_b	$3\,\mathrm{kg/m^3}$	$2.5\,\mathrm{kg/m^3}$
Attachment rate parameter $c_{a,1}$	7.40×10^{-3}	
Attachment rate parameter $c_{a,2}$	7.88×10^{-2}	

The experiments have been simulated with the model developed in Chapter 2. However, since this is a one-phase flow problem, the mass balance equation for CO_2 is not necessary,

and both wetting-phase saturations are equal to unity. Thus, one is left with a system of equations which is a lot simpler than that of Table 1. This is advantageous because the number of empirical parameters which require fitting is less than in the original system.

The initial and boundary conditions for the problem are given in Table 4. Since the problem is one-dimensional, only boundary conditions at the ends of the columns are given (see Figure 25). The domain is discretised with 22 uniform elements, i.e., a discretisation length of 0.0236 m. In Section 2.7, the parameters needed to describe changes in permeability were

Table 4: Initial and boundary conditions.

Parameter	Value	
	Column 1	Column 2
Initial conditions		
p_w	101325 Pa	
C_w^b	$0\,\mathrm{kg/m^3}$	
$C_{w,p}^s$	$7.20 \times 10^{-3}\,\mathrm{kg/m^3}$	$5.59 \times 10^{-3}\,\mathrm{kg/m^3}$
$C_{w,f}^s$	$0\,\mathrm{kg/m^3}$	
Boundary conditions at $x = 0\,\mathrm{m}$		
Water flux (Neumann)	as given in Table 2	
C_w^b (Dirichlet)	$5 \times 10^{-3}\,\mathrm{kg/m^3}$ for $t \leq 0.212\,\mathrm{days}$	
(Neumann)	$0\,\mathrm{kg/m^3}$ otherwise	
$C_{w,p}^s$ (Dirichlet)	as given in Table 2	
$C_{w,f}^s$ (Neumann)	no flow	
Boundary conditions at $x = 0.52\,\mathrm{m}$		
p_w (Dirichlet)	101325 Pa	
C_w^b (Dirichlet)	$0\,\mathrm{kg/m^3}$	
C_w^s (Dirichlet)	$0\,\mathrm{kg/m^3}$	
C_f^s (Dirichlet)	$0\,\mathrm{kg/m^3}$	

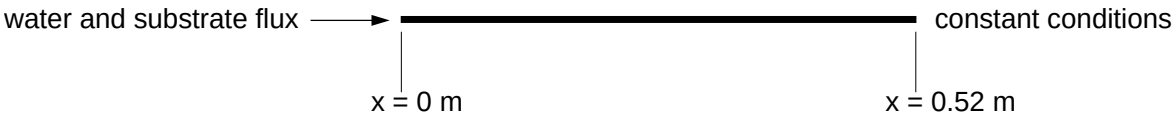

Figure 25: Schematic diagram of experiment with boundary conditions at the ends of the column.

Table 5: Values of fitted parameters.

Parameter	Value
$c_{d,1}$	2.9×10^{-8}
$\tilde{c}_{d,2}$	6
$K_{\min}$	$7.33 \times 10^{-20}\,\mathrm{m^2}$

fitted to data given by Cunningham *et al.* (1991) for sands with median grain sizes of 0.54 mm

and 0.70 mm. The permeabilites of these sands were $2.17 \times 10^{-10}\,\mathrm{m}^2$ and $3.19 \times 10^{-10}\,\mathrm{m}^2$, respectively. These values are very close to those of the sand used by Taylor and Jaffé (1990a) (mean grain size: 0.70 mm, permeability: $2.93 \times 10^{-10}\,\mathrm{m}^2$). Thus, the set of parameters from Section 2.7 shown in Figure 22 are deemed appropriate for the description of changes in permeability in this experiment. They include $\phi_{p,c}/\phi_0 = 0.6$, $n_k = 3$, and $\phi'_{p,c}/\phi_0 = 0.8$. However, $K_{\min}$ is assumed to be unknown and will be fitted to the experimental results. The sand used by Taylor and Jaffé (1990a) had a declared permeability of $2.93 \times 10^{-10}\,\mathrm{m}^2$. However, judging from their results, the measured permeabilities of the sands unaffected by biomass was a bit lower than K_0. For this reason, in the simulations, the maximum permeability is taken to be $1.42 \times 10^{-10}\,\mathrm{m}^2$.

Other parameters used in the simulation include water density $\varrho_w = 1000\,\mathrm{kg/m}^3$, the dispersion coefficients $D_p^b = D_p^s = \phi_p \times 10^{-8}\,\mathrm{m}^2/\mathrm{s}$ and $D_f^s = \phi_f \times 10^{-8}\,\mathrm{m}^2/\mathrm{s}$, and the effective diffusion coefficient $D_{eff}^s = \varepsilon \times 10^{-9}\,\mathrm{m}^2/\mathrm{s}$. The average pore diameter of the sand is estimated using the empirical relation $d_r = 6\phi_0/M$, therefore, $d_r = 0.07$ mm. Zhang and Bishop (1994) observed variations in biofilm porosity ε ranging from 0.58 to 0.93. Here, ε is assigned a value of 0.8. However, the results of the simulation were not very sensitive to changes in ε. The attachment parameters $c_{a,1}$ and $c_{a,2}$ were fitted in the simulations by Taylor and Jaffé (1990a) (see Table 2).

Three parameters had to be fitted in the simulation of the experiments. They include the two detachment rate parameters $c_{d,1}$ and $\tilde{c}_{d,2}$, and the permeability value $K_{\min}$. They were fitted in the simulation of Column 1 and remained unchanged for Column 2. See Table 5 for the values. $c_{d,1}$ directly influences the speed of the biofilm front moving through the column. The value for $K_{\min}$ is relatively low suggesting that advective flow of fluids through the biofilm may be negligible for the prediction of changes in permeability in these experiments.

3.1.3 Results

Figure 26 shows the results of the simulations using the parameters and conditions described above. The logarithmic reduction of permeability caused by biofilm growth is plotted over distance into the columns. The biofilm grows by utilising the substrate at the inlet causing a decrease in permeability. Since the inflow rate is kept constant, this results in a pressure build-up near the inlet. High pressure gradients cause high biomass detachment from the biofilm. Detached cells get transported downstream, where they reattach. This results in an encroachment of the biofilm into the column, the extent of which is dependent on the inflow rate. Three parameters were fitted to the observed results of Column 1 and were used in the prediction of the permeability reduction in Column 2. The simulated permeability reduction in Column 1 was less than observed in the experiments. In Column 2, the simulated biofilm advanced further into the column than in the experiments. The differences between simulations and experiments may result from shortcomings of the model concept, e.g., the assumption that the biofilm density is constant or the way biofilm decay is treated. Biofilm density may vary with biofilm age and external conditions. This is not accounted for in the model. In the model concept, decay of biomass within the biofilm immediately leads to a reduction of the pore space occupied by the biofilm. In reality, obviously, it may

take some amount of time for dead biomass to be removed. However, as discussed in Section 3.1.1, due to problems which occurred in the experiments, the aim of this comparison is mostly qualitative. Column 1 is affected by biomass throughout the column, whereas the biofilm affects only part of Column 2. This can be seen in both the experimental and the simulated results. The permeability values of both experimental and numerical results near the inlet fluctuate in space. However, these fluctuations are more pronounced in the simulation. This is probably due to the instability of the solution just before or after Continuum P becomes fully clogged ($K_P = 0$). This is however exaggerated by the logarithmic scale. Figure 27 shows the distribution of attached biomass within the two columns. Further results of the simulation are shown in Figure 28. Suspended biomass concentrations are highest near the inlet. Since, the experiments were run with constant flow, the distribution of pressure depends on permeability. Consequently, the pressure gradient is high in areas with high amounts of attached biomass.

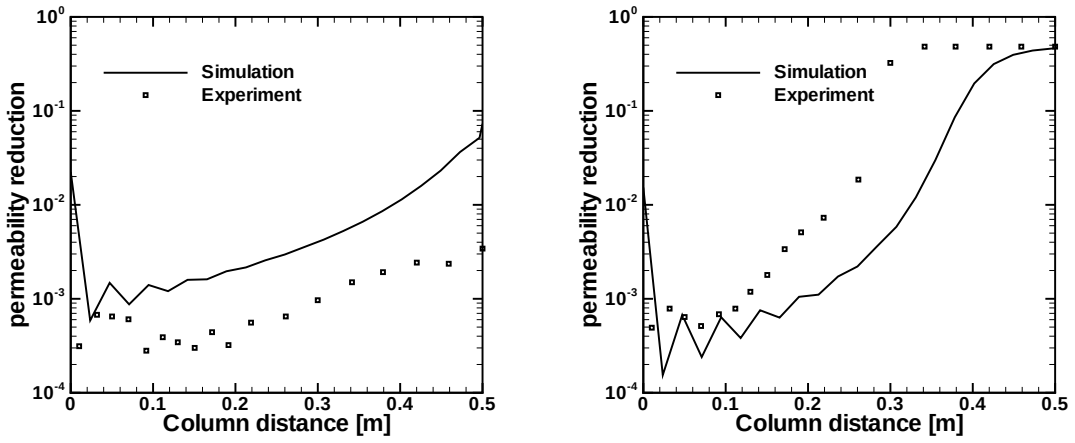

(a) Column 1 (b) Column 2

Figure 26: Comparison of simulated permeability reduction to the experimental results of Taylor and Jaffé (1990a). The parameters $c_{d,2}$, $\tilde{c}_{d,2}$, and $K_{\min}$ were fitted to the experimental data in Column 1. Possible reasons for the differences between simulations and experimental results are discussed in Section 3.1.3

3.2 Experiments by Mitchell *et al.* (2009) with Two Phases

3.2.1 General Description

The experiments described in Section 3.1 deal with biofilm development in a one-phase flow system and concentrate on the interaction between fluid flow and biomass accumulation. In the experiments conducted by Mitchell *et al.* (2009), the focus is on the effect of biofilm growth on the permeability of a porous medium and on the effect of supercritical CO_2 on the

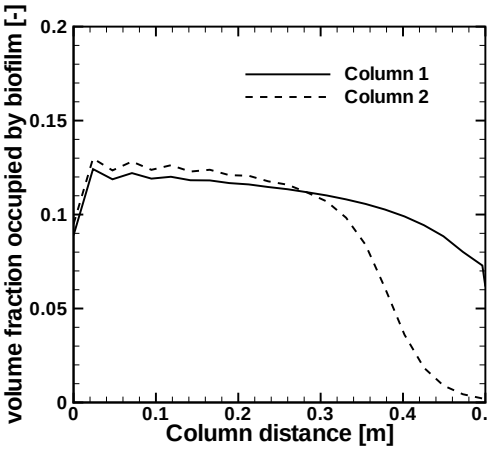

Figure 27: Simulation results: fraction of pore space occupied by biofilm ϕ_f/ε. The biofilm is almost uniformly distributed in the first half of the columns. In Column 2, there is a strong drop in the amount of attached biomass towards the outlet.

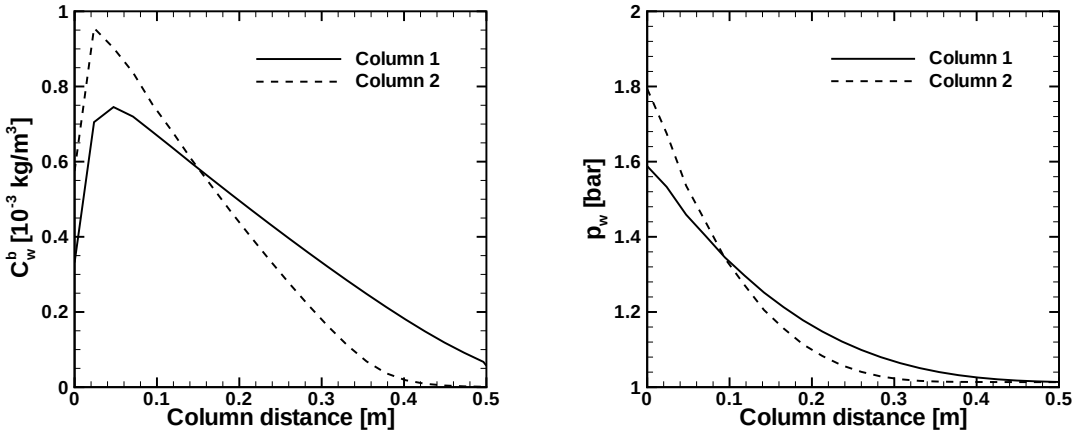

(a) Biomass concentration in water C_w^b

(b) Pressure p_w

Figure 28: Simulation results: (a) The concentrations of suspended biomass is high near the inlet and decreases continuously towards the outlet. The pressure gradient is strongly dependent on permeability (see Figure 27).

biofilm. The experiments were conducted at high pressure (89 bar) and moderate temperature (32°C). Two sandstone cores were inoculated with $Shewanella\ fridgidimarina$. The general strategy in the experiments was to grow a biofilm in the sandstone core and challenge the biofilm with supercritical CO_2. A saline nutrient media was injected once or twice a day in pulses lasting between 20 and 200 min. With each pulse, the permeability of the core was calculated. The permeabilities of both cores were observed to decrease by more than 95 % and increased only slightly after the CO_2 flood. The bacteria species $S.\ fridgidimarina$ which was used to inoculate the cores was succeeded by other species originally present in the cores, namely, $Bacillus\ mojavensis$ and $Citrobacter$ sp. Please refer to Mitchell *et al.* (2009) for further details on the experiments.

3.2.2 Simulation Parameters

The properties of the sandstone cores and the conditions at which the experiments were run are given in Table 6. Also given in the table is the duration of each experiment. The experiments can be divided into different phases depending on the influent medium. Initially, a saline nutrient medium was injected into the cores at intervals as mentioned in Section 3.2.1. This phase will be referred to as the *growth phase*. In Experiment 1, the growth phase was followed directly by a flooding of the core with CO_2. After the growth phase in Experiment 2, a nutrient-depleted saline solution was injected (*starvation phase*). This was followed by the injection of CO_2, a second starvation phase, and another CO_2 challenge. The different phases of the experiments are summarised in Table 7.

Table 6: Parameters for experiments by Mitchell *et al.* (2009).

Parameter	Experiment 1	Experiment 2
Column length	0.0508 m	0.1185 m
Sandstone porosity ϕ_0	0.22	
Sandstone permeability K_0	38.96×10^{-15} m^2	47.13×10^{-15} m^2
Pressure	89 bar	
Temperature	32 °C	
Total operation time	20.67 days	34.58 days

Table 7: Duration of the different phases of the experiments by Mitchell *et al.* (2009).

	Growth I	Starvation II	CO_2 III	Starvation IV	CO_2 V
Experiment 1	20 days	-	0.67 days	-	-
Experiment 2	12.5 days	15.13 days	4.21 days	0.75 days	2 days

Due to lack of information and for simplicity, the following assumptions will be made in the simulation.

- The periods of flow through the core are neglected. This means that no spatial discretisation is necessary since there are no spatial gradients.

- The effect of suspended biomass is neglected. This implies that the balance equation for biomass in Continuum P is omitted, and there are no attachment or detachment rates.
- During the growth phase, the nutrients needed by the bacterial cells are abundantly available, i.e., the growth rate is independent of the substrate concentration, $\mu_f = k_\mu Y$. The opposite is the case during the starvation phase, $\mu_f = 0$. Therefore, no balance equations for substrate are solved.
- The pore-size distribution and entry pressure of the rock and the biofilm are unknown. The same goes for the amount of CO_2 in the cores during the flooding of the cores with CO_2. Obviously, any fitting of parameters would not be unique. Instead, it will be assumed that λ_κ and $p_{d,\kappa}$ are known, and the CO_2 saturation at the start of the CO_2 challenge is fitted to the experimental data.

With the above assumptions, the mass balance equations from Table 1 simplify to the following.

$$\begin{aligned} \tfrac{d(\phi_p S_{w,p}+\phi_f S_{w,f})}{dt} &= q_w/\varrho_w \\ \tfrac{d(\phi_p S_{n,p}+\phi_f S_{n,f})}{dt} &= q_n/\varrho_n \\ \tfrac{1}{\phi_f}\tfrac{d\phi_f}{dt} &= \mu_f - b_0 - c_c S_{n,f}^{n_c} \end{aligned} \tag{82}$$

The source/sink term q_w is chosen in such a way that the water-phase pressure p_w remains unchanged, whereas, $q_n = 0$. The reason for this will be explained with the following example. When a sandstone core with biofilm is filled with CO_2, some biofilm decays releasing intracellular water. Since the model does not account for intracellular water within the biofilm, this would lead to an unrealistic decrease in pressure in the simulation. This transfer of intracellular to extracellular water is accounted for here with the source term q_w. During the growth phase, q_w is a sink term. The source/sink term q_n, however, is always set to zero.

In Table 8, the set of parameters used for the simulation of the two experiments are listed. Some of the parameters are estimated based on values from literature. As mentioned above, assumptions have been made for the pore-size distribution indices, entry pressures, and residual saturations of the two phases in the two continua. Three parameters have been fitted to the results of Experiment 2. One of the fitted parameters is the CO_2 saturation at the beginning of a CO_2 challenge. In the experiments, CO_2 was injected into the sandstone core for a period of time after which the core was closed and allowed to rest. The CO_2 saturation at the end of the injection is not known, and thus it is fitted to the results of Experiment 2.

The growth phase is initialised, in the experiments, by injecting bacteria suspended in water into the cores and letting the bacteria attach to the rock. In the simulation, the porosity of Continuum F is initialised with $\phi_f = 10^{-4} \cdot \varepsilon$.

3.2.3 Results

The growth of biofilm within the sandstone core causes a permeability reduction. At some point, a minimum permeability value is achieved. In the experiments, this occurs after a

Table 8: Parameters for simulation of experiments.

Parameter	Value	Comment
Growth rate μ_f	$4.63 \times 10^{-5}\,\mathrm{s}^{-1}$	
Endogenous decay rate b_0	$3.18 \times 10^{-7}\,\mathrm{s}^{-1}$	from Taylor and Jaffé (1990b)
Decay rate parameter c_c	$8.7 \times 10^{-4}\,\mathrm{s}^{-1}$	estimated from Mitchell *et al.* (2008)
Decay rate parameter n_c	3	fitted to Experiment 2
Permeability parameter $\phi_{p,c}/\phi_0$	0.35	fitted to Experiment 2
Permeability parameter n_k	3	
Minimum permeability $K_{\min}$	$5.0 \times 10^{-16}\,\mathrm{m}^2$	taken from experimental data
Biofilm porosity ε	0.8	estimated from Zhang and Bishop (1994)
Pore-size distribution indices		
λ_p	2	
λ_f	0.5	
Entry pressures		
$p_{d,p}$	0.1 bar	
$p_{d,f}$	0.25 bar	
Residual saturations		
$S_{wr,p}$	0.15	
$S_{wr,f}$	0.3	
$S_{nr,p}$	0.05	
$S_{nr,f}$	0	
$S_{n,p}$ at start of each CO_2 challenge	0.8	fitted to Experiment 2

small increase in permeability (see Figure 29). In both experiments, this occurs at about $t \approx 5$ days. The reason for this increase is not clear. Possibly, it occurs due to nutrient limitations at that point. Since no nutrient limitations are accounted for in the simulation, no such increase was modelled. Instead, the permeability decreases monotonously and stagnates at the minimum value of 5×10^{-16} m^2. In Experiment 1, the growth phase is followed directly by a CO_2 challenge in which a slight increase in permeability was observed. The simulation does not show this increase in permeability. However, the effect of the CO_2 on the biofilm can be seen in the sharp decrease in the amount of pore space occupied by the biofilm ϕ_f/ε (see Figure 29). In Experiment 2, the growth phase is followed by a starvation phase. In the first starvation phase, the permeability remains constantly low. The simulation shows a steady decrease in ϕ_f/ε corresponding to the endogenous decay rate. This first starvation phase is followed by the first CO_2 challenge, a second short starvation phase, and finally the second CO_2 challenge. Both the experiment and simulation show slight increases in permeability in each of the last three phases.

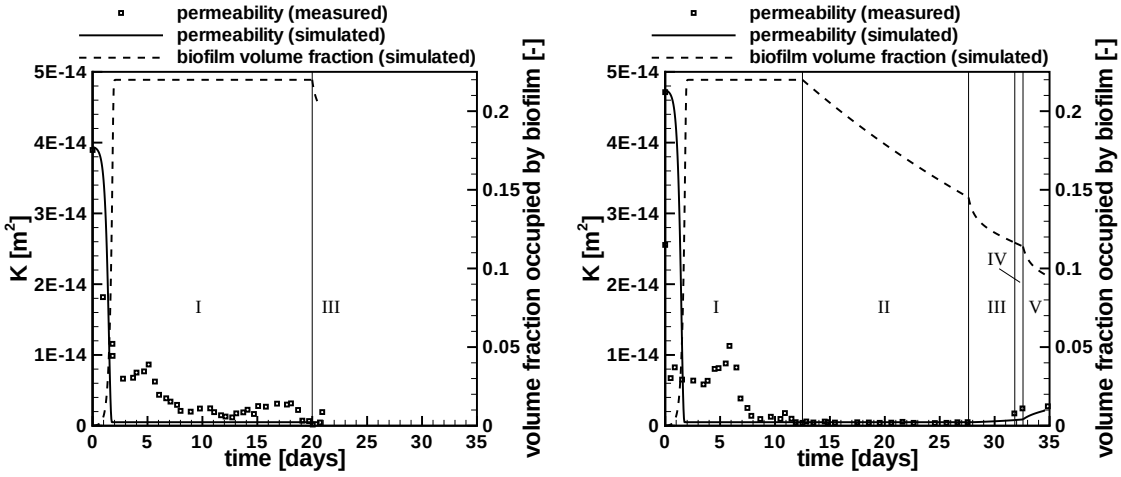

(a) Experiment 1

(b) Experiment 2

Figure 29: Comparison of simulated permeability changes to the experimental results of Mitchell *et al.* (2009). Three parameters were fitted to Experiment 2 and remained unchanged for the simulation of Experiment 1. The symbols show the measured permeabilities of the sandstone cores in the experiments by Mitchell *et al.* (2009), and the continuous lines show the permeabilities of the cores in the simulation. The dashed lines show the volume fractions of pore space occupied by attached biomass, which is equivalent to ϕ_f/ε.

3.3 Remarks

The model described in Chapter 2 was tested by modelling experiments from literature and comparing the simulations to experimental results. Two experiments were chosen, one dealing primarily with the interaction between flow and biofilm growth, and the other dealing

with the effect of supercritical CO_2 on a biofilm. In order to model these experiments numerically, a number of assumptions and simplifications had to be made. Each of the experiments consisted of two runs, each with a different set of parameters and conditions. The model was fitted to one of the two runs and used to predict the results of the other. For the experiments by Taylor and Jaffé (1990a), three model parameters were fitted, and three other parameters were fitted to the experiments by Mitchell *et al.* (2009). The values of the fitted parameters may not be unique. This may question the capability of these comparisons to verify the model. However, it is an excellent way of testing the model and getting a feel for the important parameters and the implications of the modelling assumptions.

4 Model Application

A model which describes biomass accumulation in the subsurface by accounting for growth of attached biomass, transport of suspended biomass and one growth-limiting substrate, and the flow of two fluid phases was introduced in Chapter 2 and tested in Chapter 3. This chapter focuses on the application of the model in simulations of processes in the vicinity of a CO_2 injection well. The simulations are expected to give some insight into the feasibility of CO_2 leakage mitigation with biofilms.

4.1 General Description

The problem set-up is similar to that used in the leakage simulations run by Kopp *et al.* (2007) with which they investigated the thermal effects of leaking CO_2 (see also Pruess, 2004). In this work, however, the interest is on the caprock and the target formation which are both included in the model domain as is shown in Figure 30. The caprock around the well is assumed to have been damaged, for example, during the drilling of the well or as a result of high pressures during injection. The damaged caprock is a leakage pathway for CO_2 from the storage reservoir. In the following, different strategies aimed at minimising CO_2 leakage using biofilms will be investigated with simulations.

4.2 Description of Model Domain and Simulation Parameters

The model domain is radially symmetric, i.e., two-dimensional (r, z), with a radius of 100 m and a thickness of 20 m. The bottom of the domain is at 1000 m depth. As shown in Figure 31, the caprock and the storage aquifer both have a thickness of 10 m, and the caprock is damaged up to a radius of 0.5 m. The properties of the formation are summarised in Table 9. Also given in Table 9 are biofilm porosity ε and the parameters required to calculate permeability changes. These have been taken from the simulations in Section 3.2 (see Table 8 on page 49). Fluid properties as used in the simulations are given in Table 10. The properties of brine are assumed to be constant, whereas those of CO_2 vary with pressure. The biological parameters, i.e., growth and decay parameters used in the simulations are given in Table 11. Biomass attachment and detachment parameters have been taken from the simulations in Section 3.1 (see Table 12). Capillary pressure and relative permeabilities are calculated with the parameters given in Table 13. Other parameters include the specific surface area of the rock formation $M = 2.2 \times 10^4\,\mathrm{m}^{-1}$, the dispersion coefficients $D_p^b = D_p^s = \phi_p \times 10^{-8}\,\mathrm{m}^2/\mathrm{s}$ and $D_f^s = \phi_f \times 10^{-8}\,\mathrm{m}^2/\mathrm{s}$, and the effective diffusion coefficient $D_{eff}^s = \varepsilon \times 10^{-9}\,\mathrm{m}^2/\mathrm{s}$.

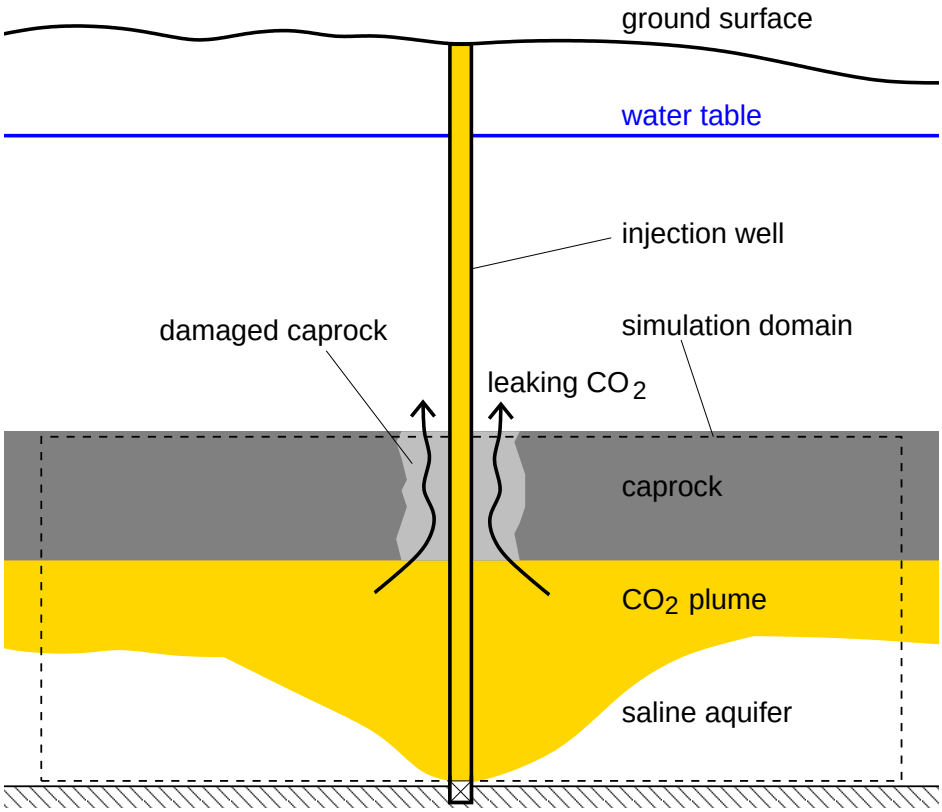

Figure 30: Sketch of leakage scenario. The caprock near the injection well is damaged and serves as a leakage pathway for CO_2. The simulation domain comprises the caprock and the saline aquifer in which the CO_2 is stored.

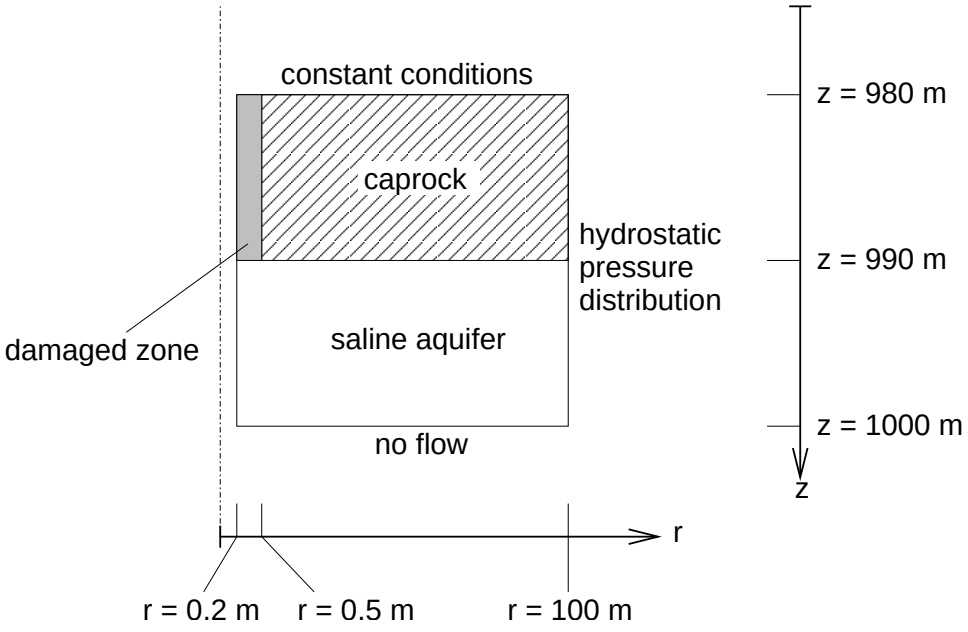

Figure 31: Boundary conditions for the radially symmetric domain.

Table 9: Properties of formation and hydraulic properties of biofilm.

Property	Value	Comment
Aquifer permeability	$50 \times 10^{-15}\,\mathrm{m}^2$	
Aquifer porosity	0.22	
Aquifer thickness	10 m	
Caprock permeability	$1 \times 10^{-18}\,\mathrm{m}^2$	
Caprock porosity	0.22	
Caprock thickness	10 m	
Permeability of damaged zone	$20 \times 10^{-15}\,\mathrm{m}^2$	
Porosity of damaged zone	0.22	
Radius of damaged zone	0.5 m	
Permeability parameter $\phi_{p,c}/\phi_0$	0.35	from Table 8 on page 49
Permeability parameter n_k	3	
Minimum permeability $K_{\min}$	$0.01 \cdot K_0$	
Biofilm porosity ε	0.8	
Depth at bottom of aquifer	1000 m	
Injection well radius	0.2 m	
Domain radius	100 m	
Temperature T	$40\,^\circ\mathrm{C}$	isothermal

Table 10: Fluid properties.

Property	Value	Comment
Brine salinity	0.15 kg/kg	see Section 2.3.2
Brine density ϱ_w	$1102\,\mathrm{kg/m^3}$	Batzle and Wang (1992)
Brine viscosity μ_w	$9.63 \times 10^{-4}\,\mathrm{Pa \cdot s}$	Batzle and Wang (1992)
CO_2 density ϱ_n	$f(p,T)$	Span and Wagner (1996)
CO_2 viscosity μ_n	$f(p,T)$	Fenghour *et al.* (1998)

Table 11: Biological parameters.

Parameter	Value	Comment
Maximum substrate utilisation rate k_μ	$8.91 \times 10^{-5}\,\mathrm{s}^{-1}$	from Table 3 on page 42
Monod half-saturation coefficient K_s	$7.99 \times 10^{-4}\,\mathrm{kg/m^3}$	
Yield coefficient Y	0.0975 kg/kg	
Endogenous decay rate b_0	$3.18 \times 10^{-7}\,\mathrm{s}^{-1}$	
Decay rate parameter c_c	$8.7 \times 10^{-4}\,\mathrm{s}^{-1}$	from Table 8 on page 49
Decay rate parameter n_c	3	
Biofilm density ϱ_b	$15\,\mathrm{kg/m^3}$	

Table 12: Biomass attachment and detachment parameters.

Parameter	Value	Comment
Attachment rate parameter $c_{a,1}$	7.40×10^{-3}	from Section 3.1
Attachment rate parameter $c_{a,2}$	7.88×10^{-2}	
Detachment rate parameter $c_{d,1}$	2.9×10^{-8}	
Detachment rate parameter $\tilde{c}_{d,2}$	6	

Table 13: Capillary pressure and relative permeabilities (from Table 8 on page 49).

Parameter	Value
Pore-size distribution indices	
λ_p	2
λ_f	0.5
Entry pressures	
$p_{d,p}$	0.1 bar
$p_{d,f}$	0.25 bar
Residual saturations	
$S_{wr,p}$	0.15
$S_{wr,f}$	0.3
$S_{nr,p}$	0.05
$S_{nr,f}$	0

Even though the model domain has a radius of 100 m, only the first 10 m are of interest and are finely meshed. This is done to capture relevant processes near the well. The mesh in the outer region ($r > 10\,\mathrm{m}$) is very coarse and only supposed to reduce the influence of the lateral boundary conditions, especially pressure, on the system. Figure 32 shows the mesh over the whole domain, and Figure 33 shows the area near the well. In vertical direction, the mesh is uniform with a size of 0.5 m, whereas in the horizontal direction, the element size varies between 0.2 m at the injection well and 42 m at the outer boundary.

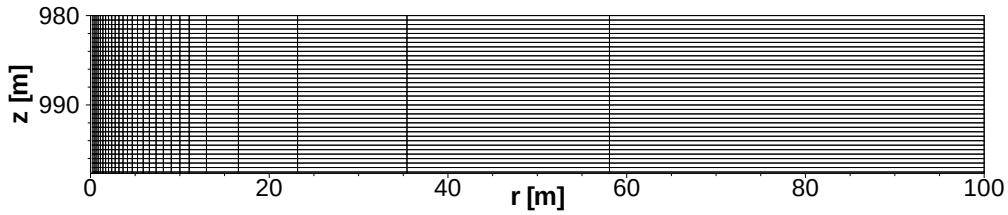

Figure 32: Simulation mesh.

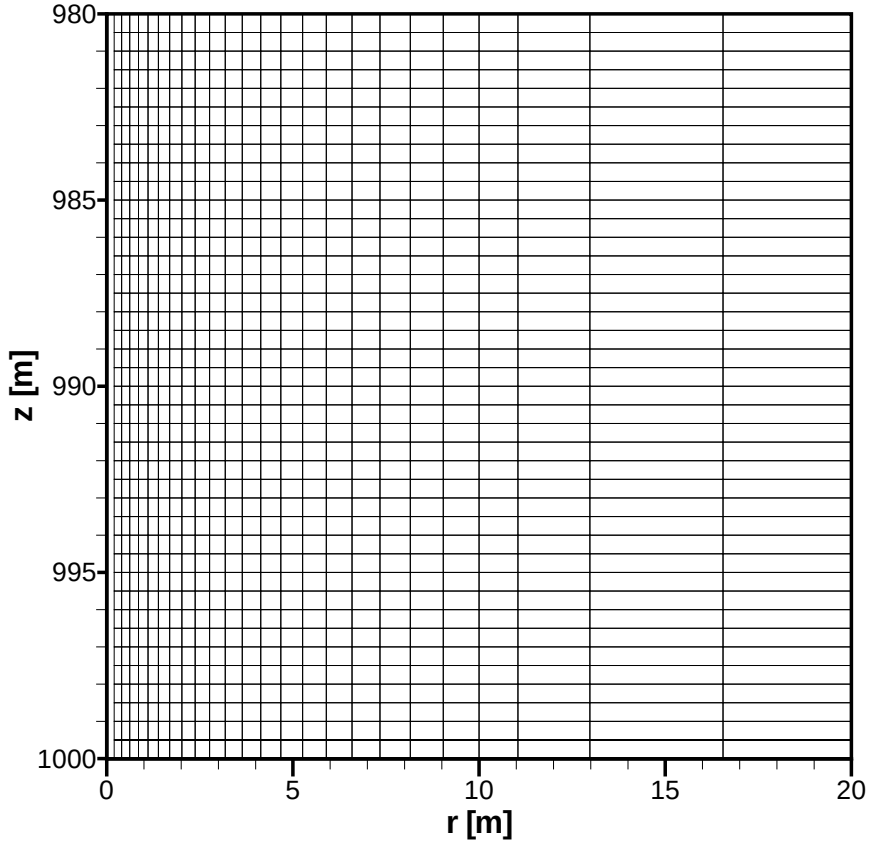

Figure 33: Simulation mesh near the well.

4.3 Reference Simulation: Clogging of Damaged Caprock

The simulation in this section describes the injection of bacteria and substrate into the formation described in Section 4.2 and the subsequent injection of CO_2. The injected bacteria is expected to attach to the surface of the formation rock. Given the abundance of nutrients near the well, the bacteria can reproduce to form a biofilm occupying pore space and reducing the permeability of the formation rock, thus, preventing the CO_2 from leaking out of the formation.

4.3.1 Initial and Boundary Conditions

The formation is assumed to be initially filled with brine under hydrostatic conditions. It is also assumed that there is no biomass or substrate in the system. These conditions are assigned to the top and outer boundaries as boundary conditions. The bottom boundary is a no-flow boundary. The boundary conditions are shown in Figure 31. The inner boundary, i.e., the injection well is also a no-flow boundary except at the interval over which water or CO_2 is being injected. Initially, water with suspended biomass is injected into the formation. This is followed by the injection of the nutrient medium containing the substrate. This, in turn, is followed by the injection of CO_2. This injection strategy is illustrated in Figure 34. Different regions $A, B, C,$ and D have been demarcated, each representing a different set of

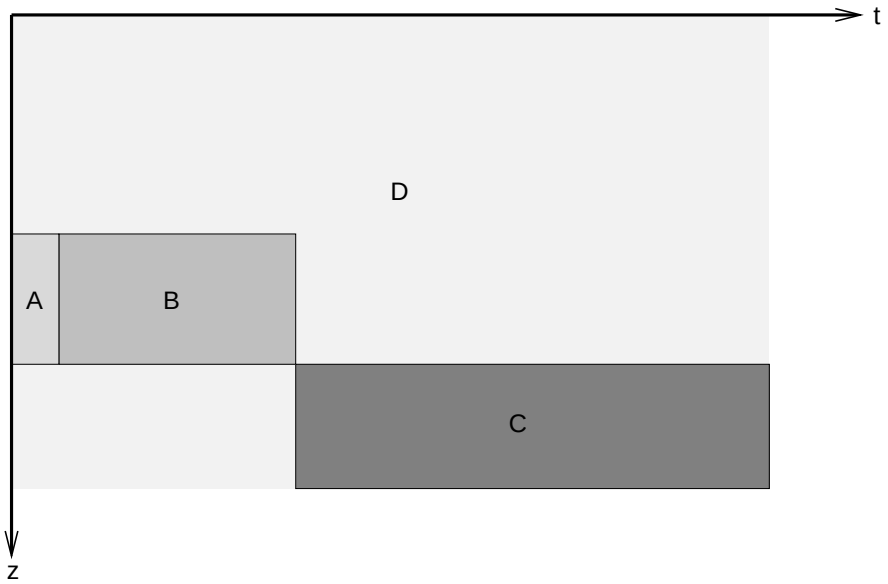

Figure 34: Reference simulation: Boundary conditions at the well.

boundary conditions at the well as listed below. The total simulation time is 400 days.

A $(0 \leq t < 0.167\,\text{days}; 989.25 < z < 994.75\,\text{m})$

- Water flow: $0.5\,\text{kg/s}$

- CO_2 flow: no flow
- Biomass flow: $4.54 \times 10^{-7}\,\mathrm{kg/s}$.
  This corresponds to a biomass concentration in the injected medium of $10^{-3}\,\mathrm{kg/m^3}$.
- Substrate flow: no flow

B $(0.167 \leq t < 90\,\mathrm{days};\ 989.25 < z < 994.75\,\mathrm{m})$

- Water flow: 0.5 kg/s
- CO_2 flow: no flow
- Biomass flow: no flow
- Substrate flow (Continuum P): $1.13 \times 10^{-4}\,\mathrm{kg/s}$.
  This corresponds to a substrate concentration in the injected medium of $0.25\,\mathrm{kg/m^3}$.
- Substrate flow (Continuum F): no flow

C $(90 \leq t \leq 400\,\mathrm{days};\ 994.75 < z \leq 1000\,\mathrm{m})$

- Water flow: no flow
- CO_2 flow: 0.5 kg/s
- Biomass flow: no flow
- Substrate flow: no flow

D $(0 \leq t \leq 400\,\mathrm{days})$

- No-flow conditions.

4.3.2 Results

The development of the biofilm in the vicinity of the injection well with time can be seen in Figure 35. The figures show the biofilm volume fraction ϕ_f/ε at six different times (10, 40, 90, 100, 140, and 400 days). The biofilm develops in the region into which the bacteria and substrate are injected. At $t = 90\,\mathrm{days}$, the injection of substrate is stopped and the injection of CO_2 starts leading to a reduction of attached biomass with time. At the end of the simulation ($t = 400\,\mathrm{days}$), there is almost no biofilm left in the formation. The reduction of the amount of attached biomass is caused primarily by endogenous decay because the bacteria within the biofilm are protected from the supercritical CO_2. Suspended bacteria, however, are not protected from the biocidal effects of supercritical CO_2. That is why the concentration of suspended biomass in water drops strongly when CO_2 is injected into the formation as can be seen in Figure 36. At $t = 100\,\mathrm{days}$, most of the suspended biomass has been destroyed by CO_2. Before the injection of CO_2, the concentration of suspended biomass in water C_w^b is high within the region in which the biofilm is developing. Some of the suspended biomass attaches to the biofilm, while some of the attached biomass detaches

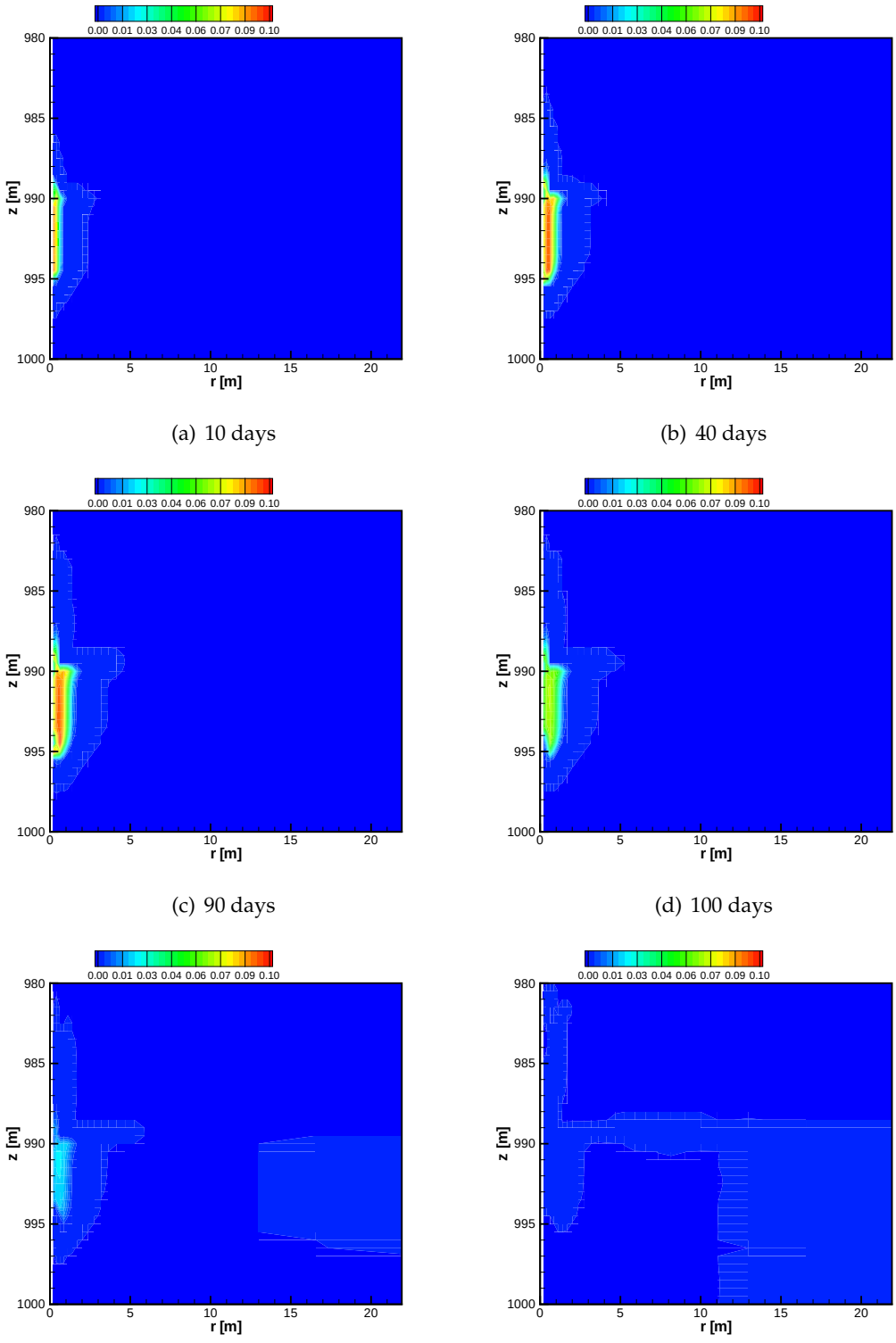

(a) 10 days

(b) 40 days

(c) 90 days

(d) 100 days

(e) 140 days

(f) 400 days

Figure 35: Results of reference simulation: Volume fraction of space occupied by biofilm ϕ_f/ε.

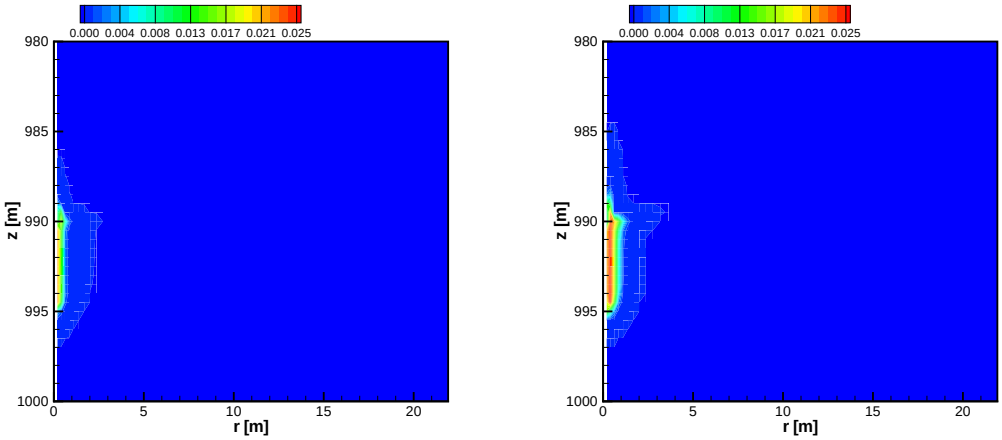

(a) 10 days

(b) 40 days

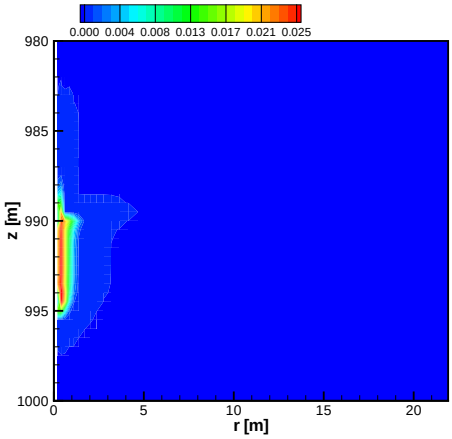

(c) 90 days

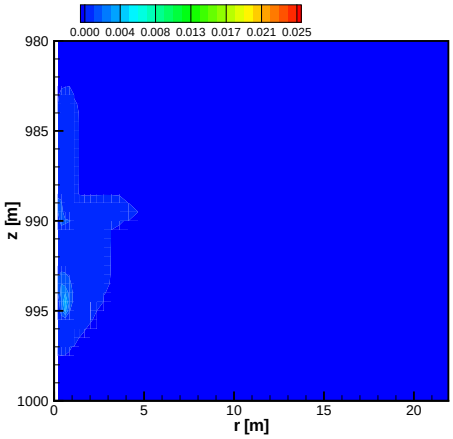

(d) 100 days

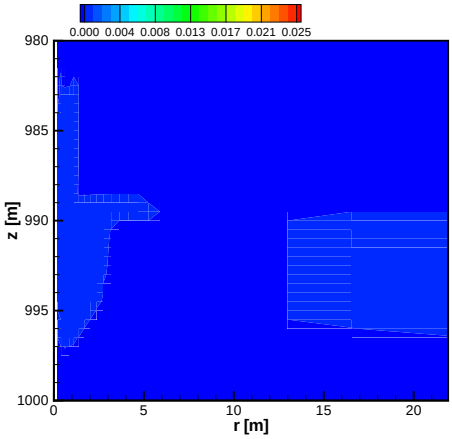

(e) 140 days

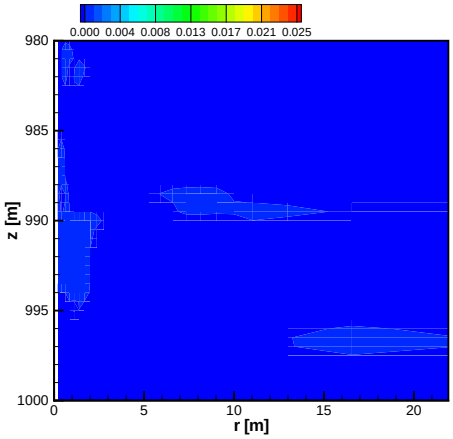

(f) 400 days

Figure 36: Results of reference simulation: Concentration of suspended biomass in water C_w^b.

(especially in the regions with high pressure gradients) and is transported advectively with the injected water.

Figure 37 shows the total amount of attached and suspended biomass in the formation with respect to time. As substrate is injected, the biomass in the system increases steadily. When the injection of substrate is stopped, the amount of biomass reduces strongly. As mentioned earlier, this is as a result of the combination of endogenous decay and the biocidal effect of supercritical CO_2. However, one can see in the figure that the CO_2 kills almost all the suspended bacteria in a very short time, whereas the bacteria in the biofilm are – to an extent – protected from the CO_2.

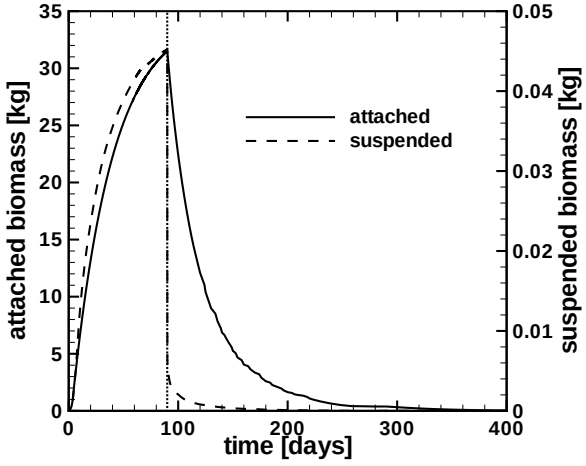

Figure 37: Reference simulation: Amount of biomass (attached and suspended) in the formation. The dotted vertical line at $t = 90\,\mathrm{days}$ marks the end of substrate injection and the start of CO_2 injection. Since suspended bacteria are more susceptible to the adverse effects of supercritical CO_2, the amount of suspended biomass drops more rapidly than the amount of attached biomass when CO_2 is injected. Note that the amount of suspended biomass is about two orders of magnitude less than that of the attached biomass.

The effect of the biofilm on the permeability of the formation can be seen in Figure 38. The right column of figures shows the total permeability, i.e., the sum of the permeabilities of the two continua ($K = K_p + K_f$) at $t = 100, 140,$ and $400\,\mathrm{days}$, and the left column shows the CO_2 saturation $S_{n,p}$ in Continuum P. The biofilm causes a considerable reduction of permeability preventing the CO_2, which is injected below the biofilm, from leaking through the damaged zone. However, as biomass decay within the biofilm progresses, the permeability increases. At $t = 400\,\mathrm{days}$, no influence of attached biomass on the permeability can be seen. This would mean that a renewal of the biofilm by the injection of nutrients would be necessary at some point. A more lasting solution would be the use of biofilms which actively precipitate $CaCO_3$ minerals as mentioned in Section 1.3.

In Section 4.4, a renewal of the substrate at regular intervals even during CO_2 injection is modelled. However, mineral precipitation cannot be simulated in this work since the model

does not account for that. Section 4.5 deals with the injection of bacteria into a formation already containing CO_2.

4.4 Variation 1: Continued Injection of Substrate Medium

In the reference simulation, the biobarrier only lasts for a limited amount of time. At the end of the substrate injection phase, the biofilm stops growing and steadily decays. This section is a variation of the reference simulation in which substrate is injected into the formation at intervals during the injection of CO_2. This is done in order to maintain the biofilm during the injection of CO_2. All the parameters, mesh, domain, etc. are exactly the same as in the reference simulation. Only the boundary conditions at the injection well differ from those of the reference simulation.

4.4.1 Initial and Boundary Conditions

The initial conditions are the same as those used in the reference simulation, i.e., a formation filled only with brine. The boundary conditions are also the same except at the injection well. These are illustrated using Figure 39. The injection well is divided into different regions (A, B, C, D, E) in space z and time t. The regions A, B, C, and D are identical to those of the reference simulation. See Section 4.3.1 for the definitions of these regions. E represents the injection of substrate at intervals and is simultaneous to C (the injection of CO_2). The boundary conditions in E are defined below.

E $(90 \leq t \leq 400\,\text{days};\ 989.25 < z \leq 994.75\,\text{m})$

- Water flow: $f_e(t) \cdot 0.5\,\text{kg/s}$
- CO_2 flow: no flow
- Biomass flow: no flow
- Substrate flow (Continuum P): $f_e(t) \cdot 1.13 \times 10^{-4}\,\text{kg/s}$.
  This corresponds to a substrate concentration in the injected medium of $0.25\,\text{kg/m}^3$.
- Substrate flow (Continuum F): no flow

$f_e(t)$ is the positive part of a sine function of time with a period T of 120 days and a unit amplitude as defined in Equation 83.

$$f_e(t) = \max\left(0, -\sin\left(\frac{t - t_0}{T/2\pi}\right)\right), \tag{83}$$

where $t_0 = 90\,\text{days}$ marks the beginning of region E. A plot of the resulting mass flow of water over the boundary of the injection well for the regions A, B, and E is given in Figure 40.

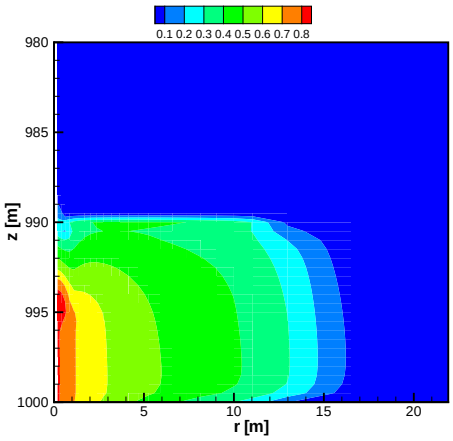

(a) $S_{n,p}$ at 100 days

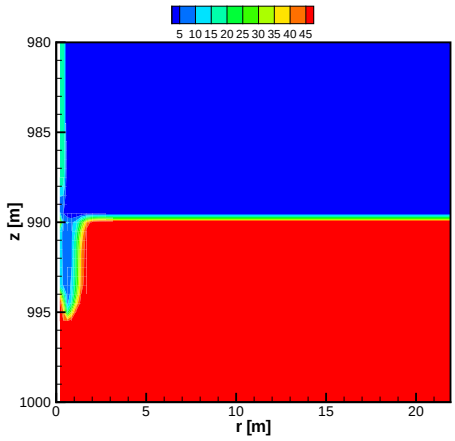

(b) K in $10^{-15}\mathrm{m}^2$ at 100 days

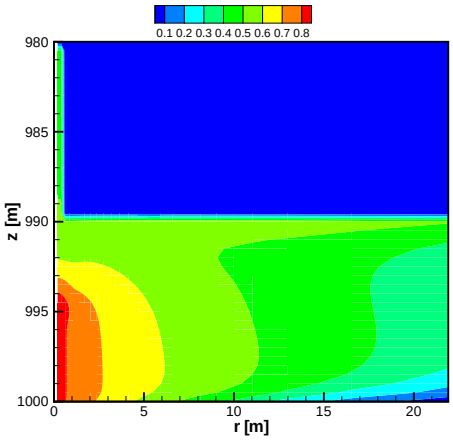

(c) $S_{n,p}$ at 140 days

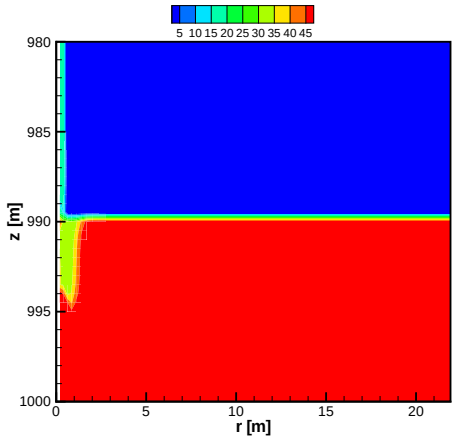

(d) K in $10^{-15}\mathrm{m}^2$ at 140 days

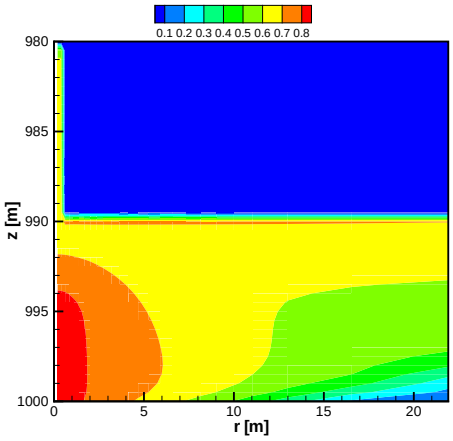

(e) $S_{n,p}$ at 400 days

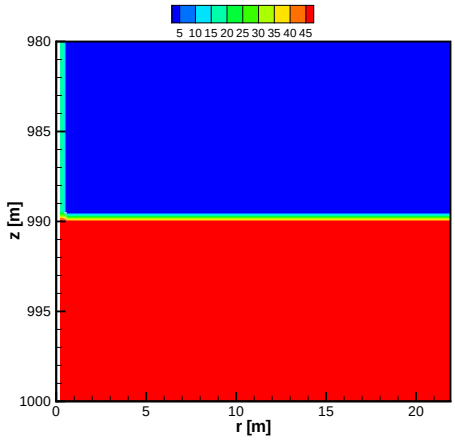

(f) K in $10^{-15}\mathrm{m}^2$ at 400 days

Figure 38: Results of reference simulation: $S_{n,p}$ (left) and $K = K_p + K_f$ (right).

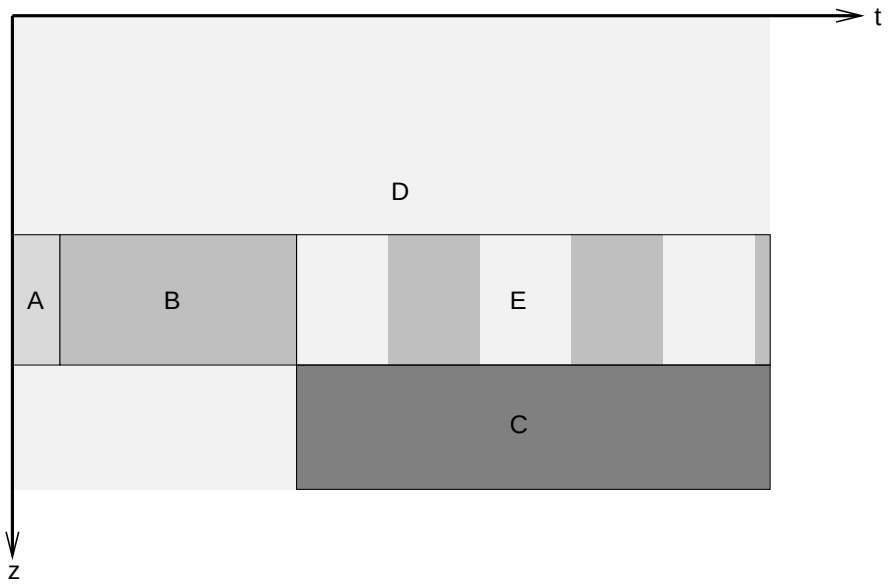

Figure 39: Variation 1: Boundary conditions at the well.

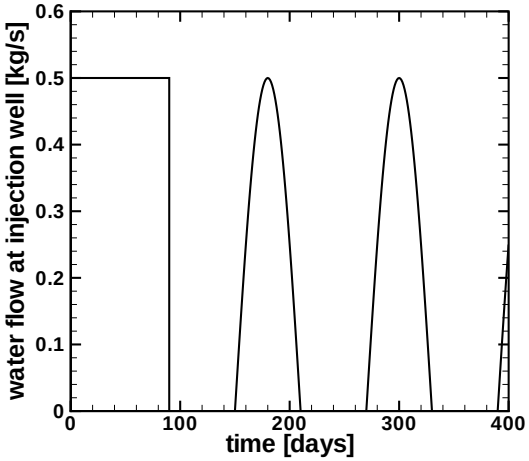

Figure 40: Injection strategy of water. Water is injected initially at a constant rate of $0.5\,\mathrm{kg/s}$ (A and B). As from $90\,\mathrm{days}$ (E), the injection rate is a function of time. The substrate concentration of the injected water is $0.25\,\mathrm{kg/m^3}$ in B and E and $0\,\mathrm{kg/m^3}$ in A.

4.4.2 Results

Figure 41 shows the total amount of biomass in the formation over time. As is the case in the reference simulation, there is a build-up of attached and suspended biomass in the formation during the first 90 days. This is followed by a strong drop when the substrate injection is stopped and CO_2 is injected. However, in contrast to the reference simulation, the amount of biomass in the system increases again when the injection of the nutrient medium is resumed. There is a cyclic pattern corresponding to the injection strategy as shown in Figure 40. One can see that the amount of suspended biomass reduces very quickly when the medium injection is shut down compared to that of the attached biomass. This has been discussed in Section 4.3.2 and is attributed to the protection of the bacteria within the biofilm from supercritical CO_2.

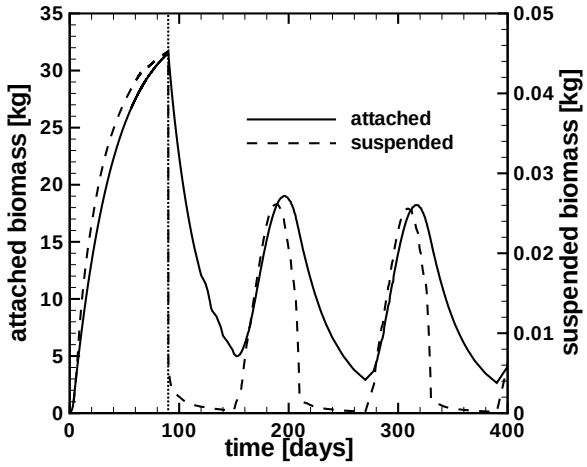

Figure 41: Variation 1: Amount of biomass (attached and suspended) in the formation.

The CO_2 saturation and the total permeability of the formation at three time-steps, i.e., at 180, 270, and 400 days are shown in Figure 42. The magnitude and extent of permeability reduction changes with time. They are greatest in the middle of an injection phase, e.g., at $t = 180\,\mathrm{days}$ and lowest at the end of a starvation phase, e.g., at $t = 270\,\mathrm{days}$.

4.5 Variation 2: Biofilm Growth in a Formation Containing CO_2

Assuming CO_2 is injected into the formation described in Sections 4.1 and 4.2, and the CO_2 leakage from the reservoir through the damaged zone of the caprock is detected only after some time, one may consider using a biofilm to stop the leakage. This would entail injecting biofilm-forming bacteria into the formation in the presence of supercritical CO_2. The effect CO_2 has on the rate of biofilm formation is of interest, thus, only the first 90 days are simulated which is the biofilm growth phase.

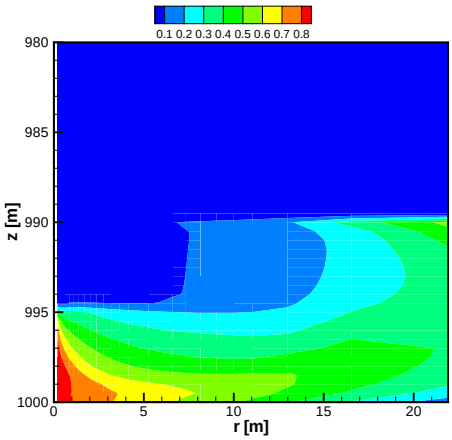

(a) $S_{n,p}$ at 180 days

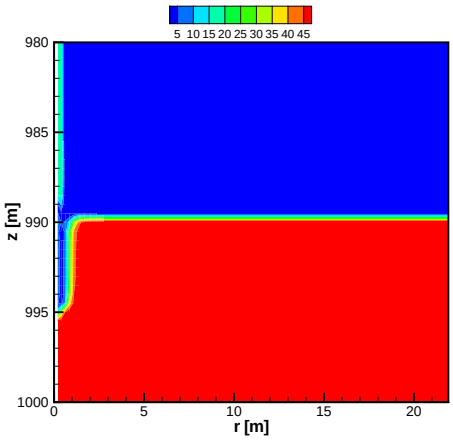

(b) K in $10^{-15}\mathrm{m}^2$ at 180 days

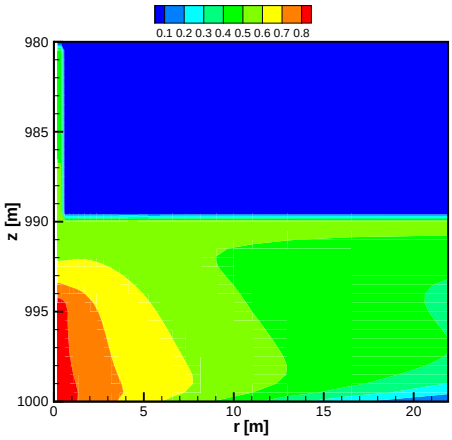

(c) $S_{n,p}$ at 270 days

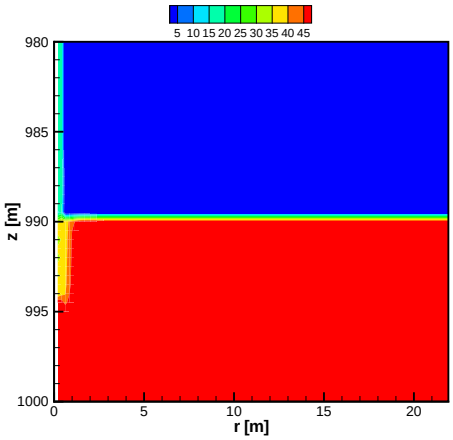

(d) K in $10^{-15}\mathrm{m}^2$ at 270 days

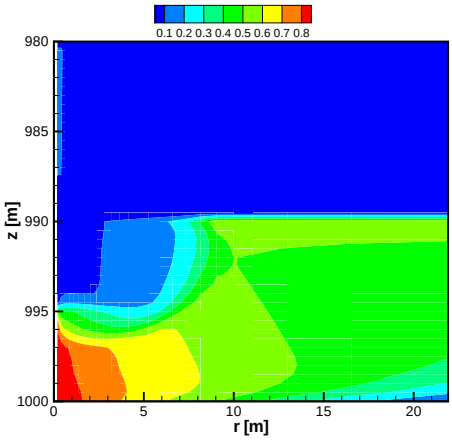

(e) $S_{n,p}$ at 400 days

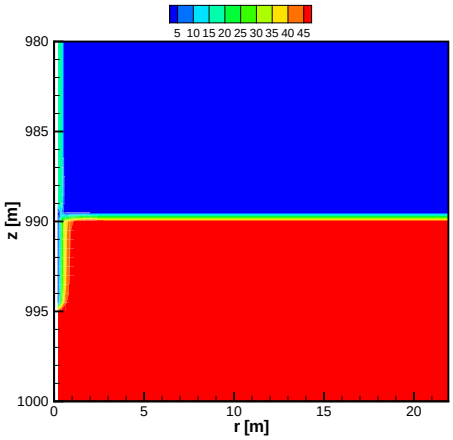

(f) K in $10^{-15}\mathrm{m}^2$ at 400 days

Figure 42: Results of Variation 1: $S_{n,p}$ (left) and $K = K_p + K_f$ (right).

4.5.1 Initial and Boundary Conditions

Since the formation contains CO_2, the initial conditions differ from those described in the reference simulation in Section 4.3.1 by the CO_2 saturation. Here, it is assumed that $S_n = 0.8$ within the saline aquifer, and $S_n = 0$ in the caprock. The initial conditions which are identical to those of the reference simulation are hydrostatic pressure conditions, no biomass, and no substrate.

The conditions at the outer boundary of the domain (see Figure 31) are equal to the initial conditions. At the inner boundary, i.e., the injection well, the boundary conditions are time-dependent. They are the same as those given in the reference simulation (see Figure 34).

4.5.2 Results

The results of the simulation are shown in Figures 43 and 44. Both figures clearly show that biofilm growth is inhibited in the presence of supercritical CO_2. The amounts of suspended

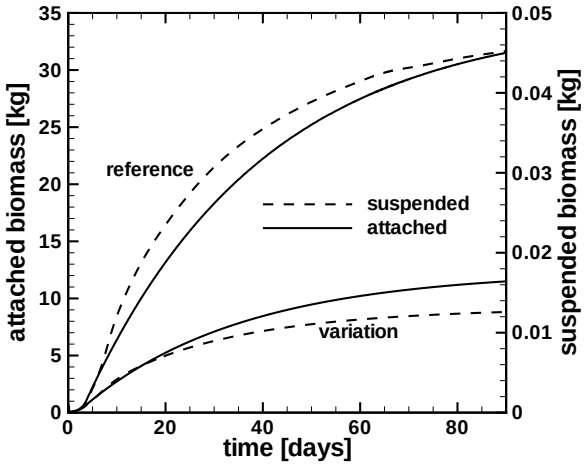

Figure 43: Variation 2: Amount of biomass (attached and suspended) in the formation

and attached biomass in the formation over time are shown in Figure 43. The biomass in the system is three to four times less than in the reference simulation. Supercritical CO_2 is a biocide and kills the suspended bacterial cells making it difficult for the biofilm to grow and spread. The left column of figures in Figure 44 shows the volume fraction occupied by the biofilm ϕ_f/ε at three different time-steps. They show that it is possible to grow a biofilm in a CO_2 storage reservoir, albeit more difficulty. The right column of figures in Figure 44 shows the CO_2 saturation. Due to the injection of water, most of the CO_2 gets displaced from the injection well making it easier for the biofilm to develop.

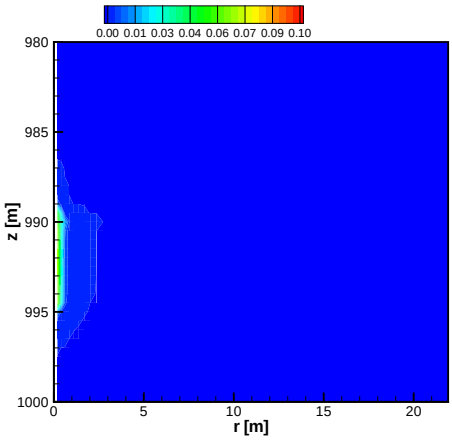

(a) ϕ_f/ε at 10 days

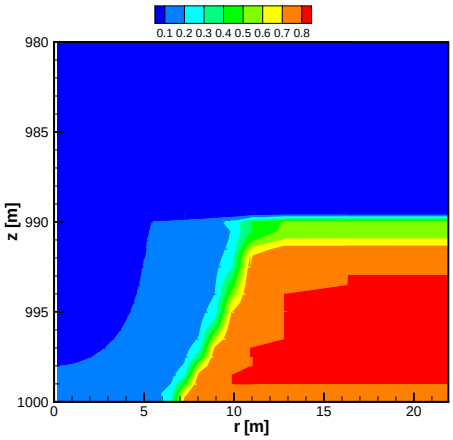

(b) $S_{n,p}$ at 10 days

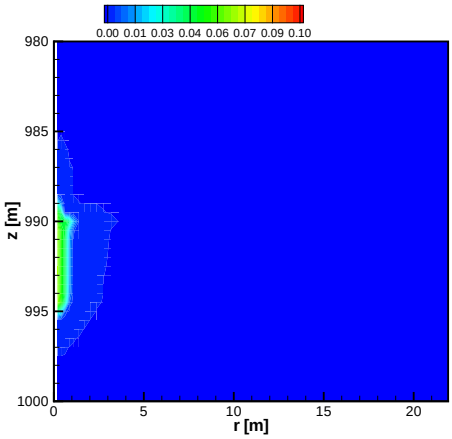

(c) ϕ_f/ε at 40 days

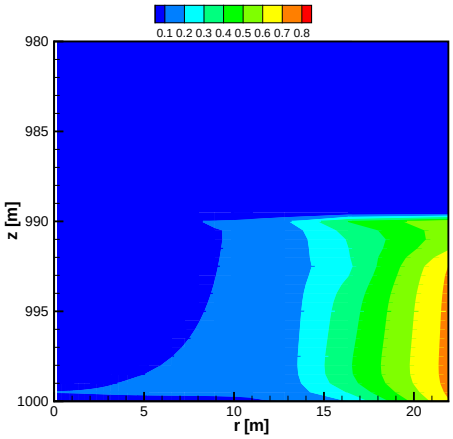

(d) $S_{n,p}$ at 40 days

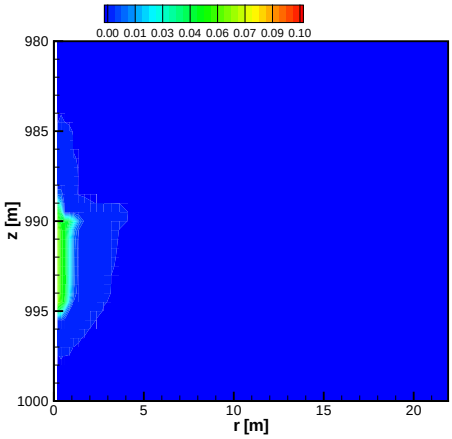

(e) ϕ_f/ε at 90 days

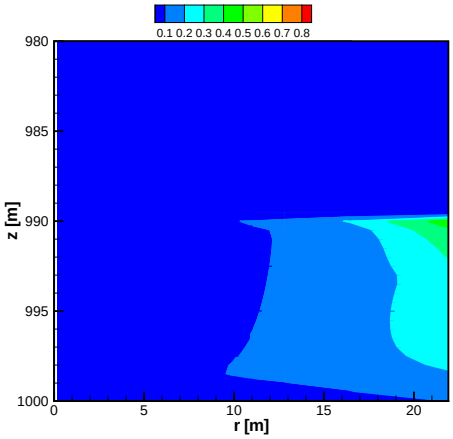

(f) $S_{n,p}$ at 90 days

Figure 44: Results of Variation 2: ϕ_f/ε (left) and $S_{n,p}$ (right).

4.6 Remarks

The simulations in this chapter show that the model developed in this thesis is capable of qualitatively modelling the accumulation of biomass in a geological formation in the presence of water and CO_2 as well as the effects of the accumulated biomass on the hydraulic properties of the formation. In the simulations, the bacterial cells embedded in the biofilm are protected from supercritical CO_2, and thus the biofilm persists longer than the suspended cells. The biofilm can even grow in the presence of CO_2 when nutrients are injected. These are important prerequisites for the use of biofilms to increase storage safety. However, in the presence of supercritical CO_2, an important process which enhances the spreading of the biofilm is strongly inhibited, i.e., the transport of detached cells and subsequent reattachment at new sites. Since detached cells leave the protective environment of the biofilm, the presence of a biocide in the bulk fluid prevents them from successfully colonising new surfaces.

For the given example, it was possible to plug the damaged caprock with biofilm. However, the biofilm is temporary and requires regular feeding. This problem could be solved by the use of biofilms which serve as catalysts for the precipitation of minerals, leading to longer-lasting clogging. The described model does not account for geochemical processes, and such scenarios cannot be modelled yet. Thus, in future work, an extension of the model to account for such processes is important. If it is possible to transport the chemical species necessary for biomineralisation to the biofilm, the use of this technology to plug leakage pathways can be a very useful method of mitigating leakage and increasing storage safety.

One of the assumptions made in the description of the model is that there is only one growth-limiting factor which is the availability of a substrate. This limits the applicability of the model to simulations of more sophisticated injection strategies which may target fractures at some distance from the injection well. For example, if one would also account for the availability of an electron acceptor, it would be possible to simulate scenarios in which a substrate and an electron acceptor are injected at different time intervals in order to increase the extent of the biofilm-affected zone in the formation. Thus, the description of bacterial growth as a function of more than one growth-limiting factor is a crucial step in the further development of the model.

5 Further Applications

In the previous chapters, a model was developed (Chapter 2) with the purpose of modelling biomass accumulation in a CO_2 storage reservoir (Chapter 4). However, the model could be used in the simulation of other processes involving microbial activity in the subsurface, e.g., the biological remediation of a contaminated aquifer or in the enhancement of oil recovery using microbes. This will be discussed in the following sections.

5.1 In Situ Biodegradation

Subsurface contamination, usually caused by industrial waste, often poses a serious threat to groundwater quality. Non-aqueous phase liquids (NAPLs) may remain trapped within the pores of aquifers for long periods of time and serve as a source of contaminants as components of the NAPL slowly dissolve into the groundwater. There are a number of possible methods to treat contaminated sites including pump and treat, air sparging, thermally enhanced treatment, enhanced in situ biodegradation, etc. (see Wiedemeier *et al.*, 1999; Valdes, 2000; Class and Helmig, 2002).

In this section, a simple simulation of the treatment of a site contaminated with residually saturated NAPL using enhanced in situ biodegradation is run. The model, at its current state, is not able to model such a scenario fully since it does not consider the dissolution of the phases in each other. However, the purpose of the exercise is to show possible applications of the model. To this aim, a few modifications to the model are made in the following.

- $C^s_{w,\kappa}$ is the concentration of an electron acceptor (e.g., oxygen) in water in Continuum κ.
- The NAPL is assumed to be the carbon source. It is assumed to be abundantly available as long as it exists as a separate phase.
- It is assumed that the bacteria can consume either components of the NAPL which are dissolved in water or can attach to the interface between the fluids and degrade the NAPL directly. Both mechanisms would lead to a reduction of NAPL saturation due to biomass growth. The source/sink term q_n from Equation 35 is rewritten as follows.

$$q_n = -(r_{g,p} + r_{g,f})/Y \tag{84}$$

  $r_{g,p}$ and $r_{g,f}$ are given in Equation 37. This accounts for the reduction of NAPL mass due to biomass growth.

- The rate of consumption of the electron acceptor given in Equation 46 is multiplied with the mass ratio R of electron acceptor per substrate consumed (see Murphy and Ginn, 2000).

$$q^s_{w,\kappa} = -R \cdot r_{g,\kappa}/Y \tag{85}$$

With these modifications, biomass growth is now dependent on two factors, i.e., the availability of the electron acceptor and the presence of the NAPL.

5.1.1 Simulation

An aquifer contamination is to be treated by injecting water with an electron acceptor, e.g., oxygen into the source zone of contamination which is a region containing immobile NAPL. This is supposed to increase the activity of microorganisms native to the aquifer which use components of the NAPL as substrates. The microorganisms degrade the contaminant to less harmful compounds.

The same mesh as in Chapter 4 is used in this simulation. Hence, the simulation domain has the same dimensions as in the previous chapter. It is radially symmetric around the injection well. Figure 45 shows geometry and boundary conditions of the domain. It is

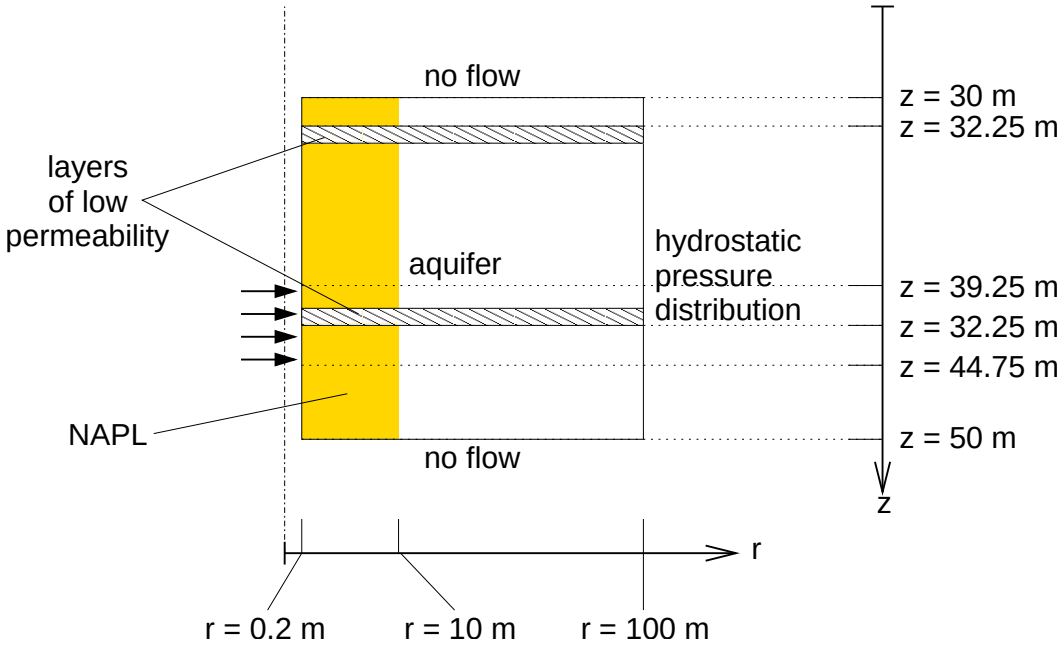

Figure 45: Radially symmetric domain with boundary conditions. Water is injected over the inner boundary ($r = 0.2\,\mathrm{m}$) as shown by the arrows. The NAPL contamination is also shown.

100 m long and lies 30 to 50 m below the groundwater table. The injection well has a radius of 0.2 m. There are two layers which have a lower permeability than the rest of the aquifer (see Figure 45 and Table 14). Each of these layers is 1 m thick.

Initial and Boundary Conditions

The initial conditions used in the simulation are as follows.

- Pressure is hydrostatically distributed, $p_n = p_n(z)$;
- the contaminated zone ($r < 10\,\mathrm{m}$) contains an immobile NAPL phase with $S_{n,p} = 0.01$;
- the concentration of the electron acceptor in the aquifer water is equal to zero, $C^s_{w,\kappa} = 0\,\mathrm{kg/m^3}$;
- and the indigenous bacteria are modelled by assuming that an initial amount of attached biomass is present, $\phi_f = 10^{-4} \cdot \varepsilon$, $C^b_w = 0\,\mathrm{kg/m^3}$. Biofilm porosity ε is given in Table 14.

The boundary conditions are shown in Figure 45 and are stated below.

- The top and bottom boundaries are no-flow boundaries.
- Dirichlet conditions are assigned to the outer boundary ($r = 100\,\mathrm{m}$) with a hydrostatic pressure distribution and no nutrients or biomass.
- Neumann conditions are assigned to the inner boundary, i.e., the injection well ($r = 0.2\,\mathrm{m}$). Water with an oxygen concentration of $0.01\,\mathrm{kg/m^3}$ is injected at a rate of $0.1\,\mathrm{kg/s}$ between $z = 39.25\,\mathrm{m}$ and $z = 44.75\,\mathrm{m}$. There is no flow over the rest of the inner boundary.

Simulation Parameters

All the parameters used in the simulation are given in this section. The properties of the aquifer including its geometry, permeability, and porosity are given in Table 14. Table 15 shows the properties of the fluids (water and NAPL) which have been assumed to be constant. In the simulation, the NAPL saturation is always less than its residual saturation. Therefore, there is no advective NAPL flow, and the viscosity of the NAPL is not needed in the simulation. Biological parameters, e.g., substrate utilisation rate, decay rate, etc. are given in Table 16. The attachment and detachment parameters are the same as those given in Table 12 in Section 4.2. Similarly, the parameters used in this simulation for the calculation of capillary pressure and relative permeability are identical to those used in Section 4.2 and are given in Table 13 on page 55. Finally, other parameters include the specific surface area of the rock formation $M = 5 \times 10^3\,\mathrm{m^{-1}}$, the dispersion coefficients $D^b_p = D^s_p = \phi_p \times 10^{-8}\,\mathrm{m^2/s}$ and $D^s_f = \phi_f \times 10^{-8}\,\mathrm{m^2/s}$, and the effective diffusion coefficient $D^s_{eff} = \varepsilon \times 10^{-9}\,\mathrm{m^2/s}$.

Table 14: Properties of groundwater aquifer and hydraulic properties of biofilm.

Property	Value	Comment
Aquifer permeability	$100 \times 10^{-15}\,\mathrm{m}^2$	
Permeability of layers	$50 \times 10^{-15}\,\mathrm{m}^2$	
Aquifer porosity	0.3	
Aquifer thickness	20 m	
Radius of contaminated zone	10 m	
Permeability parameter $\phi_{p,c}/\phi_0$	0.35	from Table 8 on page 49
Permeability parameter n_k	3	
Minimum permeability K_{min}	$0.01 \cdot K_0$	
Biofilm porosity ε	0.8	
Depth at bottom of aquifer	50 m	
Injection well radius	0.2 m	
Domain radius	100 m	

Table 15: Fluid properties.

Property	Value
Water density ϱ_w	$1000\,\mathrm{kg/m^3}$
Water viscosity μ_w	$10^{-3}\,\mathrm{Pa \cdot s}$
NAPL density ϱ_n	$250\,\mathrm{kg/m^3}$

Table 16: Biological parameters.

Parameter	Value
Maximum substrate utilisation rate k_μ	$1.16 \times 10^{-4}\,\mathrm{s}^{-1}$
Monod half-saturation coefficient K_s	$1 \times 10^{-4}\,\mathrm{kg/m^3}$
Yield coefficient Y	0.1 kg/kg
Endogenous decay rate b_0	$3.18 \times 10^{-7}\,\mathrm{s}^{-1}$
Mass ratio of electron acceptor per substrate consumed R	0.1
Biofilm density ϱ_b	$15\,\mathrm{kg/m^3}$

Results

The results of the simulation are shown in Figures 46–48. A very important difference to the simulations in the previous chapter is that biomass growth is dependent on two conditions. In most of the domain, only one of the two conditions is met. Thus, most of the bacterial activity takes place within a small part of the domain. An explanation for this is given below.

Figure 46 shows the volume fraction occupied by attached biomass ϕ_f/ε and the concentration of biomass in water C_w^b at three time-steps ($t = 10, 400,$ and $1000\,\mathrm{days}$). Initially, biomass (attached and suspended) grows near the injection zone since there is an abundance of the electron acceptor and substrate. At some point, however, the biomass near the injection decreases. This is due to the fact that all the NAPL within that region is degraded as can be seen in Figure 47. Two distinct zones emerge within the aquifer with each zone lacking either an electron acceptor or donor. Biodegradation and biomass growth only takes place at the interface between the two zones. Note that the dissolved components of the NAPL have not been accounted for by the model. These would be mobile and could mix better with the electron acceptor-rich water. Thus, mixing is a very important process in biodegradation (see Cirpka *et al.*, 1999). The distribution of the electron acceptor in the aquifer is influenced by the permeability of the aquifer. This, in turn, influences the biomass distribution. The permeability of the aquifer is shown in Figure 48. The influence of the biofilm on permeability can be seen.

These simulations are supposed to show that the model could be applied to other applications other than CO_2 storage. For a proper simulation of biodegradation, however, it would have to be extended to account for the dissolution of NAPL components in water and for bacterial attachment to the water-NAPL interface.

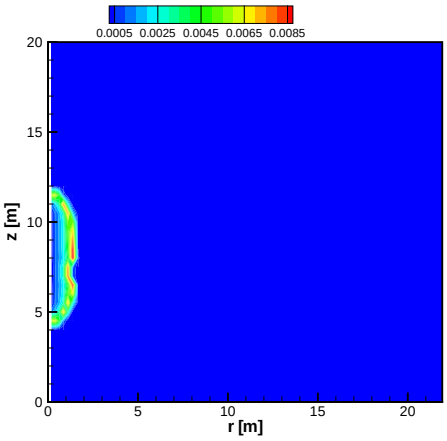

(a) ϕ_f/ε at 10 days

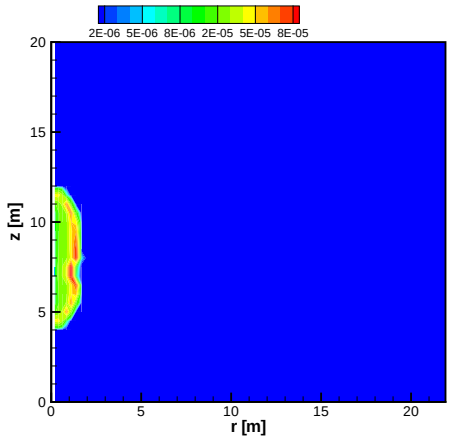

(b) C_w^b in kg/m^3 at 10 days

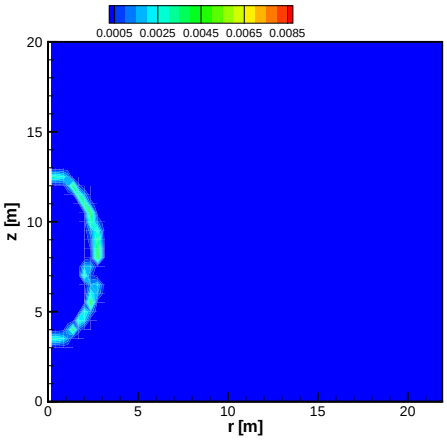

(c) ϕ_f/ε at 400 days

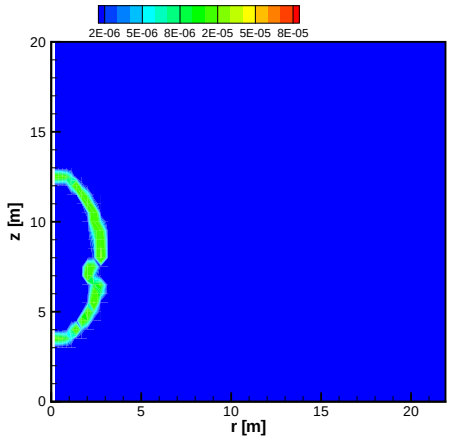

(d) C_w^b in kg/m^3 at 400 days

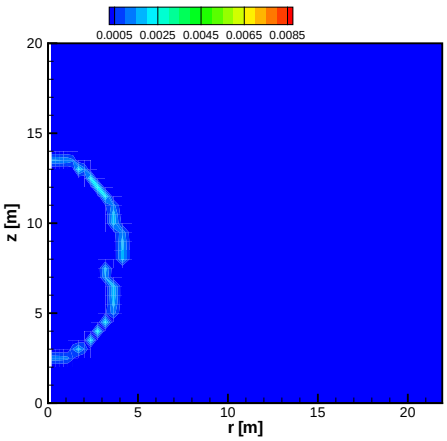

(e) ϕ_f/ε at 1000 days

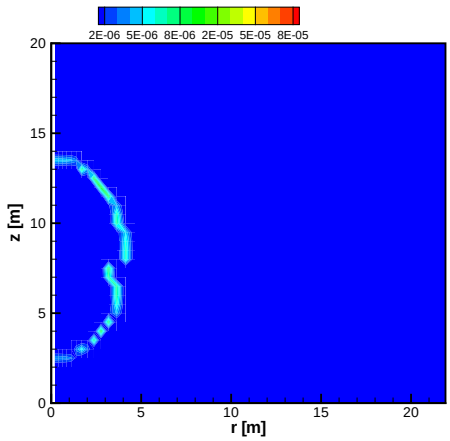

(f) C_w^b in kg/m^3 at 1000 days

Figure 46: Simulation results of in situ biodegradation: ϕ_f/ε (left) and C_w^b (right).

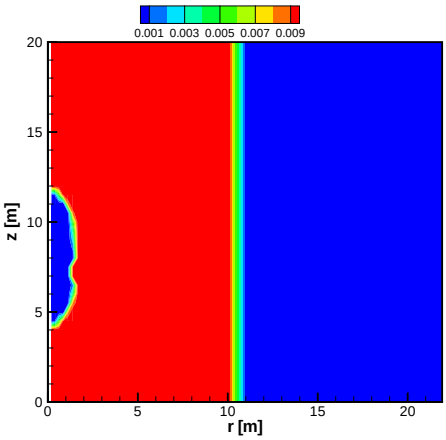

(a) $S_{n,p}$ at 10 days

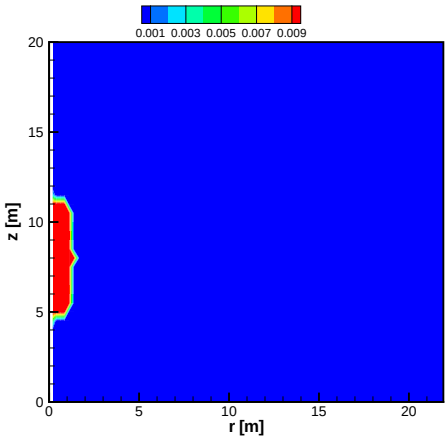

(b) $C^s_{w,p}$ in kg/m^3 at 10 days

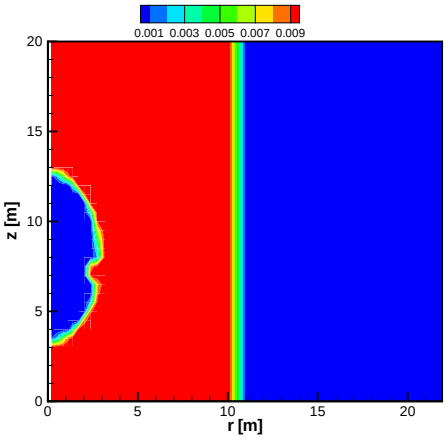

(c) $S_{n,p}$ at 400 days

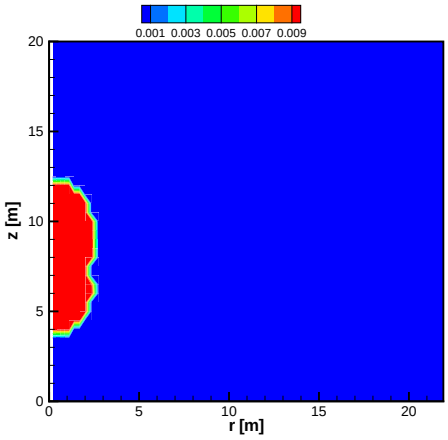

(d) $C^s_{w,p}$ in kg/m^3 at 400 days

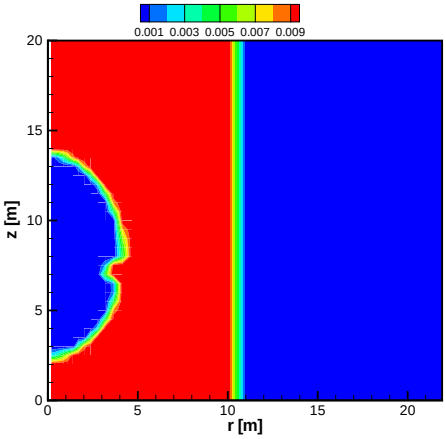

(e) $S_{n,p}$ at 1000 days

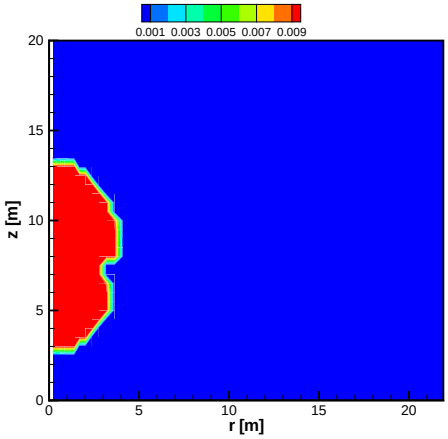

(f) $C^s_{w,p}$ in kg/m^3 at 1000 days

Figure 47: Simulation results of in situ biodegradation: $S_{n,p}$ (left) and $C^s_{w,p}$ (right).

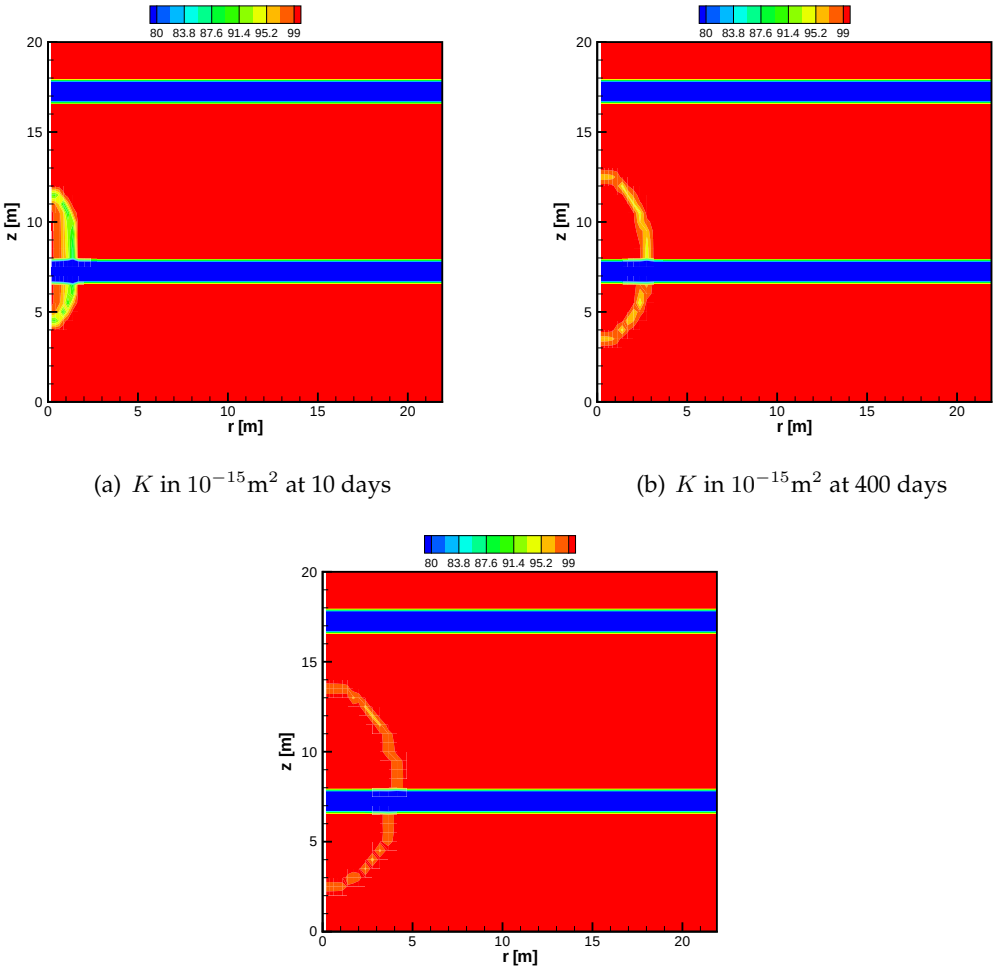

(a) K in $10^{-15}\mathrm{m}^2$ at 10 days

(b) K in $10^{-15}\mathrm{m}^2$ at 400 days

(c) K in $10^{-15}\mathrm{m}^2$ at 1000 days

Figure 48: Simulation results of in situ biodegradation: $K = K_p + K_f$.

5.2 Microbially Enhanced Oil Recovery

The recovery of hydrocarbons (oil/gas) from reservoirs is often divided into *primary, secondary*, and *tertiary recovery* stages. Primary recovery involves the use of the natural pressure drive in the reservoir. Production rates from primary production, however, decline as the pressure in the reservoir drops. The primary recovery stage can be prolonged by actively pumping the hydrocarbon to the surface. In secondary recovery, production is augmented by the injection of fluids such as water or natural gas. The injection of water to improve oil recovery is referred to as *water-flooding*. The fluids are injected in order to maintain the pressure in the reservoir which tends to drop during primary production. The injected fluids displace the oil or gas towards the production well. Further enhancement of recovery can be achieved in the tertiary recovery stage by further improving hydrocarbon flow to the well. Mobilisation of trapped oil by surfactants, reduction of oil viscosity by the injection of CO_2 or steam, injection of acids to increase permeability, and the use of polymers to increase the viscosity of the injected water are some of the techniques used in tertiary production (also called enhanced recovery).

Microbially enhanced oil recovery (MEOR) exploits the properties of microbes to achieve the goals of tertiary oil recovery. For example, biosurfactants produced by microorganisms can be used to reduce the interfacial tension between oil and water, biofilm-forming bacteria can be used to plug preferential flow paths during water-flooding. It is possible to inject microbes with specific properties for MEOR or use indigenous microbes. MEOR can be achieved at low costs compared to conventional enhanced oil recovery. A recent overview of MEOR technology is given by Sen (2008).

The model developed in this work could be used to model MEOR. However, it would have to be extended to some extent. Since the oil-water interface is a site of significant microbial activity, the most important extension of the model would probably be to account for microbial activity at this interface. This implies accounting for attachment and detachment of bacteria at the fluids' interface. The effect of bacterial activity on the interfacial tension between the fluids would also have to be accounted for. However, a very important process in MEOR is already included in the model, i.e., the changes in permeability caused by biofilm growth.

6 Summary and Outlook

This work deals primarily with the development of a numerical model capable of describing the accumulation of biomass in the subsurface and its application to the plugging of damaged caprock in a subsurface CO_2 storage reservoir. This involves the description of fluid flow and microbial activity in porous media. On the one hand, the accumulation of biomass in a porous medium changes the hydraulic properties of the medium which affects flow. Flow processes, on the other hand, determine the transport of nutrients to the microbes, and thus directly influence the rate and distribution of biomass growth. Thus, the proper description of the interaction between flow and microbial processes is an essential challenge for such a model.

Microbial Biomass in the Subsurface

Microbes (particularly bacteria) can exist as floating cells in a medium. These suspended cells are referred to as planktonic. In the subsurface, however, most microbial cells are sessile which means that they are attached to a solid surface (substratum). This tends to be the more successful mode of growth. A group of sessile cells attached to a common substratum and held together by extrapolymeric substances (EPS) is called a biofilm. A biofilm forms on a surface in the following steps.

- Organic molecules dissolved in water adhere to a solid surface forming a conditioning film.
- Planktonic cells which come in contact with a conditioned surface may adsorb at the surface.
- Adsorbed cells produce EPS which strengthen their bond to the surface and to other attached cells.
- In conducive environments, these attached cells reproduce and colonise the substratum forming a biofilm.
- Sessile cells may detach from a biofilm and reattach to a downstream surface.

The structure of biofilms is very heterogeneous. Cells within a biofilm tend to form clusters leaving open spaces within the structure. Thus, the biofilm itself may be seen as a porous medium which can be characterised with a porosity and a density.

Biofilm growth in a porous medium blocks pore throats thereby changing the properties of the medium. This is often used in biological filtration (e.g., wastewater treatment), bioremediation (for the creation of biobarriers), etc. A biobarrier could be used in a carbon dioxide (CO_2) storage reservoir to prevent leakage of CO_2.

CO_2 Storage in Geological Formations

CO_2 is the most important anthropogenic greenhouse gas. The increase in atmospheric concentrations of greenhouse gases in the past decades due to the burning of fossil fuels is mainly responsible for global warming and its adverse effects on the environment. The use of more efficient technology and alternative energy sources can help in reducing CO_2 production. CO_2 emissions can be reduced by capturing CO_2 from large point sources and storing in deep geological formations. At the conditions which persist in such underground reservoirs, CO_2 is a supercritical fluid with a high density and a low viscosity. The reservoirs contain saline water which is denser than CO_2. Buoyant CO_2 is prevented from rising to the atmosphere by an impermeable layer called caprock. Cracks in the caprock could, however, lead to leakage. The caprock in the vicinity of the CO_2 injection is particularly at risk. The high pressure build-up during the initial injection phase, corrosion of well cement by CO_2-rich formation water, or damage to the caprock during drilling could cause leakage of CO_2. Biobarriers could be used to minimise such risk by plugging potential leakage pathways and protecting well cement against corrosion. The biobarrier could be either the biofilm itself, mineral precipitates which form in the presence of the biofilm, or both.

Model Concept

In the field of flow and transport in porous media, at least two characteristic scales can be defined. At the microscale, the geometry of the porous medium and the flow of the individual fluids through the pores can be resolved. An averaging over the microscale leads to the macroscale. Information such as the geometry of the medium are represented by effective parameters, e.g., porosity and permeability. The model described in this work is defined on the macroscale.

The formation water and injected CO_2 form separate phases. The flow of these two phases within the porous medium is described using the extended Darcy equation. The interaction between the fluids and the porous medium is accounted for with constitutive relationships.

As stated above, the biofilm has a porous structure. Both fluids may be contained within the pores of the biofilm. It seems obvious that flow and transport within the biofilm occur at a considerably different rate than outside the biofilm. In order to account for this, two continua are defined in the model. One continuum describes the flow processes through the pores of the biofilm, and the other describes the flow processes through the pores of the porous medium. This so-called dual-continuum concept also defines exchange terms which describe the interaction between the two continua. This means that a set of balance equations is set up for each continuum and then coupled by the exchange terms. Simplifications

help reduce the complexity of the system of equations. Some of the simplifications, however, are restrictive and need to be addressed in further work. The most important assumptions are stated below.

- Solute exchange between the two continua is diffusive, i.e., due to gradients in concentration between the two continua.
- The distribution of the two fluids within the continua is entirely dependent on capillary forces.
- Empirical functions are used to describe the exchange of biomass between the two continua, i.e., attachment of suspended biomass and detachment of attached biomass.
- Only one growth-limiting substrate is accounted for. Thus, it is assumed that all other prerequisites for growth are fulfilled.

Clogging: This is obviously a very important part of any concept which aims to model biobarriers in the subsurface. A biofilm growing within the pores of a porous medium occupies space and changes the properties of the medium. A permeability can be assigned to each of the continua mentioned above. Changes in the amount of attached biomass cause changes in permeability of each continuum. These are described with constitutive relationships. The total permeability of the biofilm-filled porous medium is the sum of the permeabilities of the individual continua. Comparison to experimental data (Cunningham *et al.*, 1991) shows that the typical permeability–porosity relationship observed in experiments can be reproduced with this concept.

The properties of the fluids are important for the proper description of flow. Water in deep geological formations, often called brine, is mostly very saline. Salinity affects the density and viscosity of brine. The critical point of CO_2 is at 73.8 bar and $31\,^{\circ}\mathrm{C}$. The properties of CO_2 can vary considerably with temperature and pressure. The equation of state of Span and Wagner (1996) is used for the calculation of density. Supercritical CO_2 is a very good solvent. Its high solvency makes supercritical CO_2 an efficient biocide since it causes the extraction of intracellular material. This is accounted for in the model by a saturation-dependent decay term.

The set of partial differential equations resulting from the mass balance equations is discretised in space using a vertex-centered finite volume method called the Box method. A control volume (box) is assigned to each node. First-order ansatz functions are used for the approximation of unknowns and geometry. The weighting function at each node is equal to unity within the control volume belonging to the node and zero outside. Discretisation in time is done with a fully implicit Euler scheme (backward finite difference method). The numerical model is implemented within the framework of the multiphase flow simulator MUFTE-UG which has previously been used in the simulation of the infiltration of non-aqueous phase liquids in saturated and unsaturated soils, CO_2 geosequestration, salt water intrusion, flow in the cathode of fuel cells, and leakage of contaminant gas from atomic waste containers in deep rock repositories.

Verification of the model

Every numerical model which is to be used predictively requires verification. This can be achieved by comparing numerical results to experimental data. The numerical model developed in this work is tested in this manner. Two experiments with particular relevance to the processes of interest were chosen, each consisting of two runs.

The experiments by Taylor and Jaffé (1990a) focus on the interaction between biofilm growth and fluid flow processes. The exchange of biomass between the two continua, i.e., attachment and detachment is particularly important in these experiments. Biofilms were grown in sand columns under constant-flow conditions. Three parameters of the numerical model were fitted to one of the runs and applied to the second run. The results of the numerical simulation fitted satisfactorily to those of the experiments.

Mitchell *et al.* (2009) performed experiments in which supercritical CO_2 was injected into sandstone cores. They were conducted at high pressure and moderate temperature to ensure the supercritical state of aggregation of CO_2. Two sandstone cores were inoculated with biofilm-forming bacteria, and the permeabilities of the cores were measured regularly. The biofilms reduced the permeabilities of the cores by about 95 %. The biofilms were then challenged with supercritical CO_2. The CO_2 challenges had a small effect on the permeabilities of the cores. Due to lack of information, a number of assumptions have to be made in the simulations, and a simplified version of the model is used. This makes a rigorous quantitative comparison between the two results difficult. However, the model can reproduce the permeability changes observed in the first of the two experimental runs very well. Three parameters were fitted to this run. A prediction of the results of the second run by the model compares satisfactorily to the experimental results.

These comparisons help to gain a better understanding as to which processes and parameters are important for the given conditions. They are also an excellent way of finding mistakes and wrong assumptions in the model.

Application

As mentioned above, the aim of the model development is to be able to simulate the accumulation of biomass in a CO_2 storage reservoir. The model described in this work accounts for the following processes:

- biomass growth,
- biomass decay,
- attachment of planktonic cells to the surface of the formation rock,
- detachment of sessile cells,
- transport of suspended cells with bulk fluid,

- the effect of biofilm formation on the hydraulic properties of the formation,
- the effect of supercritical CO_2 on the microbial cells, etc.

This model is applied to a fictitious test scenario. The caprock of a CO_2 storage reservoir is damaged at the injection well. Injected CO_2 would leak through the damaged zone. Bacterial cells and nutrients are injected into the formation just below the caprock until a biofilm is formed within the damaged zone. CO_2 is then injected into the formation. The simulations show that the biobarrier prevents the injected CO_2 from leaking for a limited amount of time. Other simulations were run in which the substrate was injected at intervals in order to maintain the biobarrier. As proposed by Cunningham *et al.* (2009), biofilms could serve as catalysts for mineral precipitation. This would produce a longer-lasting biobarrier. At its current state, the model does not account for such processes. In a final simulation, the development of a biobarrier in a formation already containing CO_2 was shown. In all three simulations, the supercritical CO_2 inhibited the development of the biofilm. Even though bacterial cells are protected from the harmful effects of the CO_2 within the biofilm, a spreading of the biofilm is difficult since this entails the detachment of microbes from the biofilm and transport within the fluids to a surface downstream. Suspended cells are very susceptible to biocides.

Further Applications

With some extensions, this model could be used in other applications which deal with microbial activity and two-phase fluid flow. Two examples are bioremediation and microbially enhanced oil recovery.

- In bioremediation, microbial activity in contaminated soil helps degrade toxic substances. This activity could be natural or artificially enhanced. Biobarriers are also used in bioremediation for the containment of contaminant plumes . A simple simulation was run to demonstrate in situ biodegradation.
- Oil recovery can be enhanced by microbial activity. Bacteria attached to the oil–water interface can produce surfactants which reduce interfacial tension and aid in the mobilisation of oil. Biofilms can be used to plug preferential flow paths in water-flooding.

For a proper description of the processes mentioned above, the most important extensions to the model are to account for microbial activity at the interface between the fluids and the mutual dissolution of the fluids.

Outlook

This work describes the process of development and verification of a numerical model, and its application to a test case. The capabilities of the model allow the simulation of biofilm formation in the subsurface. However, there is very much room for improvement. Further work on this topic should include the following points.

- Some of the simplifications made in the development of the model are restrictive and need to be revisited. A good example is the assumption that both continua have the same pressure. This way, the advective exchange of solutes between the two continua cannot be accounted for. Instead, both pressures could be solved for independently and linked only with the exchange term. The exchange of solutes would then be driven by a combination of solute and pressure gradients.

- The model assumes that there is only one growth-limiting substrate and that all other nutrients necessary for growth are abundantly available. This is a strong restriction. An injection strategy could involve the injection of a substrate and the delayed injection of an electron acceptor with the aim of growing a biofilm at some distance from the injection. This cannot be simulated with the model. Thus, an electron acceptor needs to be accounted for by the model.

- The model makes use of many empirical parameters and relationships. Sensitivity studies are necessary to determine the parameters which have the strongest influence on the system. Values for these parameters need to be determined in experimental investigations. Experiments are also necessary to gain a better understanding of the relevant mechanisms involved.

- All the equations, correlations, and parameters used in the model are defined on the macroscale. However, it is often easier to understand and describe processes on the microscale. Well-understood microscale phenomena should be properly depicted on the macroscale. This is not always easy. Therefore, research on the upscaling of microscale processes relevant to biofilms in porous media to the macroscale (e.g., Golfier *et al.*, 2009) is absolutely necessary.

- The conservation equations of the different components (water, CO_2, biomass, and substrate) are solved simultaneously. This is computationally expensive. Future work could focus on decoupling processes of different time scales. For example, the simulation of flow processes, involving water and CO_2, could be partly decoupled from transport and biological processes, involving biomass and substrate.

- Under starvation conditions, the biobarrier slowly loses its efficiency. A more enduring option is the use of mineral-precipitating biofilms. In further work, it could be of interest to extend the model to account for the transport of the chemical species necessary for such mineralisation.

Bibliography

Assteerawatt, A., Bastian, P., Bielinski, A., Breiting, T., Class, H., Ebigbo, A., Eichel, H., Freiboth, S., Helmig, R., Kopp, A., Niessner, J., Ochs, S. O., Papafotiou, A., Paul, M., Sheta, H., Werner, D., and Ölmann, U. (2005). MUFTE-UG: Structure, Applications and Numerical Methods. *Newsletter, International Groundwater Modeling Centre, Colorado School of Mines*, **23(2)**.

Barenblatt, G. I. and Zheltov, I. P. (1960). Fundamental equations for the filtration of homogeneous fluids through fissured rocks. *Doklady Akademii Nauk Sssr*, **132**(3), 545–548.

Bastian, P. and Helmig, R. (1999). Efficient Fully-Coupled Solution Techniques for Two-Phase Flow in Porous Media. Parallel Multigrid Solution and Large Scale Computations. *Adv. Water Resour.*, **23**, 199–216.

Bastian, P., Birken, K., Johannsen, K., Lang, S., Eckstein, K., Neuss, N., Rentz-Reichert, H., and Wieners, C. (1997). UG – A Flexible Software Toolbox for Solving Partial Differential Equations. *Computing and Visualization in Science*, **1**(1), 27–40.

Batzle, M. and Wang, Z. J. (1992). Seismic properties of pore fluids. *Geophysics*, **57**(11), 1396–1408.

Bear, J. (1988). *Dynamics of Fluids in Porous Media*. Dover Publications.

Bielinski, A. (2006). *Numerical Simulation of CO_2 Sequestration in Geological Formations*. Ph.D. thesis, Universität Stuttgart.

Bouwer, E. J., Rijnaarts, H. H. M., Cunningham, A. B., and Gerlach, R. (2000). *Biofilms II: Process Analysis and Applications*, chapter 2.5 Biofilms in Porous Media, pages 123–158. Wiley.

Bradford, S. A., Simunek, J., Bettahar, M., Van Genuchten, M. T., and Yates, S. R. (2003). Modeling colloid attachment, straining, and exclusion in saturated porous media. *Environmental Science & Technology*, **37**(10), 2242–2250.

Brooks, R. H. and Corey, A. T. (1964). Hydraulic properties of porous media. *Colorado State University Hydrology Paper*, (3).

Bryers, J. D. (2000). *Biofilms II: Process Analysis and Applications*, chapter 1.1 Biofilms: An Introduction, pages 3–12. Wiley.

Cary, J. W. (1994). Estimating the surface-area of fluid-phase interfaces in porous-media. *Journal Of Contaminant Hydrology*, **15**(4), 243–248.

Chambless, J. D., Hunt, S. M., and Stewart, P. S. (2006). A three-dimensional computer model of four hypothetical mechanisms protecting biofilms from antimicrobials. *Applied And Environmental Microbiology*, **72**(3), 2005–2013.

Cirpka, O. A., Frind, E. O., and Helmig, R. (1999). Numerical simulation of biodegradation controlled by transverse mixing. *Journal Of Contaminant Hydrology*, **40**(2), 159–182.

Class, H. and Helmig, R. (2002). Numerical simulation of non-isothermal multiphase multicomponent processes in porous media. – 2. Applications for the injection of steam and airc. *Adv. Water Resour.*, **25**, 551–564.

Clement, T. P., Hooker, B. S., and Skeen, R. S. (1996). Macroscopic models for predicting changes in saturated porous media properties caused by microbial growth. *Ground Water*, **34**(5), 934–942.

Clement, T. P., Peyton, B. M., Ginn, T. R., and Skeen, R. S. (1999). Modeling bacterial transport and accumulation processes in saturated porous media: A review. *Advances in Nuclear Science and Technology*, **26**, 59–78.

Corapcioglu, M. Y. and Haridas, A. (1984). Transport and fate of microorganisms in porous media: A theoretical investigation. *Journal of Hydrology*, **72**(1-2), 149–169.

Corey, A. T. (1994). *Mechanics of Immiscible Fluids in Porous media*. Water Resources Publications.

Costerton, J. W., Geesey, G. G., and Cheng, K. J. (1978). How bacteria stick. *Scientific American*, **238**(1), 86–95.

Cullimore, R. (2000). *Microbiology of Well Biofouling*. Lewis.

Cunningham, A. B., Characklis, W. G., Abedeen, F., and Crawford, D. (1991). Influence of biofilm accumulation on porous media hydrodynamics. *Environmental Science Technology*, **25**(7), 1305–1311.

Cunningham, A. B., Gerlach, R., Spangler, L., and Mitchell, A. C. (2009). Microbially enhanced geologic containment of sequestered supercritical CO_2. *Energy Procedia*, **1**(1), 3245–3252.

De Beer, D. and Stoodley, P. (2006). *The Prokaryotes*, chapter 3.10 Microbial Biofilms, pages 904–937. Springer.

De Beer, D., Stoodley, P., and Lewandowski, Z. (1994). Liquid flow in heterogeneous biofilms. *Biotechnology And Bioengineering*, **44**(5), 636–641.

Dietrich, P., Helmig, R., Sauter, M., Hötzl, H., Köngeter, J., and Teutsch, G. (2005). *Flow and Transport in Fractured Porous Media*. Springer.

Ebigbo, A., Class, H., and Helmig, R. (2007). CO_2 leakage through an abandoned well: problem-oriented benchmarks. *Computational Geosciences*, **11**(2), 103–115.

Fenghour, A., Wakeham, W. A., and Vesovic, V. (1998). The Viscosity of Carbon Dioxide. *J. Phys. Chem. Ref. Data*, **27**(1), 31–44.

Gargiulo, G., Bradford, S., Simunek, J., Ustohal, P., Vereecken, H., and Klumpp, E. (2007). Bacteria transport and deposition under unsaturated conditions: The role of the matrix grain size and the bacteria surface protein. *Journal Of Contaminant Hydrology*, **92**(3-4), 255–273.

Gerke, H. H. and van Genuchten, M. T. (1993). A dual-porosity model for simulating the preferential movement of water and solutes in structured porous-media. *Water Resources Research*, **29**(2), 305–319.

Golfier, F., Wood, B. D., Orgogozo, L., Quintard, M., and Buès, M. (2009). Biofilms in porous media: Development of macroscopic transport equations via volume averaging with closure for local mass equilibrium conditions. *Advances in Water Resources*, **32**, 463–485.

Helmig, R. (1997). *Multiphase Flow and Transport Processes in the Subsurface*. Springer.

Huber, R. (1999). *Immiscible and Compositional Multiphase Flow and Transport in Heterogeneous Porous Media: Modelling, Formulation, and Numerical Simulation.* Ph.D. thesis, Technische Universität Braunschweig, Institut für Computeranwendungen im Bauingenieurwesen.

IPCC (2005). *Intergovernmental Panel on Climate Change: Special Report on Carbon Capture and Storage*. Cambridge Univ. Press.

Kopp, A., Ebigbo, A., Bielinski, A., Class, H., and Helmig, R. (2007). Numerical Simulation of Temperature Changes Caused by CO_2 Injection in Geological Reservoirs. In M. Grobe, J. C. Pashin, and R. L. Dodge, editors, *Carbon dioxide sequestration in gelogical media–State of the science*, chapter 26, pages 1–18.

Kopp, A., Binning, P. J., Johannsen, K., Class, H., and Helmig, R. (2009). Risk Analysis for Leakage through Abandoned Wells in Geological CO_2 Storage. *submitted to Energy Conversion and Management*.

Lewandowski, Z. (2000). Notes on biofilm porosity. *Water Research*, **34**(9), 2620–2624.

Lewandowski, Z. and Cunningham, A. B. (1998). *Bioremediation: Principles and Practice*, volume 1. Fundamentals and Applications, chapter Biofilm Process Fundamentals, pages 511–546. Technomic Publications.

Maggi, F. and Porporato, A. (2007). Coupled moisture and microbial dynamics in unsaturated soils. *Water Resources Research*, **43**(7), W07444.

Michaelides, E. E. (1981). Thermodynamic properties of geothermal fluids. *Geothermal Resources Council Transactions*, **5**, 361–364.

Mitchell, A. C., Phillips, A. J., Hamilton, M. A., Gerlach, R., Hollis, W. K., Kaszuba, J. P., and Cunningham, A. B. (2008). Resilience of planktonic and biofilm cultures to supercritical CO_2. *The Journal of Supercritical Fluids*, **47**(2), 318–325.

Mitchell, A. C., Phillips, A. J., Hiebert, R., Gerlach, R., Spangler, L. H., and Cunningham, A. B. (2009). Biofilm enhanced geologic sequestration of supercritical CO_2. *International Journal Of Greenhouse Gas Control*, **3**(1), 90–99.

Mostafa, M. and Van Geel, P. J. (2007). Conceptual models and simulations for biological clogging in unsaturated soils. *Vadose Zone Journal*, **6**(1), 175–185.

Mukhopadhyay, M. (2009). Extraction and processing with supercritical fluids. *Journal Of Chemical Technology And Biotechnology*, **84**(1), 6–12.

Murphy, E. M. and Ginn, T. R. (2000). Modeling microbial processes in porous media. *Hydrogeology Journal*, **8**(1), 142–158.

Niemet, M. R., Rockhold, M. L., Weisbrod, N., and Selker, J. S. (2002). Relationships between gas-liquid interfacial surface area, liquid saturation, and light transmission in variably saturated porous media. *Water Resources Research*, **38**(8), 1135.

Nordbotten, J. M., Celia, M. A., Bachu, S., and Dahle, H. K. (2005). Semi-Analytical Solution for CO_2 Leakage through an Abandoned Well. *Environmental Science and Technology*, **39(2)**, 602–611.

Oldenburg, C. M. (2008). Screening and ranking framework for geologic CO_2 storage site selection on the basis of health, safety, and environmental risk. *Environmental Geology*, **54**(8), 1687–1694.

Peyton, B. M. and Characklis, W. G. (1993). A statistical analysis of the effect of substrate uitlization and shear stress on the kinetics of biofilm detachment. *Biotechnology and Bioengineering*, **41**(7), 728–735.

Picioreanu, C., van Loosdrecht, M. C. M., and Heijnen, J. J. (2001). Two-dimensional model of biofilm detachment caused by internal stress from liquid flow. *Biotechnology And Bioengineering*, **72**(2), 205–218.

Pruess, K. (2004). Thermal Effects During CO_2 Leakage from a Geologic Storage Reservoir. Technical Report LBNL-55913, Lawrence Berkeley National Laboratory.

Pruess, K. (2005). Numerical studies of fluid leakage from a geologic disposal reservoir for co_2 show self-limiting feedback between fluid flow and heat transfer. *Geophysical Research Letters*, **32**(14), L14404.

Pruess, K., Faybishenko, B., and Bodvarsson, G. S. (1999). Alternative concepts and approaches for modeling flow and transport in thick unsaturated zones of fractured rocks. *Journal Of Contaminant Hydrology*, **38**(1-3), 281–322.

Rittmann, B. E. (1982). The effect of shear stress on biofilm loss rate. *Biotechnology and Bioengineering*, **24**(2), 501–506.

Rittmann, B. E. (1993). The significance of biofilms in porous media. *Water Resources Research*, **29**, 2195–2202.

Rockhold, M. L., Yarwood, R. R., Niemet, M. R., Bottomley, P. J., and Selker, J. S. (2002). Considerations for modeling bacterial-induced changes in hydraulic properties of variably saturated porous media. *Advances In Water Resources*, **25**(5), 477–495.

Rockhold, M. L., Yarwood, R. R., and Selker, J. S. (2004). Coupled microbial and transport processes in soils. *Vadose Zone J*, **3**(2), 368–383.

Schaefer, A., Ustohal, P., Harms, H., Stauffer, F., Dracos, T., and Zehnder, A. J. B. (1998). Transport of bacteria in unsaturated porous media. *Journal Of Contaminant Hydrology*, **33**(1-2), 149–169.

Seki, K. and Miyazaki, T. (2001). A mathematical model for biological clogging of uniform porous media. *Water Resources Research*, **37**(12), 2995–2999.

Sen, R. (2008). Biotechnology in petroleum recovery: The microbial EOR. *Progress In Energy And Combustion Science*, **34**(6), 714–724.

Span, R. and Wagner, W. (1996). A New Equation of State for Carbon Dioxide Covering the Fluid Region from the Triple-Point Temperature to 1100 K at Pressures up to 800 MPa. *J. Phys. Chem. Ref. Data*, **25**(6), 1509–1596.

Speitel, G. E. and DiGiano, F. A. (1987). Biofilm shearing under dynamic conditions. *Journal Of Environmental Engineering-Asce*, **113**(3), 464–475.

Stewart, P. S. (1993). A model of biofilm detachment. *Biotechnology and Bioengineering*, **41**(1), 111–117.

Stewart, P. S. (1998). A review of experimental measurements of effective diffusive permeabilities and effective diffusion coefficients in biofilms. *Biotechnology And Bioengineering*, **59**(3), 261–272.

Stoodley, P., De Beer, D., and Lewandowski, Z. (1994). Liquid flow in biofilm systems. *Applied And Environmental Microbiology*, **60**(8), 2711–2716.

Taylor, S. W. and Jaffé, P. R. (1990a). Biofilm Growth and the Related Changes in the Physical Properties of a Porous Medium 1. Experimental Investigation. *Water Resources Research*, **26**(9), 2153–2159.

Taylor, S. W. and Jaffé, P. R. (1990b). Substrate and Biomass Transport in a Porous Medium. *Water Resources Research*, **26**(9), 2181–2194.

Taylor, S. W., Milly, P. C. D., and Jaffé, P. R. (1990). Biofilm Growth and the Related Changes in the Physical Properties of a Porous Medium 2. Permeability. *Water Resources Research*, **26**(9), 2161–2169.

Tchobanoglous, G., Burton, F. L., and Stensel, H. D. (2003). *Wastewater Engineering, Treatment and Reuse*. McGraw-Hill.

Thullner, M. and Baveye, P. (2008). Computational pore network modeling of the influence of biofilm permeability on bioclogging in porous media. *Biotechnology And Bioengineering*, **99**(6), 1337–1351.

Thullner, M., Zeyer, J., and Kinzelbach, W. (2002). Influence of microbial growth on hydraulic properties of pore networks. *Transport In Porous Media*, **49**(1), 99–122.

Tijhuis, L., van Loosdrecht, M. C. M., and Heijnen, J. J. (1995). Dynamics of biofilm detachment in biofilm airlift suspension reactors. *Biotechnology and Bioengineering*, **45**(6), 481–487.

Tufenkji, N. and Elimelech, M. (2004). Correlation equation for predicting single-collector efficiency in physicochemical filtration in saturated porous media. *Environmental Science & Technology*, **38**(2), 529–536.

Valdes, J. J., editor (2000). *Bioremediation*. Kluwer.

van Loosdrecht, M. C. M. and Henze, M. (1999). Maintenance, endogeneous respiration, lysis, decay and predation. *Water Science And Technology*, **39**(1), 107–117.

van Loosdrecht, M. C. M., Lyklema, J., Norde, W., and Zehnder, A. J. (1990). Influence of interfaces on microbial activity. *Microbiol. Mol. Biol. Rev.*, **54**(1), 75–87.

van Loosdrecht, M. C. M., Eikelboom, D., Gjaltema, A., Mulder, A., Tijhuis, L., and Heijnen, J. J. (1995). Biofilm structures. *Water Science And Technology*, **32**(8), 35–43.

van Loosdrecht, M. C. M., Heijnen, J. J., Eberl, H., Kreft, J., and Picioreanu, C. (2002). Mathematical modelling of biofilm structures. *Antonie van Leeuwenhoek*, **81(12)**, 245–256.

Vandevivere, P. (1995). Bacterial clogging of porous-media - a new modeling approach. *Biofouling*, **8**(4), 281–291.

Vandevivere, P. and Baveye, P. (1992). Effect of bacterial extracellular polymers on the saturated hydraulic conductivity of sand columns. *Applied and Environmental Microbiology*, **58**(5), 1690–1698.

White, F. M. (2003). *Fluid Mechanics*. McGraw-Hill.

Wiedemeier, T. H., Rifai, H. S., Newell, C. J., and Wilson, J. T. (1999). *Natural Attenuation of Fuels and Chlorinated Solvents in the Subsurface*. Wiley.

Wimpenny, J. W. T. and Colasanti, R. (1997). A unifying hypothesis for the structure of microbial biofilms based on cellular automaton models. *Fems Microbiology Ecology*, **22**(1), 1–16.

Wood, B. D., Quintard, M., and Whitaker, S. (2002). Calculation of effective diffusivities for biofilms and tissues. *Biotechnology And Bioengineering*, **77**(5), 495–516.

Wu, Y. S., Pan, L. H., and Pruess, K. (2004). A physically based approach for modeling multiphase fracture-matrix interaction in fractured porous media. *Advances In Water Resources*, **27**(9), 875–887.

Xu, T. F., Ontoy, Y., Molling, P., Spycher, N., Parini, M., and Pruess, K. (2004). Reactive transport modeling of injection well scaling and acidizing at Tiwi field, Philippines. *Geothermics*, **33**(4), 477–491.

Zekri, A. Y. (2001). Microbial enhanced oil recovery - a short review. *Oil Gas European Magazine*, **1**, 22–25.

Zhang, J., Davis, T. A., Matthews, M. A., Drews, M. J., LaBerge, M., and An, Y. H. (2006). Sterilization using high-pressure carbon dioxide. *The Journal of Supercritical Fluids*, **38**(3), 354–372.

Zhang, T. C. and Bishop, P. L. (1994). Density, porosity, and pore structure of biofilms. *Water Research*, **28**(11), 2267–2277.

Institut für Wasserbau
Universität Stuttgart

Pfaffenwaldring 61
70569 Stuttgart (Vaihingen)
Telefon (0711) 685 - 64717/64749/64752/64679
Telefax (0711) 685 - 67020 o. 64746 o. 64681
E-Mail: iws@iws.uni-stuttgart.de
http://www.iws.uni-stuttgart.de

Verzeichnis der Mitteilungshefte

5 Plate, Erich: *Beitrag zur Bestimmung der Windgeschwindigkeitsverteilung in der durch eine Wand gestörten bodennahen Luftschicht*,
und
Röhnisch, Arthur; Marotz, Günter: *Neue Baustoffe und Bauausführungen für den Schutz der Böschungen und der Sohle von Kanälen, Flüssen und Häfen; Gestehungskosten und jeweilige Vorteile*, sowie Unny, T.E.: *Schwingungsuntersuchungen am Kegelstrahlschieber*, 1967

6 Seiler, Erich: *Die Ermittlung des Anlagenwertes der bundeseigenen Binnenschiffahrtsstraßen und Talsperren und des Anteils der Binnenschiffahrt an diesem Wert*, 1967

7 *Sonderheft anläßlich des 65. Geburtstages von Prof. Arthur Röhnisch mit Beiträgen von* Benk, Dieter; Breitling, J.; Gurr, Siegfried; Haberhauer, Robert; Honekamp, Hermann; Kuz, Klaus Dieter; Marotz, Günter; Mayer-Vorfelder, Hans-Jörg; Miller, Rudolf; Plate, Erich J.; Radomski, Helge; Schwarz, Helmut; Vollmer, Ernst; Wildenhahn, Eberhard; 1967

8 Jumikis, Alfred: *Beitrag zur experimentellen Untersuchung des Wassernachschubs in einem gefrierenden Boden und die Beurteilung der Ergebnisse*, 1968

9 Marotz, Günter: *Technische Grundlagen einer Wasserspeicherung im natürlichen Untergrund*, 1968

10 Radomski, Helge: *Untersuchungen über den Einfluß der Querschnittsform wellenförmiger Spundwände auf die statischen und rammtechnischen Eigenschaften*, 1968

11 Schwarz, Helmut: *Die Grenztragfähigkeit des Baugrundes bei Einwirkung vertikal gezogener Ankerplatten als zweidimensionales Bruchproblem*, 1969

12 Erbel, Klaus: *Ein Beitrag zur Untersuchung der Metamorphose von Mittelgebirgsschneedecken unter besonderer Berücksichtigung eines Verfahrens zur Bestimmung der thermischen Schneequalität*, 1969

13 Westhaus, Karl-Heinz: *Der Strukturwandel in der Binnenschiffahrt und sein Einfluß auf den Ausbau der Binnenschiffskanäle*, 1969

14 Mayer-Vorfelder, Hans-Jörg: *Ein Beitrag zur Berechnung des Erdwiderstandes unter Ansatz der logarithmischen Spirale als Gleitflächenfunktion*, 1970

15 Schulz, Manfred: *Berechnung des räumlichen Erddruckes auf die Wandung kreiszylindrischer Körper*, 1970

16 Mobasseri, Manoutschehr: *Die Rippenstützmauer. Konstruktion und Grenzen ihrer Standsicherheit*, 1970

17 Benk, Dieter: *Ein Beitrag zum Betrieb und zur Bemessung von Hochwasserrückhaltebecken*, 1970

18 Gàl, Attila: *Bestimmung der mitschwingenden Wassermasse bei überströmten Fischbauchklappen mit kreiszylindrischem Staublech*, 1971, vergriffen

19 Kuz, Klaus Dieter: *Ein Beitrag zur Frage des Einsetzens von Kavitationserscheinungen in einer Düsenströmung bei Berücksichtigung der im Wasser gelösten Gase*, 1971, vergriffen

20 Schaak, Hartmut: *Verteilleitungen von Wasserkraftanlagen*, 1971

21 *Sonderheft zur Eröffnung der neuen Versuchsanstalt des Instituts für Wasserbau der Universität Stuttgart mit Beiträgen von* Brombach, Hansjörg; Dirksen, Wolfram; Gàl, Attila; Gerlach, Reinhard; Giesecke, Jürgen; Holthoff, Franz-Josef; Kuz, Klaus Dieter; Marotz, Günter; Minor, Hans-Erwin; Petrikat, Kurt; Röhnisch, Arthur; Rueff, Helge; Schwarz, Helmut; Vollmer, Ernst; Wildenhahn, Eberhard; 1972

22 Wang, Chung-su: *Ein Beitrag zur Berechnung der Schwingungen an Kegelstrahlschiebern*, 1972

23 Mayer-Vorfelder, Hans-Jörg: *Erdwiderstandsbeiwerte nach dem Ohde-Variationsverfahren*, 1972

24 Minor, Hans-Erwin: *Beitrag zur Bestimmung der Schwingungsanfachungsfunktionen überströmter Stauklappen*, 1972, vergriffen

25 Brombach, Hansjörg: *Untersuchung strömungsmechanischer Elemente (Fluidik) und die Möglichkeit der Anwendung von Wirbelkammerelementen im Wasserbau*, 1972, vergriffen

26 Wildenhahn, Eberhard: *Beitrag zur Berechnung von Horizontalfilterbrunnen*, 1972

27 Steinlein, Helmut: *Die Eliminierung der Schwebstoffe aus Flußwasser zum Zweck der unterirdischen Wasserspeicherung, gezeigt am Beispiel der Iller*, 1972

28 Holthoff, Franz Josef: *Die Überwindung großer Hubhöhen in der Binnenschiffahrt durch Schwimmerhebewerke*, 1973

29 Röder, Karl: *Einwirkungen aus Baugrundbewegungen auf trog- und kastenförmige Konstruktionen des Wasser- und Tunnelbaues*, 1973

30 Kretschmer, Heinz: *Die Bemessung von Bogenstaumauern in Abhängigkeit von der Talform*, 1973

31 Honekamp, Hermann: *Beitrag zur Berechnung der Montage von Unterwasserpipelines*, 1973

32 Giesecke, Jürgen: *Die Wirbelkammertriode als neuartiges Steuerorgan im Wasserbau*, und Brombach, Hansjörg: *Entwicklung, Bauformen, Wirkungsweise und Steuereigenschaften von Wirbelkammerverstärkern*, 1974

33 Rueff, Helge: *Untersuchung der schwingungserregenden Kräfte an zwei hintereinander angeordneten Tiefschützen unter besonderer Berücksichtigung von Kavitation*, 1974

34 Röhnisch, Arthur: *Einpreßversuche mit Zementmörtel für Spannbeton - Vergleich der Ergebnisse von Modellversuchen mit Ausführungen in Hüllwellrohren*, 1975

35 *Sonderheft anläßlich des 65. Geburtstages von Prof. Dr.-Ing. Kurt Petrikat mit Beiträgen von*: Brombach, Hansjörg; Erbel, Klaus; Flinspach, Dieter; Fischer jr., Richard; Gàl, Attila; Gerlach, Reinhard; Giesecke, Jürgen; Haberhauer, Robert; Hafner Edzard; Hausenblas, Bernhard; Horlacher, Hans-Burkhard; Hutarew, Andreas; Knoll, Manfred; Krummet, Ralph; Marotz, Günter; Merkle, Theodor; Miller, Christoph; Minor, Hans-Erwin; Neumayer, Hans; Rao, Syamala; Rath, Paul; Rueff, Helge; Ruppert, Jürgen; Schwarz, Wolfgang; Topal-Gökceli, Mehmet; Vollmer, Ernst; Wang, Chung-su; Weber, Hans-Georg; 1975

36 Berger, Jochum: *Beitrag zur Berechnung des Spannungszustandes in rotationssymmetrisch belasteten Kugelschalen veränderlicher Wandstärke unter Gas- und Flüssigkeitsdruck durch Integration schwach singulärer Differentialgleichungen*, 1975

37 Dirksen, Wolfram: *Berechnung instationärer Abflußvorgänge in gestauten Gerinnen mittels Differenzenverfahren und die Anwendung auf Hochwasserrückhaltebecken*, 1976

38 Horlacher, Hans-Burkhard: *Berechnung instationärer Temperatur- und Wärmespannungsfelder in langen mehrschichtigen Hohlzylindern*, 1976

39 Hafner, Edzard: *Untersuchung der hydrodynamischen Kräfte auf Baukörper im Tiefwasserbereich des Meeres*, 1977, ISBN 3-921694-39-6

40 Ruppert, Jürgen: *Über den Axialwirbelkammerverstärker für den Einsatz im Wasserbau*, 1977, ISBN 3-921694-40-X

41 Hutarew, Andreas: *Beitrag zur Beeinflußbarkeit des Sauerstoffgehalts in Fließgewässern an Abstürzen und Wehren*, 1977, ISBN 3-921694-41-8, vergriffen

42 Miller, Christoph: *Ein Beitrag zur Bestimmung der schwingungserregenden Kräfte an unterströmten Wehren*, 1977, ISBN 3-921694-42-6

43 Schwarz, Wolfgang: *Druckstoßberechnung unter Berücksichtigung der Radial- und Längsverschiebungen der Rohrwandung*, 1978, ISBN 3-921694-43-4

44 Kinzelbach, Wolfgang: *Numerische Untersuchungen über den optimalen Einsatz variabler Kühlsysteme einer Kraftwerkskette am Beispiel Oberrhein*, 1978, ISBN 3-921694-44-2

45 Barczewski, Baldur: *Neue Meßmethoden für Wasser-Luftgemische und deren Anwendung auf zweiphasige Auftriebsstrahlen*, 1979, ISBN 3-921694-45-0

46 Neumayer, Hans: *Untersuchung der Strömungsvorgänge in radialen Wirbelkammerverstärkern*, 1979, ISBN 3-921694-46-9

47 Elalfy, Youssef-Elhassan: *Untersuchung der Strömungsvorgänge in Wirbelkammerdioden und -drosseln*, 1979, ISBN 3-921694-47-7

48 Brombach, Hansjörg: *Automatisierung der Bewirtschaftung von Wasserspeichern*, 1981, ISBN 3-921694-48-5

49 Geldner, Peter: *Deterministische und stochastische Methoden zur Bestimmung der Selbstdichtung von Gewässern*, 1981, ISBN 3-921694-49-3, vergriffen

50 Mehlhorn, Hans: *Temperaturveränderungen im Grundwasser durch Brauchwassereinleitungen*, 1982, ISBN 3-921694-50-7, vergriffen

51 Hafner, Edzard: *Rohrleitungen und Behälter im Meer*, 1983, ISBN 3-921694-51-5

52 Rinnert, Bernd: *Hydrodynamische Dispersion in porösen Medien: Einfluß von Dichteunterschieden auf die Vertikalvermischung in horizontaler Strömung*, 1983, ISBN 3-921694-52-3, vergriffen

53 Lindner, Wulf: *Steuerung von Grundwasserentnahmen unter Einhaltung ökologischer Kriterien*, 1983, ISBN 3-921694-53-1, vergriffen

54 Herr, Michael; Herzer, Jörg; Kinzelbach, Wolfgang; Kobus, Helmut; Rinnert, Bernd: *Methoden zur rechnerischen Erfassung und hydraulischen Sanierung von Grundwasserkontaminationen*, 1983, ISBN 3-921694-54-X

55 Schmitt, Paul: *Wege zur Automatisierung der Niederschlagsermittlung*, 1984, ISBN 3-921694-55-8, vergriffen

56 Müller, Peter: *Transport und selektive Sedimentation von Schwebstoffen bei gestautem Abfluß*, 1985, ISBN 3-921694-56-6

57 El-Qawasmeh, Fuad: *Möglichkeiten und Grenzen der Tropfbewässerung unter besonderer Berücksichtigung der Verstopfungsanfälligkeit der Tropfelemente*, 1985, ISBN 3-921694-57-4, vergriffen

58 Kirchenbaur, Klaus: *Mikroprozessorgesteuerte Erfassung instationärer Druckfelder am Beispiel seegangsbelasteter Baukörper*, 1985, ISBN 3-921694-58-2

59 Kobus, Helmut (Hrsg.): *Modellierung des großräumigen Wärme- und Schadstofftransports im Grundwasser*, Tätigkeitsbericht 1984/85 (DFG-Forschergruppe an den Universitäten Hohenheim, Karlsruhe und Stuttgart), 1985, ISBN 3-921694-59-0, vergriffen

60 Spitz, Karlheinz: *Dispersion in porösen Medien: Einfluß von Inhomogenitäten und Dichteunterschieden*, 1985, ISBN 3-921694-60-4, vergriffen

61 Kobus, Helmut: *An Introduction to Air-Water Flows in Hydraulics*, 1985, ISBN 3-921694-61-2

62 Kaleris, Vassilios: *Erfassung des Austausches von Oberflächen- und Grundwasser in horizontalebenen Grundwassermodellen*, 1986, ISBN 3-921694-62-0

63 Herr, Michael: *Grundlagen der hydraulischen Sanierung verunreinigter Porengrundwasserleiter*, 1987, ISBN 3-921694-63-9

64 Marx, Walter: *Berechnung von Temperatur und Spannung in Massenbeton infolge Hydratation*, 1987, ISBN 3-921694-64-7

65 Koschitzky, Hans-Peter: *Dimensionierungskonzept für Sohlbelüfter in Schußrinnen zur Vermeidung von Kavitationsschäden*, 1987, ISBN 3-921694-65-5

66 Kobus, Helmut (Hrsg.): *Modellierung des großräumigen Wärme- und Schadstofftransports im Grundwasser*, Tätigkeitsbericht 1986/87 (DFG-Forschergruppe an den Universitäten Hohenheim, Karlsruhe und Stuttgart) 1987, ISBN 3-921694-66-3

67 Söll, Thomas: *Berechnungsverfahren zur Abschätzung anthropogener Temperaturanomalien im Grundwasser*, 1988, ISBN 3-921694-67-1

68 Dittrich, Andreas; Westrich, Bernd: *Bodenseeufererosion, Bestandsaufnahme und Bewertung*, 1988, ISBN 3-921694-68-X, vergriffen

69 Huwe, Bernd; van der Ploeg, Rienk R.: *Modelle zur Simulation des Stickstoffhaushaltes von Standorten mit unterschiedlicher landwirtschaftlicher Nutzung*, 1988, ISBN 3-921694-69-8, vergriffen

70 Stephan, Karl: *Integration elliptischer Funktionen*, 1988, ISBN 3-921694-70-1

71 Kobus, Helmut; Zilliox, Lothaire (Hrsg.): *Nitratbelastung des Grundwassers, Auswirkungen der Landwirtschaft auf die Grundwasser- und Rohwasserbeschaffenheit und Maßnahmen zum Schutz des Grundwassers*. Vorträge des deutsch-französischen Kolloquiums am 6. Oktober 1988, Universitäten Stuttgart und Louis Pasteur Strasbourg (Vorträge in deutsch oder französisch, Kurzfassungen zweisprachig), 1988, ISBN 3-921694-71-X

72 Soyeaux, Renald: *Unterströmung von Stauanlagen auf klüftigem Untergrund unter Berücksichtigung laminarer und turbulenter Fließzustände*,1991, ISBN 3-921694-72-8

73 Kohane, Roberto: *Berechnungsmethoden für Hochwasserabfluß in Fließgewässern mit überströmten Vorländern*, 1991, ISBN 3-921694-73-6

74 Hassinger, Reinhard: *Beitrag zur Hydraulik und Bemessung von Blocksteinrampen in flexibler Bauweise*, 1991, ISBN 3-921694-74-4, vergriffen

75 Schäfer, Gerhard: *Einfluß von Schichtenstrukturen und lokalen Einlagerungen auf die Längsdispersion in Porengrundwasserleitern*, 1991, ISBN 3-921694-75-2

76 Giesecke, Jürgen: *Vorträge, Wasserwirtschaft in stark besiedelten Regionen; Umweltforschung mit Schwerpunkt Wasserwirtschaft*, 1991, ISBN 3-921694-76-0

77 Huwe, Bernd: *Deterministische und stochastische Ansätze zur Modellierung des Stickstoffhaushalts landwirtschaftlich genutzter Flächen auf unterschiedlichem Skalenniveau*, 1992, ISBN 3-921694-77-9, vergriffen

78 Rommel, Michael: *Verwendung von Kluftdaten zur realitätsnahen Generierung von Kluftnetzen mit anschließender laminar-turbulenter Strömungsberechnung*, 1993, ISBN 3-92 1694-78-7

79 Marschall, Paul: *Die Ermittlung lokaler Stofffrachten im Grundwasser mit Hilfe von Einbohrloch-Meßverfahren*, 1993, ISBN 3-921694-79-5, vergriffen

80 Ptak, Thomas: *Stofftransport in heterogenen Porenaquiferen: Felduntersuchungen und stochastische Modellierung*, 1993, ISBN 3-921694-80-9, vergriffen

81 Haakh, Frieder: *Transientes Strömungsverhalten in Wirbelkammern,* 1993, ISBN 3-921694-81-7

82 Kobus, Helmut; Cirpka, Olaf; Barczewski, Baldur; Koschitzky, Hans-Peter: *Versucheinrichtung zur Grundwasser und Altlastensanierung VEGAS, Konzeption und Programmrahmen*, 1993, ISBN 3-921694-82-5

83 Zang, Weidong: *Optimaler Echtzeit-Betrieb eines Speichers mit aktueller Abflußregenerierung*, 1994, ISBN 3-921694-83-3, vergriffen

84 Franke, Hans-Jörg: *Stochastische Modellierung eines flächenhaften Stoffeintrages und Transports in Grundwasser am Beispiel der Pflanzenschutzmittelproblematik*, 1995, ISBN 3-921694-84-1

85 Lang, Ulrich: *Simulation regionaler Strömungs- und Transportvorgänge in Karstaquiferen mit Hilfe des Doppelkontinuum-Ansatzes: Methodenentwicklung und Parameteridentifikation*, 1995, ISBN 3-921694-85-X, vergriffen

86 Helmig, Rainer: *Einführung in die Numerischen Methoden der Hydromechanik*, 1996, ISBN 3-921694-86-8, vergriffen

87 Cirpka, Olaf: *CONTRACT: A Numerical Tool for Contaminant Transport and Chemical Transformations - Theory and Program Documentation* -, 1996, ISBN 3-921694-87-6

88 Haberlandt, Uwe: *Stochastische Synthese und Regionalisierung des Niederschlages für Schmutzfrachtberechnungen*, 1996, ISBN 3-921694-88-4

89 Croisé, Jean: *Extraktion von flüchtigen Chemikalien aus natürlichen Lockergesteinen mittels erzwungener Luftströmung*, 1996, ISBN 3-921694-89-2, vergriffen

90 Jorde, Klaus: *Ökologisch begründete, dynamische Mindestwasserregelungen bei Ausleitungskraftwerken*, 1997, ISBN 3-921694-90-6, vergriffen

91 Helmig, Rainer: *Gekoppelte Strömungs- und Transportprozesse im Untergrund - Ein Beitrag zur Hydrosystemmodellierung*-, 1998, ISBN 3-921694-91-4, vergriffen

92 Emmert, Martin: *Numerische Modellierung nichtisothermer Gas-Wasser Systeme in porösen Medien,* 1997, ISBN 3-921694-92-2

93 Kern, Ulrich: *Transport von Schweb- und Schadstoffen in staugeregelten Fließgewässern am Beispiel des Neckars*, 1997, ISBN 3-921694-93-0, vergriffen

94 Förster, Georg: *Druckstoßdämpfung durch große Luftblasen in Hochpunkten von Rohrleitungen 1997*, ISBN 3-921694-94-9

95 Cirpka, Olaf: *Numerische Methoden zur Simulation des reaktiven Mehrkomponententransports im Grundwasser*, 1997, ISBN 3-921694-95-7, vergriffen

96 Färber, Arne: *Wärmetransport in der ungesättigten Bodenzone: Entwicklung einer thermischen In-situ-Sanierungstechnologie*, 1997, ISBN 3-921694-96-5

97 Betz, Christoph: *Wasserdampfdestillation von Schadstoffen im porösen Medium: Entwicklung einer thermischen In-situ-Sanierungstechnologie*, 1998, ISBN 3-921694-97-3

98 Xu, Yichun: *Numerical Modeling of Suspended Sediment Transport in Rivers*, 1998, ISBN 3-921694-98-1, vergriffen

99 Wüst, Wolfgang: *Geochemische Untersuchungen zur Sanierung CKW-kontaminierter Aquifere mit Fe(0)-Reaktionswänden,* 2000, ISBN 3-933761-02-2

100 Sheta, Hussam: *Simulation von Mehrphasenvorgängen in porösen Medien unter Einbeziehung von Hysterese-Effekten*, 2000, ISBN 3-933761-03-4

101 Ayros, Edwin: *Regionalisierung extremer Abflüsse auf der Grundlage statistischer Verfahren*, 2000, ISBN 3-933761-04-2, vergriffen

102 Huber, Ralf: *Compositional Multiphase Flow and Transport in Heterogeneous Porous Media*, 2000, ISBN 3-933761-05-0

103 Braun, Christopherus: *Ein Upscaling-Verfahren für Mehrphasenströmungen in porösen Medien*, 2000, ISBN 3-933761-06-9

104 Hofmann, Bernd: *Entwicklung eines rechnergestützten Managementsystems zur Beurteilung von Grundwasserschadensfällen*, 2000, ISBN 3-933761-07-7

105 Class, Holger: *Theorie und numerische Modellierung nichtisothermer Mehrphasenprozesse in NAPL-kontaminierten porösen Medien,* 2001, ISBN 3-933761-08-5

106 Schmidt, Reinhard: *Wasserdampf- und Heißluftinjektion zur thermischen Sanierung kontaminierter Standorte*, 2001, ISBN 3-933761-09-3

107 Josef, Reinhold:, *Schadstoffextraktion mit hydraulischen Sanierungsverfahren unter Anwendung von grenzflächenaktiven Stoffen*, 2001, ISBN 3-933761-10-7

108 Schneider, Matthias: *Habitat- und Abflussmodellierung für Fließgewässer mit unscharfen Berechnungsansätzen*, 2001, ISBN 3-933761-11-5

109 Rathgeb, Andreas: *Hydrodynamische Bemessungsgrundlagen für Lockerdeckwerke an überströmbaren Erddämmen*, 2001, ISBN 3-933761-12-3

110 Lang, Stefan: *Parallele numerische Simulation instätionärer Probleme mit adaptiven Methoden auf unstrukturierten Gittern*, 2001, ISBN 3-933761-13-1

111 Appt, Jochen; Stumpp Simone: *Die Bodensee-Messkampagne 2001, IWS/CWR Lake Constance Measurement Program 2001*, 2002, ISBN 3-933761-14-X

112 Heimerl, Stephan: *Systematische Beurteilung von Wasserkraftprojekten,* 2002, ISBN 3-933761-15-8

113 Iqbal, Amin: *On the Management and Salinity Control of Drip Irrigation,* 2002, ISBN 3-933761-16-6

114 Silberhorn-Hemminger, Annette: *Modellierung von Kluftaquifersystemen: Geostatistische Analyse und deterministisch-stochastische Kluftgenerierung,* 2002, ISBN 3-933761-17-4

115 Winkler, Angela: *Prozesse des Wärme- und Stofftransports bei der In-situ-Sanierung mit festen Wärmequellen,* 2003, ISBN 3-933761-18-2

116 Marx, Walter: *Wasserkraft, Bewässerung, Umwelt - Planungs- und Bewertungsschwerpunkte der Wasserbewirtschaftung,* 2003, ISBN 3-933761-19-0

117 Hinkelmann, Reinhard: *Efficient Numerical Methods and Information-Processing Techniques in Environment Water,* 2003, ISBN 3-933761-20-4

118 Samaniego-Eguiguren, Luis Eduardo: *Hydrological Consequences of Land Use / Land Cover and Climatic Changes in Mesoscale Catchments*, 2003, ISBN 3-933761-21-2

119 Neunhäuserer, Lina: *Diskretisierungsansätze zur Modellierung von Strömungs- und Transportprozessen in geklüftet-porösen Medien*, 2003, ISBN 3-933761-22-0

120 Paul, Maren: *Simulation of Two-Phase Flow in Heterogeneous Poros Media with Adaptive Methods*, 2003, ISBN 3-933761-23-9

121 Ehret, Uwe: *Rainfall and Flood Nowcasting in Small Catchments using Weather Radar*, 2003, ISBN 3-933761-24-7

122 Haag, Ingo: *Der Sauerstoffhaushalt staugeregelter Flüsse am Beispiel des Neckars - Analysen, Experimente, Simulationen -,* 2003, ISBN 3-933761-25-5

123 Appt, Jochen: *Analysis of Basin-Scale Internal Waves in Upper Lake Constance,* 2003, ISBN 3-933761-26-3

124 Hrsg.: Schrenk, Volker; Batereau, Katrin; Barczewski, Baldur; Weber, Karolin und Koschitzky, Hans-Peter: *Symposium Ressource Fläche und VEGAS - Statuskolloquium 2003, 30. September und 1. Oktober 2003,* 2003, ISBN 3-933761-27-1

125 Omar Khalil Ouda: *Optimisation of Agricultural Water Use: A Decision Support System for the Gaza Strip,* 2003, ISBN 3-933761-28-0

126 Batereau, Katrin: *Sensorbasierte Bodenluftmessung zur Vor-Ort-Erkundung von Schadensherden im Untergrund*, 2004, ISBN 3-933761-29-8

127 Witt, Oliver: *Erosionsstabilität von Gewässersedimenten mit Auswirkung auf den Stofftransport bei Hochwasser am Beispiel ausgewählter Stauhaltungen des Oberrheins*, 2004, ISBN 3-933761-30-1

128 Jakobs, Hartmut: *Simulation nicht-isothermer Gas-Wasser-Prozesse in komplexen Kluft-Matrix-Systemen*, 2004, ISBN 3-933761-31-X

129 Li, Chen-Chien: *Deterministisch-stochastisches Berechnungskonzept zur Beurteilung der Auswirkungen erosiver Hochwasserereignisse in Flussstauhaltungen,* 2004, ISBN 3-933761-32-8

130 Reichenberger, Volker; Helmig, Rainer; Jakobs, Hartmut; Bastian, Peter; Niessner, Jennifer: *Complex Gas-Water Processes in Discrete Fracture-Matrix Systems: Upscaling, Mass-Conservative Discretization and Efficient Multilevel Solution,* 2004, ISBN 3-933761-33-6

131 Hrsg.: Barczewski, Baldur; Koschitzky, Hans-Peter; Weber, Karolin; Wege, Ralf: *VEGAS - Statuskolloquium 2004,* Tagungsband zur Veranstaltung am 05. Oktober 2004 an der Universität Stuttgart, Campus Stuttgart-Vaihingen, 2004, ISBN 3-933761-34-4

132 Asie, Kemal Jabir: *Finite Volume Models for Multiphase Multicomponent Flow through Porous Media*. 2005, ISBN 3-933761-35-2

133 Jacoub, George: *Development of a 2-D Numerical Module for Particulate Contaminant Transport in Flood Retention Reservoirs and Impounded Rivers,* 2004, ISBN 3-933761-36-0

134 Nowak, Wolfgang: *Geostatistical Methods for the Identification of Flow and Transport Parameters in the Subsurface,* 2005, ISBN 3-933761-37-9

135 Süß, Mia: *Analysis of the influence of structures and boundaries on flow and transport processes in fractured porous media*, 2005, ISBN 3-933761-38-7

136 Jose, Surabhin Chackiath: *Experimental Investigations on Longitudinal Dispersive Mixing in Heterogeneous Aquifers,* 2005, ISBN: 3-933761-39-5

137 Filiz, Fulya: *Linking Large-Scale Meteorological Conditions to Floods in Mesoscale Catchments,* 2005, ISBN 3-933761-40-9

138 Qin, Minghao: *Wirklichkeitsnahe und recheneffiziente Ermittlung von Temperatur und Spannungen bei großen RCC-Staumauern*, 2005, ISBN 3-933761-41-7

139 Kobayashi, Kenichiro: *Optimization Methods for Multiphase Systems in the Subsurface - Application to Methane Migration in Coal Mining Areas*, 2005, ISBN 3-933761-42-5

140 Rahman, Md. Arifur: *Experimental Investigations on Transverse Dispersive Mixing in Heterogeneous Porous Media,* 2005, ISBN 3-933761-43-3

141 Schrenk, Volker: *Ökobilanzen zur Bewertung von Altlastensanierungsmaßnahmen,* 2005, ISBN 3-933761-44-1

142 Hundecha, Hirpa Yeshewatesfa: *Regionalization of Parameters of a Conceptual Rainfall-Runoff Model*, 2005, ISBN: 3-933761-45-X

143 Wege, Ralf: *Untersuchungs- und Überwachungsmethoden für die Beurteilung natürlicher Selbstreinigungsprozesse im Grundwasser,* 2005, ISBN 3-933761-46-8

144 Breiting, Thomas: *Techniken und Methoden der Hydroinformatik - Modellierung von komplexen Hydrosystemen im Untergrund*, 2006, 3-933761-47-6

145 Hrsg.: Braun, Jürgen; Koschitzky, Hans-Peter; Müller, Martin: *Ressource Untergrund: 10 Jahre VEGAS: Forschung und Technologieentwicklung zum Schutz von Grundwasser und Boden,* Tagungsband zur Veranstaltung am 28. und 29. September 2005 an der Universität Stuttgart, Campus Stuttgart-Vaihingen, 2005, ISBN 3-933761-48-4

146 Rojanschi, Vlad: *Abflusskonzentration in mesoskaligen Einzugsgebieten unter Berücksichtigung des Sickerraumes,* 2006, ISBN 3-933761-49-2

147 Winkler, Nina Simone: *Optimierung der Steuerung von Hochwasserrückhaltebecken-systemen,* 2006, ISBN 3-933761-50-6

148 Wolf, Jens: *Räumlich differenzierte Modellierung der Grundwasserströmung alluvialer Aquifere für mesoskalige Einzugsgebiete*, 2006, ISBN: 3-933761-51-4

149 Kohler, Beate: *Externe Effekte der Laufwasserkraftnutzung*, 2006, ISBN 3-933761-52-2

150 Hrsg.: Braun, Jürgen; Koschitzky, Hans-Peter; Stuhrmann, Matthias: *VEGAS-Statuskolloquium 2006,* Tagungsband zur Veranstaltung am 28. September 2006 an der Universität Stuttgart, Campus Stuttgart-Vaihingen, 2006, ISBN 3-933761-53-0

151 Niessner, Jennifer: *Multi-Scale Modeling of Multi-Phase - Multi-Component Processes in Heterogeneous Porous Media*, 2006, ISBN 3-933761-54-9

152 Fischer, Markus: *Beanspruchung eingeerdeter Rohrleitungen infolge Austrocknung bindiger Böden,* 2006, ISBN 3-933761-55-7

153 Schneck, Alexander: *Optimierung der Grundwasserbewirtschaftung unter Berücksichtigung der Belange der Wasserversorgung, der Landwirtschaft und des Naturschutzes*, 2006, ISBN 3-933761-56-5

154 Das, Tapash: *The Impact of Spatial Variability of Precipitation on the Predictive Uncertainty of Hydrological Models,* 2006, ISBN 3-933761-57-3

155 Bielinski, Andreas: *Numerical Simulation of CO_2 sequestration in geological formations*, 2007, ISBN 3-933761-58-1

156 Mödinger, Jens: *Entwicklung eines Bewertungs- und Entscheidungsunterstützungssystems für eine nachhaltige regionale Grundwasserbewirtschaftung*, 2006, ISBN 3-933761-60-3

157 Manthey, Sabine: *Two-phase flow processes with dynamic effects in porous media - parameter estimation and simulation,* 2007, ISBN 3-933761-61-1

158 Pozos Estrada, Oscar: *Investigation on the Effects of Entrained Air in Pipelines,* 2007, ISBN 3-933761-62-X

159 Ochs, Steffen Oliver: *Steam injection into saturated porous media – process analysis including experimental and numerical investigations*, 2007, ISBN 3-933761-63-8

160 Marx, Andreas: *Einsatz gekoppelter Modelle und Wetterradar zur Abschätzung von Niederschlagsintensitäten und zur Abflussvorhersage, 2007,* ISBN 3-933761-64-6

161 Hartmann, Gabriele Maria: *Investigation of Evapotranspiration Concepts in Hydrological Modelling for Climate Change Impact Assessment*, 2007, ISBN 3-933761-65-4

162 Kebede Gurmessa, Tesfaye: *Numerical Investigation on Flow and Transport Characteristics to Improve Long-Term Simulation of Reservoir Sedimentation*, 2007, ISBN 3-933761-66-2

163 Trifković, Aleksandar: *Multi-objective and Risk-based Modelling Methodology for Planning, Design and Operation of Water Supply Systems*, 2007, ISBN 3-933761-67-0

164 Götzinger, Jens: *Distributed Conceptual Hydrological Modelling - Simulation of Climate, Land Use Change Impact and Uncertainty Analysis*, 2007, ISBN 3-933761-68-9

165 Hrsg.: Braun, Jürgen; Koschitzky, Hans-Peter; Stuhrmann, Matthias: *VEGAS – Kolloquium 2007,* Tagungsband zur Veranstaltung am 26. September 2007 an der Universität Stuttgart, Campus Stuttgart-Vaihingen, 2007, ISBN 3-933761-69-7

166 Freeman, Beau: *Modernization Criteria Assessment for Water Resources Planning; Klamath Irrigation Project, U.S.*, 2008, ISBN 3-933761-70-0

167 Dreher, Thomas: *Selektive Sedimentation von Feinstschwebstoffen in Wechselwirkung mit wandnahen turbulenten Strömungsbedingungen*, 2008, ISBN 3-933761-71-9

168 Yang, Wei: *Discrete-Continuous Downscaling Model for Generating Daily Precipitation Time Series*, 2008, ISBN 3-933761-72-7

169 Kopecki, Ianina: *Calculational Approach to FST-Hemispheres for Multiparametrical Benthos Habitat Modelling,* 2008*,* ISBN 3-933761-73-5

170 Brommundt, Jürgen: *Stochastische Generierung räumlich zusammenhängender Niederschlagszeitreihen*, 2008, ISBN 3-933761-74-3

171 Papafotiou, *Alexandros: Numerical Investigations of the Role of Hysteresis in Heterogeneous Two-Phase Flow Systems*, 2008, ISBN 3-933761-75-1

172 He, Yi: *Application of a Non-Parametric Classification Scheme to Catchment Hydrology*, 2008, ISBN 978-3-933761-76-7

173 Wagner, Sven: *Water Balance in a Poorly Gauged Basin in West Africa Using Atmospheric Modelling and Remote Sensing Information*, 2008, ISBN 978-3-933761-77-4

174 Hrsg.: Braun, Jürgen; Koschitzky, Hans-Peter; Stuhrmann, Matthias; Schrenk, Volker: *VEGAS-Kolloquium 2008 Ressource Fläche III*, Tagungsband zur Veranstaltung am 01. Oktober 2008 an der Universität Stuttgart, Campus Stuttgart-Vaihingen, 2008, ISBN 978-3-933761-78-1

175 Patil, Sachin: *Regionalization of an Event Based Nash Cascade Model for Flood Predictions in Ungauged Basins*, 2008, ISBN 978-3-933761-79-8

176 Assteerawatt, Anongnart: *Flow and Transport Modelling of Fractured Aquifers based on a Geostatistical Approach,* 2008, ISBN 978-3-933761-80-4

177 Karnahl, Joachim Alexander: *2D numerische Modellierung von multifraktionalem Schwebstoff- und Schadstofftransport in Flüssen*, 2008, ISBN 978-3-933761-81-1

178 Hiester, Uwe: *Technologieentwicklung zur In-situ-Sanierung der ungesättigten Bodenzone mit festen Wärmequellen,* 2009, ISBN 978-3-933761-82-8

179 Laux, Patrick: *Statistical Modeling of Precipitation for Agricultural Planning in the Volta Basin of West Africa,* 2009, ISBN 978-3-933761-83-5

180 Ehsan, Saqib: *Evaluation of Life Safety Risks Related to Severe Flooding,* 2009, ISBN 978-3-933761-84-2

181 Prohaska, Sandra: *Development and Application of a 1D Multi-Strip Fine Sediment Transport Model for Regulated Rivers,* 2009, ISBN 978-3-933761-85-9

182 Kopp, Andreas: *Evaluation of CO_2 Injection Processes in Geological Formations for Site Screening,* 2009, ISBN 978-3-933761-86-6

183 Ebigbo, Anozie: *Modelling of biofilm growth and its influence on CO_2 and water (two-phase) flow in porous media,* 2009, ISBN 978-3-933761-87-3

Die Mitteilungshefte ab der Nr. 134 (Jg. 2005) stehen als pdf-Datei über die Homepage des Instituts: www.iws.uni-stuttgart.de zur Verfügung.